STUDIES IN IONOSPHERIC RAY TRACING

A thesis submitted in fulfilment of the requirements
for the degree of Master of Science at

Rhodes University, Grahamstown

by

SHERIDAN LAMBERT

Supervisor: Professor J.A. Gledhill

March, 1977

--- o0o ---

A C K N O W L E D G E M E N T S

I should like to express my gratitude to Professor J.A. Gledhill, my supervisor, for all his advice and encouragement during the course of this project. On many occasions his insight into the physics of the ionosphere revealed profitable and fascinating new aspects for me to investigate.

I also wish to thank Dr. Pat Terry for his cheerful and willing help with the computing side, and for explanations of some of the subtleties of ray tracing.

Help and advice provided by my colleagues in the Antarctic and Ionosphere Research Group, in particular Allon Poole and John Rash, have been appreciated. My thanks for the assistance I received go, too, to the staff of the Rhodes Computer Centre - manager Mike Lawrie, programmers Martin Urry, Alistair Morrison and Ray Diederiks, senior operator Eugene de Jager, and operators Moosa Sha and Hiram Major.

I wish to thank the University for the award of a Muirhead Bursary, and the C.S.I.R. for its post-graduate bursary, both of which provided financial support for the project.

Finally, I should like to express my appreciation to Heather Kew for her fine typing, my mother for all her support, and Mike Gaylard for aid both concrete and intangible.

Sheridan Lambert.

CONTENTS

Page

CHAPTER 3

THE IONOSPHERE MODEL.

CHAPTER 4

THE GEOMAGNETIC FIELD MODEL.

CHAPTER 5

THE RAY TRACING PROGRAM.

Page

CHAPTER 6

VERTICAL AND SHORT DISTANCE RAY TRACING.

CHAPTER 7

LONG DISTANCE RAY TRACING.

A B S T R A C T

The use of ray tracing in the analysis of certain daytime ionograms recorded at Grahamstown is discussed in this thesis. A computer program has been modified and used to trace rays in the frequency range 1 - 30 MHz. Vertical, short distance oblique, and long distance oblique ionograms have been synthesized from the results and compared with experimental ionograms for Grahamstown, the Alice - Grahamstown transmission path (64 km), and the SANAE - Grahamstown transmission path (4470 km) respectively. Ray paths have been calculated and related in detail to the models of the ionosphere and geomagnetic field.

The main features of the vertical and short distance oblique ionograms can, in general, be reproduced using spherically stratified ionosphere models with electron density profiles derived from vertical ionograms. A suitable model for the geomagnetic field is a tilted dipole equivalent to the actual field at Grahamstown.

The two-hop mode is shown to be, usually, the lowest on the long distance oblique records. The ionosphere model is the principal limiting factor in reproducing such ionograms, and the most satisfactory results have been those obtained with a model in which electron density is assumed to vary linearly with latitude between the profiles at SANAE and Grahamstown.

The promising results obtained by ray tracing with normal ionospheric conditions indicate that the method has further possibilities which could usefully be explored.

CHAPTER 1

THE RAY TRACING PROJECT

Investigation of the ionosphere by ground-based ionosondes, a method involving the propagation of high frequency radio waves between a transmitter and a receiver via the ionosphere, has been widely pursued since the 1930's (Ratcliffe, 1974). Much information on the structure of the ionosphere has been obtained from vertical soundings, and their interpretation in terms of theory is relatively well understood. Oblique soundings have received rather less attention from a scientific as opposed to an engineering viewpoint, although the past fifteen or so years have seen an increased interest being taken in oblique propagation.

In 1972 and 1973 the Rhodes University Physics Department acquired two Barry Research chirp-type ionosondes for the furtherance of its Antarctic Research programme. The first instrument has been operated at Grahamstown; the second, except for a brief period at Alice (South Africa), has been operated at SANAE (Antarctica). Individually, the ionosondes record vertical ionograms, and, in conjunction, oblique ionograms. This thesis represents first attempts to interpret the oblique results on a theoretical basis, and to link them to vertical results.

A ray tracing method was adopted, largely because a computer program for high frequency rays, written by Dr. P.D. Terry, was already available. The theory of radio wave propagation in an ionized medium is outlined in Chapter 2. The program is described in Chapter 5, while Chapters 3 and 4 deal with the types of models used for the ionosphere and the geomagnetic field respectively.

The program was modified by the author so as to "home in" on a selected destination for the rays, and tested by comparing output for vertical and short distance oblique rays with experimental records obtained during the trial period when the second ionosonde was operated at Alice, 64 km from Grahamstown. The results are presented in Chapter 6. In the light of these, further modifications were made to the ray tracing program. Long distance oblique results are the subject of Chapter 7. Useful information was gained about the variation of the ionosphere over the 4700 km between SANAE and Grahamstown, the delay times and frequencies propagated, and the paths followed by the radio rays.

The work is summarised, and suggestions are made for further studies, in Chapter 8.

CHAPTER 2

THEORY

2.1. Introduction.

The following, except where otherwise indicated, is condensed from Budden (1961), Kelso (1964), and Davies (1965).

The propagation of a plane electromagnetic wave in a homogeneous, anisotropic plasma is discussed in 2.2. Expressions for the direction and group refractive index of a ray are given in 2.3.

Refractive index surfaces are defined in 2.4 and used in 2.5 to make qualitative predictions about ray paths in an inhomogeneous plasma stratified in one direction. The WKBJ solutions describing an electromagnetic wave in a slowly varying medium are discussed in 2.6.

Further discussion of vertical and oblique rays follows in 2.7, with particular reference to the quantities virtual height and virtual path .

Haselgrove's general ray tracing method is summarized and applied to the chosen co-ordinate system in 2.8.

The validity of the techniques used is discussed in 2.9.

2.2. Electromagnetic wave in a homogeneous cold plasma.

The phase refractive index n for a plane harmonic wave of frequency f, propagating in a homogeneous plasma in which thermal motions of the constituent particles are negligible, in the presence of a constant external magnetic

field $\vec{B}_o$, is given by the Appleton-Hartree equation

$$n^2 = 1 - \frac{X}{U - \frac{\frac{1}{2}Y^2\sin^2\psi}{U-X} \pm \left\{\frac{\frac{1}{4}Y^4\sin^4\psi}{(U-X)^2} + Y^2\cos^2\psi\right\}^{\frac{1}{2}}} \quad \ldots(2.1)$$

where the symbols are as listed in the glossary.

The refractive index

(i) depends on plasma frequency f_N and thus electron density N, since

$$X = \frac{f_N^2}{f^2} = \frac{Ne^2}{4\pi\varepsilon_o m}\ \frac{1}{f^2} \quad \ldots(2.2)$$

(ii) depends on electron gyrofrequency f_H and thus on the magnitude of the external magnetic field, since

$$Y = \frac{f_H}{f} = \frac{eB_o}{2\pi m}\ \frac{1}{f} \quad \ldots(2.3)$$

(iii) depends on the propagation direction via the angle ψ between the wave normal and $\vec{B}_o$ (the plasma is anisotropic)

(iv) depends on frequency (the plasma is dispersive) by (2.2) and (2.3)

(v) is complex (the plasma is absorptive) since

$$U = 1 - iZ \quad \ldots(2.4a)$$

$$Z = \nu/\omega \quad \ldots(2.4b)$$

(vi) can have either of two values (the plasma is birefringent) by (2.1).

The two values of n apply to two modes of propagation, usually assumed to be independent, called ordinary and extraordinary for the + and - signs respectively in equation (2.1). Each mode has its own unique wave polarization, and when a wave of arbitrary polarization enters an ionized

region from another medium, the transmitted wave can be regarded as splitting into two waves with relative amplitudes determined by the original polarization. While the wave magnetic field is always transverse, the electric field can have a component along the wave normal.

Without the external magnetic field, the equation for the refractive index simplifies to

$$n^2 = 1 - X/U \qquad ...(2.5)$$

for a single mode of propagation with arbitrary polarization.

At high wave frequencies in media with low collision frequencies, Z is negligible, $U \simeq 1$, and n is then very nearly equal to its real part, μ. Collisions will be neglected for most of this chapter.

The dependence of n^2 on X, Y, and ψ can be illustrated by graphs of n^2 versus X for various values of Y and ψ (Ratcliffe, 1959, pp. 60, 62). It can be shown that $n^2 = 0$, the condition for reflection of a wave vertically incident on the plasma, occurs at $X = 1 - Y$ for longitudinal ($\psi = 0°$) and at $X = 1 - Y$ and $X = 1 + Y$ for intermediate and transverse ($\psi = 90°$) propagation, for the extraordinary mode; for the ordinary mode, $n^2 = 0$ at $X = 1$ for all propagation directions except $\psi = 0°$, for which $n^2 = 0$ at $X = 1 + Y$.

2.3. Ray in a homogeneous plasma.

The wave field of an actual signal may be represented by a Fourier integral of effectively plane waves with all possible frequencies and wave normal directions, the amplitude function being peaked at the centre frequency and in the predominant direction of the signal.

The energy of the signal, or the ray, moves through the medium along the ray path. From the condition of stationary

phase along the path, it can be shown that:

(i) the ray, or direction of energy propagation, is at a non-zero angle ζ to the wave normal, or direction of phase propagation, of the signal in an anisotropic plasma, where

$$\tan \zeta = \frac{1}{\mu} \frac{\partial \mu}{\partial \psi} \qquad \ldots(2.6)$$

In an isotropic plasma, $\frac{\partial \mu}{\partial \psi} = 0$, and the directions are the same.

(ii) the wave normal, ray, and the magnetic field if present, are all coplanar.

(iii) the ray travels through the plasma at group velocity V', where

$$V' = \frac{c}{\mu'} \sec \zeta \qquad \ldots(2.7)$$

and μ', the group refractive index of the ray, is related to the (phase) refractive index, μ, by

$$\mu' = \frac{\partial}{\partial f} (\mu f) \qquad \ldots(2.8)$$

The phase velocity V is the speed of a wave front in the direction of the wave normal, given by

$$V = \frac{c}{\mu} \qquad \ldots(2.9)$$

2.4. Refractive index and ray surfaces.

These will be defined in this section and used in 2.5 and 2.8.

2.4.1. Refractive index surfaces.

These are sets of surfaces for which the length of the radius vector in any direction is equal to the phase refractive index μ for a wave with its normal in that direction.

Refractive index surfaces are three dimensional representations of equations (2.1) and (2.5), defining μ for conditions ranging from free space propagation to reflection of a wave; they are usually illustrated for a fixed value of Y, the magnetic field dependent parameter, and various values of X, which is proportional to electron density.

The surface for free space is the unit sphere. For plasmas with no external magnetic field, $\vec{B}_o$, the surfaces are spheres, decreasing in radius to a point for X = 1. For anisotropic plasmas, they are surfaces of revolution about an axis parallel to $\vec{B}_o$ and the plane $\psi = 90°$ is a plane of symmetry. There are two types of surfaces, corresponding to the ordinary and extraordinary mode values of μ, for any pair of values of X and Y.

The ordinary surfaces (figure 2.1A) are elongated along $\vec{B}_o$, becoming more so with increasing X. They shrink to a line of length $2\frac{Y}{1+Y}$ along $\vec{B}_o$ at X = 1; this corresponds to an anomaly in purely longitudinal propagation mentioned in 2.2. A second set of surfaces exists but will not be discussed here as it corresponds to physical situations not usually encountered.

The extraordinary surfaces fall into two categories. For Y<1 (figure 2.1B), or propagation at frequencies above the electron gyrofrequency, they are elongated perpendicularly to $\vec{B}_o$, shrinking to a point at X = 1 - Y, and less distorted from the spherical than the ordinary surfaces. A second set exists, but will not be discussed for the reasons given above. If Y>1, the surfaces go from the unit sphere at X = 0 to unit sphere and two line segments parallel to $\vec{B}_o$

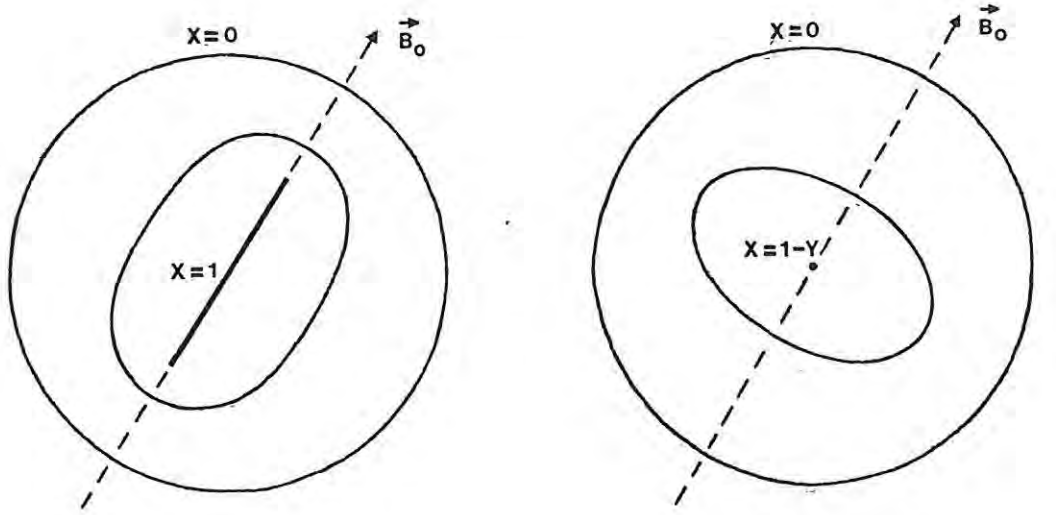

A ORDINARY MODE B EXTRAORDINARY MODE, Y<1

F 2.1 REFRACTIVE INDEX SURFACE CROSS-SECTIONS IN THE MAGNETIC MERIDIAN PLANE

at X = 1 and shrink to a point at X = 1 + Y; these are not illustrated as they apply to the lower frequencies for which collisions may not be negligible (see 2.9.2).

There is an important relationship between the direction of a ray, the direction of its wave normal, and the refractive index surface (defined by the mode and frequency of the ray and the properties of the medium). The ray is parallel to the normal to the surface at a point where the radius vector is in the direction of the wave normal.

2.4.2. Ray surfaces.

The ray velocity V_R is defined as the speed of a wave front in the ray direction. From (2.9)

$$V_R = V \sec \zeta \qquad \ldots(2.10)$$

where ζ is the angle between the ray and the wave normal given by equation (2.6).

Ray surfaces are sets of surfaces for which the length of the radius vector in any direction is equal to the ray velocity V_R of a ray in that direction.

A ray surface is the wave front, after unit time, for radiation from an isotropic point radiator at the origin. Their shapes are more complicated than those of the refractive index surfaces, except at X = 0 when the surface is a sphere of radius c.

Mathematically, the properties of the ray and refractive index surfaces are reciprocal: the normal to the ray surface at any point is parallel to the wave normal of a ray in the direction of the radius vector to that point.

2.5. Ray paths in a vertically stratified ionosphere.

When the plasma is inhomogeneous, that is, the electron density depends on position as in the ionosphere, no generally applicable analytic solution of Maxwell's equations exists. Approximate solutions are discussed in the next section. Qualitative predictions can, however, be made about the shapes of ray paths using the graphical method of Poeverlein.

2.5.1. Poeverlein's construction.

It is assumed that the plasma varies only in the vertical direction and, for simplicity, $\vec{B}_o$ is constant at all heights. The ionosphere is divided into many thin layers, each with an average value of electron density N and corresponding X, for the level. Further, the plasma is "slowly varying" in that X changes little from one layer to the next and most of the energy of a signal is transmitted. The ray path is approximated by straight line segments in each layer.

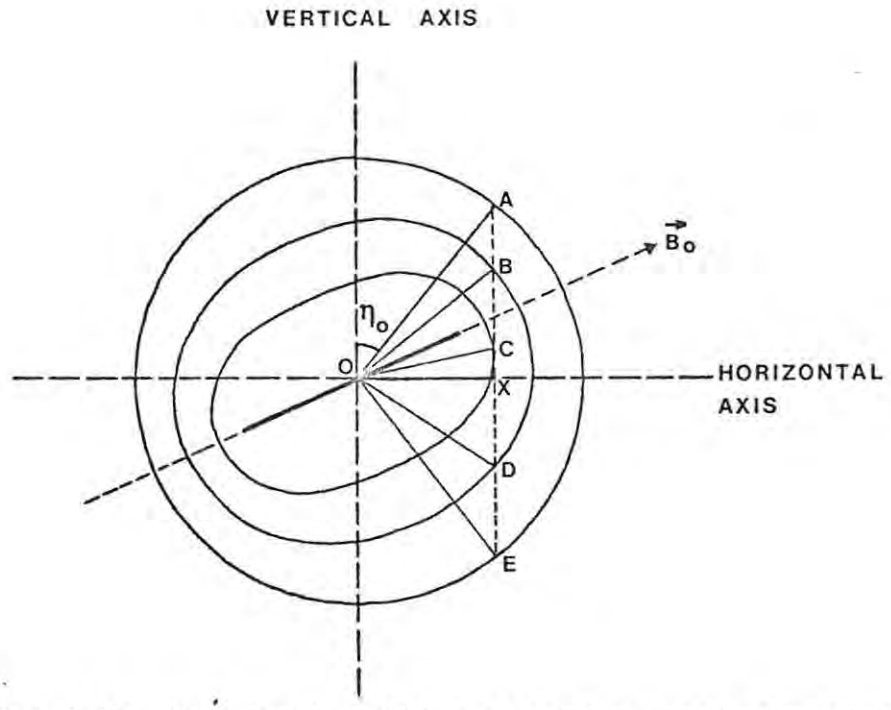

F 2.2 RAY PATH PREDICTION USING REFRACTIVE INDEX SURFACES

The angle between the wave normal and the vertical in the free space below the ionosphere is η_o, and at a level with parameter X and phase refractive index μ, it is η. Since the wave normal obeys Snell's Law,

$$\mu \sin \eta = \sin \eta_o = \text{constant} \qquad \ldots(2.11)$$

Figure 2.2 shows a set of ordinary refractive index surfaces and the vertical direction. The length OA is unity and the wave normal and ray have the same direction η_o at A. The length of OX is sin η_o and, by (2.11), constant. At the layer corresponding to point B, the wave normal makes some angle η to the vertical; OB = μ for this layer, and the ray direction is perpendicular to the refractive index surface at B. At C, the ray is horizontal; at D, the refractive index for the same level as B but for a downgoing wave, is given by OD, and at E the ray emerges into free space parallel to its wave normal.

The ray direction at any level in the medium is thus given by the perpendicular to the refractive index surface for that level at the point where the dotted line AE, parallel to the vertical axis at a distance sin η_o, intersects the surface. There are two such intersection points, for upgoing

and downgoing rays respectively, for each level except where the ray is horizontal - the reflection level.

2.5.2. Shapes of ray paths.

For a flat earth and ionosphere in which N increases monotonically with height, the following qualitative predictions can be made about the paths of rays at frequencies above the electron gyrofrequency.

For vertical rays, $\eta_o = 0$ and the line AE of figure 2.2 is the vertical axis. The rays thus remain in the magnetic meridian plane and reflect at levels where X = 1 for the ordinary, and X = 1 - Y for the extraordinary mode. Then, because N increases with height, ordinary rays reflect at greater heights than extraordinary rays of the same frequency. The ordinary rays, being perpendicular to the surface X = 1 at reflection, must be perpendicular to $\vec{B}_o$ there; extraordinary rays are not so constrained. (The angle at reflection depends on $\vec{B}_o$ and can be derived from Budden (1961), p. 247.) Unless the rays are propagating at the magnetic poles or equator, the shapes of the surfaces of figures 2.2A and 2.2B cause them to deviate from the vertical, extraordinary rays towards the magnetic equator and ordinary to the nearest magnetic pole. The greater departure from sphericity of the ordinary surfaces causes these rays to be further deviated than extraordinary rays at the same frequency. Upward and downward ray paths are identical.

Oblique rays have twisted, three dimensional paths with the planes of incidence and exit parallel; only if the plane of incidence is also that of the magnetic meridian are the paths planar. The upgoing and downgoing paths are not, in general, symmetrical. Oblique rays are also reflected lower in the ionosphere than vertical rays at the same frequency because, in general, they do not reach the levels X = 1 (ordinary) or X = 1 - Y (extraordinary). Ordinary rays in the plane of the magnetic meridian and with $\eta_o \leq \text{arc sin } \{Y/(1 + Y)\}^{\frac{1}{2}}$

are the exception: these never become horizontal but have a cusp, the "spitze", at reflection level X = 1 where the path is perpendicular to $\vec{B}_o$. The ordinary and extraordinary ray reflection points are deviated from the centre of the ground plan of the path as described above for vertical rays.

2.6. The WKBJ solutions.

When a medium is not homogeneous, but is still "slowly varying" in that its properties do not change significantly over a length of one wavelength, the WKBJ (Wentzel-Kramer-Brillouin-Jeffries) approximate solutions describe the field quantities of a harmonic wave at any point in the medium. (Wait, 1962, Chapter 6.)

A field component of the wave is then the product of an amplitude function which varies slowly with position, and an exponential containing a "phase memory" term which is the integral over position coordinates of the refractive index n.

The exact forms of the amplitude and phase memory functions depend on the physical situation, but are similar to those of the one dimensional case of a plane wave propagating along the z axis of a medium whose properties vary only with z:

$$F(z,t) = F_o n^{-\frac{1}{2}}(z) \exp\left\{i\left[\omega t \pm k \int_o^z n(z)\, dz\right]\right\} \qquad \ldots(2.12)$$

where F is an electric or magnetic field component of the wave
F_o is a constant
$n^{-\frac{1}{2}}$ is the amplitude function
ω is the wave angular frequency
k is the wave number.

The solutions break down in certain regions: where n = 0 or $\frac{dn}{dz} = 0$ in the above example.

2.7. Vertical and oblique rays.

The field of a signal in a slowly varying plasma is represented by a Fourier integral of WKBJ-type waves. Assuming a flat earth and horizontally stratified ionosphere, with z axis vertical and x and y axes in the plane of the earth, equations for the ray path and delay time τ (time of travel of a ray) can be derived. The ray paths behave as predicted in 2.5, and

$$\tau = \frac{1}{c}\left\{S_1 x + S_2 y + \int_0^z \frac{\partial}{\partial f}(qf)\,dz\right\} \qquad ...(2.13)$$

where S_1 and S_2 are the x and y direction cosines of the wave normal, and

$$q = n\cos\eta = \mu\cos\eta \qquad ...(2.14)$$

with μ and η as defined previously.

With no external magnetic field, equation (2.14) can, in principle, be solved analytically for some models of the ionosphere. This is discussed in 2.7.1 for vertical and in 2.7.3 for oblique rays. The effects of a magnetic field are considered for the two cases in 2.7.2 and 2.7.4. The quantities virtual height and path, which are recorded by ionosondes, are defined.

2.7.1. Vertical incidence with no magnetic field.

A ray of frequency f, vertically incident on the ionosphere from below, travels upwards until it reaches a height h where it is reflected. The total delay time between transmission and reception is τ. The virtual height h' of the ray is the distance it would travel in free space in the same time taken to reach the reflection level in the ionosphere. From equations (2.8), (2.13) and (2.14), with $\eta = 0$ and $S_1 = S_2 = 0$,

$$h' = \tfrac{1}{2}c\tau = \int_0^h \frac{\partial}{\partial f}(f\mu)\,dz = \int_0^h \mu'\,dz \qquad ...(2.15)$$

In the absence of an external magnetic field, the group refractive index μ', from (2.5) and (2.8), is given by

$$\mu' = \left\{1 - \frac{f_N^2}{f^2}\right\}^{\frac{1}{2}} \qquad \ldots(2.16)$$

μ' depends on ray frequency f, plasma frequency f_N and hence electron density N; the variation of N with height h, known as the electron density profile, thus determines h' for a given f. The virtual height of a ray is due both to the physical distance travelled and the delay, or group retardation, along it.

Equation (2.15) can be solved analytically to give h' as a function of ray frequency f for certain analytic functions N(h). The principal effects are that if N(h) has a maximum, that is, $\frac{dN}{dh} = 0$ at some value of N, then h'(f) is infinite when the ray frequency equals the plasma frequency corresponding to the maximum value of N. If $\frac{dN}{dh}$ is small but non-zero at a point of inflection called a ledge, the h'(f) function has a maximum.

This is illustrated in figures 2.3A and 2.3B. Below the base height, h_o, of the ionosphere, N = 0. N(h) has a local maximum at height h_{m1} with electron density N_{m1} and associated plasma frequency f_{p1}; h'(f) increases with f and becomes infinite at the penetration frequency, f_{p1}, of the lower layer. N(h) has another maximum at $h_{m2} > h_{m1}$, $N_{m2} > N_{m1}$, $f_{p2} > f_{p1}$. Without the ledge at h_L, with the profile represented by the two parabolas in figure 2.3A, h'(f) (indicated by the broken curve on figure 2.3B) has a minimum at some frequency between f_{p1} and f_{p2} since the curve is the sum of the rising (dashed) and falling (chained) curves shown - these represent the contribution to the total delay from the lower layer, and the effect of the upper layer, respectively. The effect of a ledge at h_L, N_L, f_L, is to superimpose a local maximum on the h'(f) curve at f_L (solid curve).

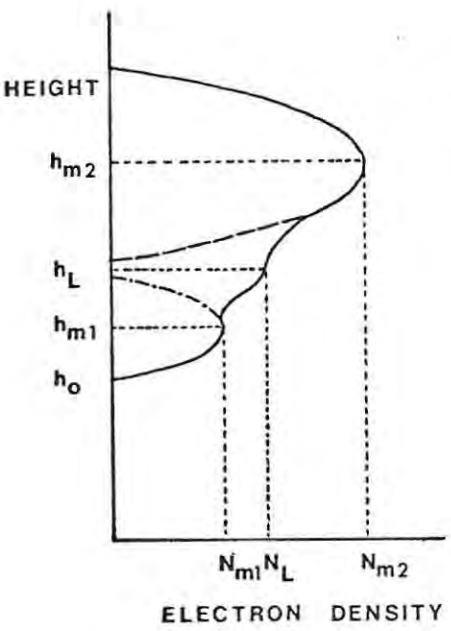

F 2.3A TYPICAL ELECTRON DENSITY PROFILE

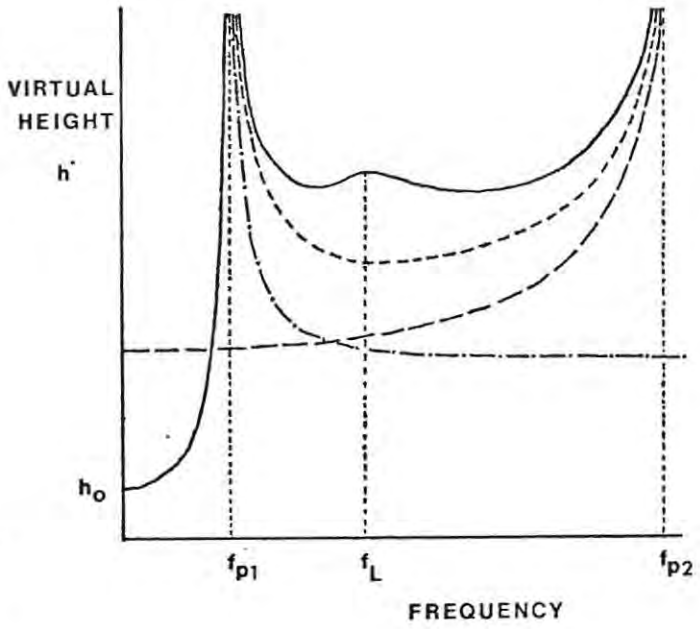

F 2.3B CORRESPONDING VARIATION OF h' WITH f

2.7.2. Vertical incidence with magnetic field.

The group refractive index μ', from (2.1) and (2.8), is such that (2.15) must be numerically evaluated to give h'(f).

The general shapes of the ordinary, extraordinary, and no-field h'(f) curves are similar, but features such as maxima and discontinuities, which occur at the same frequencies on the ordinary and no-field curves, are shifted to higher frequencies for the extraordinary case. (These effects can be seen in figures 6.1, 6.3, and 7.1A - 7.4A.) If f_p^o is the ordinary penetration frequency and $f_p^o >> \frac{1}{2}f_H$, then the extraordinary penetration frequency is

$$f_p^x \simeq f_p^o + \tfrac{1}{2} f_H \qquad \ldots(2.17)$$

2.7.3. Oblique incidence with no magnetic field.

A ray of frequency f, starting from transmitter T at the origin of the coordinate system, is obliquely incident on the ionosphere at an angle η_o to the vertical. It is reflected at some height h and received at R(x,y,0) after a delay time τ. The virtual path P' of the ray is the distance it would travel in free space in the same time τ. From (2.13)

$$P' = c\tau = \int_0^h \frac{\partial}{\partial f}(qf)\, dz + S_1 x + S_2 y \qquad ...(2.18)$$

From (2.14), $q^2 = \mu^2 - S_1^2 - S_2^2$ ...(2.19a)

and with no magnetic field, using (2.2) and (2.5),

$$q^2 = \cos^2\eta_o - f_N^2/f^2 \qquad ...(2.19b)$$

An oblique ray of frequency f reflects at the same height h as a vertical ray of frequency f_v, where

$$f_v = f \cos \eta_o \qquad ...(2.20)$$

The Theorem of Breit and Tuve links virtual path P', the horizontal distance D travelled by the ray between T and R, and the take-off angle η_o:

$$P' = D \operatorname{cosec} \eta_o \qquad ...(2.21)$$

Martyn's Equivalent Path Theorem relates the virtual height of a vertical ray at frequency f_v to the virtual path of an oblique ray with frequency f:

$$P'(f)\cos \eta_o = 2h' (f_v) \qquad ...(2.22)$$

An empirical factor is sometimes used to correct (2.22) for a curved earth.

The ray path, horizontal distance D, and virtual path P', all depend on the electron density profile. If N(h) has

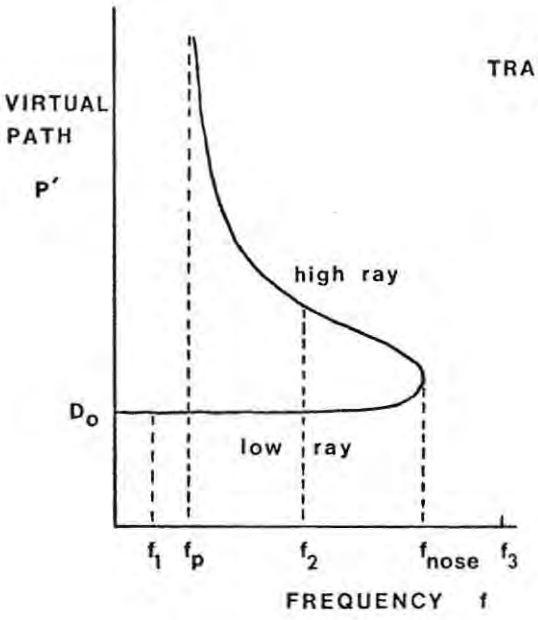

F 2.4 A VARIATION OF P' WITH f FOR TRANSMITTER - RECEIVER DISTANCE D_o

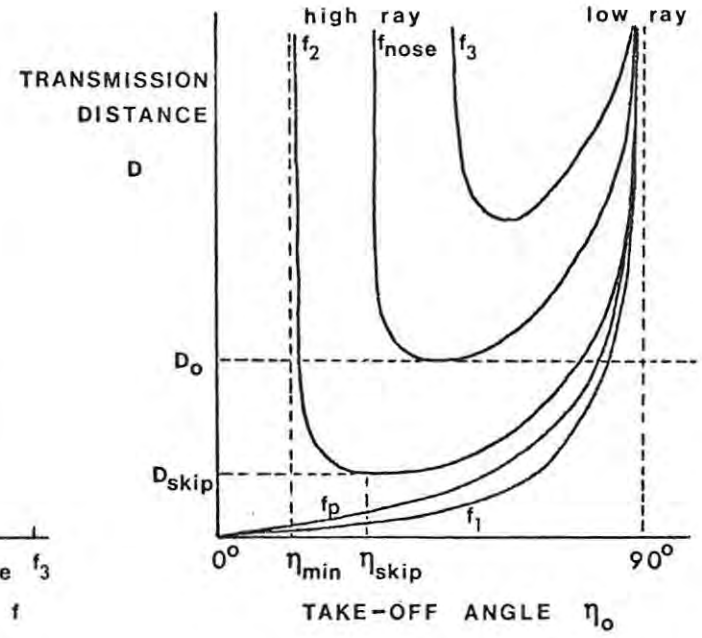

F 2.4 B VARIATION OF D WITH η_o AND f

a maximum, rays at certain frequencies can cover the same distance D via two different paths.

The P'(f) curve for a set transmitter-receiver distance D_o and a parabolic electron density profile is shown in figure 2.4A, and the relationship between frequency, take-off angle, and distance is illustrated by figure 2.4B for the same type of profile.

At frequencies below and equal to the vertical penetration frequency, f_1 and f_p in figures 2.4, the ray can travel a distance D by only one path (figure 2.4B); D is zero for vertical incidence and increases with η_o, becoming infinite when the ray leaves the transmitter tangentially to the earth. The curve of P'(f) for a fixed distance is thus single valued at these frequencies.

The curves of D versus η_o at frequencies above f_p also become infinite at some value $\eta_{min} \neq 0$ of take-off angle associated with penetration of the ionosphere, and there is a minimum

value D_{skip}, the "skip distance", which can be travelled by these rays. These are shown in figure 2.4B for the frequency f_2. A ray at this frequency can travel the distance D_o via two paths: the ray with the smaller η_o reaches a greater height in the ionosphere and has the larger virtual path - it is called the high or Pedersen ray and the other the low ray. The P'(f) curve is double valued at f_2, as shown in figure 2.4A.

The frequency for which $D_{skip} = D_o$ is the maximum useable frequency (MUF) or "nose" frequency for that distance and profile; only one ray path is possible at f_{nose} (figure 2.4B) and P'(f) is single valued (figure 2.4A).

No rays at frequencies such as f_3 above f_{nose} are received at R because their skip distances exceed D_o.

2.7.4. Oblique incidence with magnetic field.

The parameter q is no longer given by (2.19b) and equation (2.18) for the virtual path P' must be evaluated numerically for all electron density profiles.

Qualitatively, the P'(f) curve for some distance D_o is again split into ordinary and extraordinary curves. At frequencies well above (about 10x) the electron gyrofrequency, the curves closely resemble those for the no-field case and the same electron density profile, with the "nose" of the extraordinary curve shifted to higher frequencies.

2.8. Ray tracing in real space.

Haselgrove (1954) applied the methods of Hamiltonian mechanics to describe the path of a ray in a slowly varying inhomogeneous and anisotropic plasma.

Haselgrove's six canonical equations for a ray path are given

in 2.8.1 for an arbitrary system of orthonormal curvilinear co-ordinates and applied in 2.8.2 to a system of geophysical spherical polar co-ordinates formulated by Terry (1974), which are particularly suited to ray tracing over a curved earth.

2.8.1. Haselgrove's equations.

Starting with Fermat's principle of stationary time to define a ray, Haselgrove used Euler's equations and the reciprocal properties of the refractive index and ray surfaces of 2.4 to derive six first order differential equations for the position and direction of a ray in general curvilinear co-ordinates. Simplifying to orthonormal co-ordinates, these canonical equations become:

$$\frac{dx_i}{dt} = \frac{c}{h_i} \frac{\partial G}{\partial \rho_i} \qquad \ldots(2.23)$$

$$\frac{d\rho_i}{dt} = \frac{-c}{h_i} \left\{ \frac{\partial G}{\partial x_i} + \sum_{k=1}^{3} \frac{1}{h_i} \frac{\partial G}{\partial \rho_i} \left(\rho_i \frac{\partial h_i}{\partial \rho_k} - \rho_k \frac{\partial h_k}{\partial x_i} \right) \right\} \qquad \ldots(2.24)$$

where x_i, i=1,2,3 are the spatial, or position, co-ordinates

h_i are the scale factors of the co-ordinate system

ρ_i are the components of the refractive index vector, which has length μ and direction parallel to the wave normal

t is the time of travel of a wave front along the ray path.

The defining equation of the refractive index surface is

$$G(x_i,\rho_i) = \frac{(\sum_i \rho_i^2)^{\frac{1}{2}}}{\mu} = 1 \qquad \ldots(2.25)$$

The equations (2.2) and (2.4) are very general; all that is required is that the external magnetic field $\vec{B}_o$ and electron density N be defined as functions of the x_i. μ is then

completely defined, for a ray of frequency f, as a function of the x_i and ρ_i, thus allowing the calculation of the partial derivatives of G. The ray path can then be calculated by simultaneous numerical integration of the canonical equations.

Any other quantities of interest which vary along the ray path, for example delay time τ and phase p, can be found by integrating the appropriate differential equations in parallel with the canonical equations:

$$\frac{d\tau}{dt} = \frac{\mu'}{\mu} = 1 + \frac{f}{\mu}\frac{\partial \mu}{\partial f} = 1 - f\frac{\partial G}{\partial f} \qquad \ldots(2.26)$$

$$\frac{dp}{dt} = \sum_i \rho_i h_i \frac{dx_i}{dt} \qquad \ldots(2.27)$$

2.8.2. Application to geophysical co-ordinates.

In a right-handed system of spherical polar co-ordinates (r,θ,ϕ), where angle θ is measured from the equatorial plane, the position co-ordinates x_i, scale factors h_i, and direction co-ordinates ρ_i, become

$$(x_1,x_2,x_3) = (r,\theta,\phi)$$
$$(h_1,h_2,h_3) = (1,r,r\cos\theta)$$
$$(\rho_1,\rho_2,\rho_3) = (\rho_r,\rho_\theta,\rho_\phi)$$

With the integration variable changed to ds = cdt, and equations (2.23), (2.24), (2.27), (2.28) in geophysical co-ordinates, the complete set of equations to be integrated is:

$$\frac{dr}{ds} = \frac{\partial G}{\partial \rho_r}$$

$$\frac{d\theta}{ds} = \frac{1}{r}\frac{\partial G}{\partial \rho_\theta}$$

$$\frac{d\phi}{ds} = \frac{1}{r\cos\theta}\frac{\partial G}{\partial \rho_\phi} \qquad \ldots(2.28)$$

$$\frac{d\rho_r}{ds} = -\frac{\partial G}{\partial r} + \frac{\rho_\theta}{r}\frac{\partial G}{\partial \rho_\theta} + \frac{\rho_\phi}{r}\frac{\partial G}{\partial \rho_\phi}$$

$$\frac{d\rho_\theta}{ds} = -\frac{1}{r}\left\{\frac{\partial G}{\partial \theta} + \rho_\theta \frac{\partial G}{\partial \rho_r} + \rho_\phi \tan\theta \frac{\partial G}{\partial \rho_\phi}\right\}$$

$$\frac{d\rho_\phi}{ds} = \frac{-1}{r\cos\theta}\left\{\frac{\partial G}{\partial \phi} + \rho_\phi \frac{\partial G}{\partial \rho_r} - \rho_\phi \sin\theta \frac{\partial G}{\partial \rho_\theta}\right\}$$

$$\frac{d\tau}{ds} = \frac{1}{c}\left(1 - f\frac{\partial G}{\partial f}\right)$$

$$\frac{dp}{ds} = \rho_r \frac{dr}{ds} + r\rho_\theta \frac{d\theta}{ds} + r\cos\theta\,\rho_\phi \frac{d\phi}{ds}$$

2.9. Validity of the ray tracing equations.

Equations (2.28) apply to ray propagation in a collisionless, slowly varying ionosphere. The validity of these approximations will be examined briefly.

2.9.1. Slowly varying ionosphere.

Theoretically, the WKBJ solutions fail in the regions of the ionosphere where reflection occurs, and a more detailed, "full wave" treatment should be used here.

In practice, however, the ray tracing equations are stable even in such regions, and the differences between the results of the approximate and detailed treatments are slight.

2.9.2. Collisionless ionosphere.

The signal strength remains constant along the ray path if the refractive index, n, is purely real. When collisions are allowed for and n is complex, both signal strength and the path itself are affected.

If the imaginary part χ of the complex refractive index $n = \mu - i\chi$ is small compared with μ, the effect on the path is negligible and signal attenuation can be calculated by adding an equation for an absorption coefficient to the set (2.28). When χ is large, the ray path can be determined by ray tracing in complex space (Budden and Terry, 1971) or by finding the position of maximum field strength for a particular antenna beam pattern transmitting into an absorbing medium (Kimura and Kawai, 1976).

The effect of collisions on ray paths is serious at very low frequencies, but in the frequency range studied, the paths calculated from equations (2.28) are quite accurate, with one exception: the predicted penetration of the ionosphere does not actually occur - the ray is rather so heavily absorbed that a negligible signal returns to the receiver.

CHAPTER 3

THE IONOSPHERE MODEL

3.1. Introduction.

The spatial variation of the electron density is required for the solution of Haselgrove's equations (section 2.8.1).

In some circumstances, electron density need only be considered a function of height above the earth. General features of such electron density profiles are discussed in 3.2.

Analytic profiles, such as the parabolic models of section 2.7, are easily programmed but are too simplistic if a detailed analysis of frequencies propagated, ray paths, and delay times is required for a particular situation. The author used electron density profiles calculated from vertical ionograms. The theoretical basis for this type of model is outlined in 3.3, and a discussion follows in 3.4.

For long distance ray tracing, where it is not realistic to assume that the electron density profile is the same at all points along the transmission path, latitude dependent models were formulated. These are the subject of 3.5.

Criteria for the selection of suitable ionograms are given in 3.6.

3.2. General features of electron density profiles.

The ionosphere extends from about 60 km to 1000 km above the surface of the earth. Various ionospheric regions can be defined, approximately according to height, within this range. From 60 km to 80 km there is the D region, with very low electron densities. The E region extends up to 110 km.

Electron density increases with height up to this level, but may, in some cases, decrease slightly in a "valley" region above. It increases with height in the F1 region, from 180 km to 200 km, and attains its maximum value in the F2 region at a height between 200 km and 300 km. Above this, in the "topside" ionosphere, electron density decreases with height (Rawer et al., 1975). In addition to these principal features irregular "sporadic" E and "spread" or sporadic F regions can exist in the ionosphere (Al'pert, 1963, pp. 22-5).

The exact form of an electron density profile varies with position on the earth's surface and with local time. At middle to high latitudes during the day, and everywhere at night, the F1 and F2 regions merge into a single F region. Higher latitude and nighttime profiles also have smaller values of maximum electron density, and the E region is negligible at night. The ionosphere is generally most stable around midday to early afternoon and during the night at a given place. (Al'pert, 1963, pp. 126-9, 136; Davies, 1965, pp. 125-9.)

3.3. Obtaining electron density profiles from vertical ionograms.

An ionogram is, effectively, a graph of the function h'(f), where h' is the virtual height of reflection of a ray of frequency f. It can be converted to the function N(h), which is called the electron density profile and expresses the variation of electron density N with true height h, if some simplifying assumptions are made. In this case a lamination method (Poole, 1974) was chosen - it is based on standard techniques (Al'pert, 1963, pp. 118-9) and includes the effect of the earth's magnetic field.

A finite set of points (f_j, h'_j), $j = 1,\ldots, J$ where J is typically between 20 and 50, is read off the ordinary trace of a vertical ionogram. For each point the corresponding electron density N_j is calculated from the vertical incidence

reflection condition for ordinary rays, X = 1 (section 2.2); thus

$$N_j = (4\pi\varepsilon_o m/e^2)\, f_j^2 \qquad \ldots(3.1)$$

The actual electron density profile is assumed to be approximated by a function consisting of segments in which h is quadratic in N. This assumption is necessary because it is not possible to invert analytically the integral of equation (2.15),

$$h'(f) = \int_0^{h(f)} \mu' \, dh \qquad \ldots(3.2)$$

where μ' is the group refractive index of a ray of frequency f, to find h(f), the true height of reflection of the ray. At all points on the profile, then, the height h(N) corresponding to an electron density N is given by

$$h(N) = a_j(N^2 - N_{j-1}^2) + b_j(N - N_{j-1}) - h_{j-1} \quad N_{j-1} < N \leqslant N_j \qquad \ldots(3.3)$$

The form of (3.3) is determined by the condition that the profile must be continuous. Recursion formulae for the layer parameters a_j and b_j are obtained from two simultaneous equations: one arises from the requirement that h(N) should be differentiable, the other from changing the integration variable in (3.2) to N and setting each h'_j off the ionogram equal to a sum of numerically evaluated integrals over all layers up to and including the j-th. The greater the number of points between the fixed minimum and maximum discernible frequencies of the ionogram, the closer is the approximation of (3.3) to the actual profile.

Because there is no information at frequencies below the minimum, f_1, the segment from h_1 to h_2, where $h_i = h(N_i)$, is constrained to be linear and h_1 is arbitrarily set equal to h'_1. The author defined the base height h_0 of the profile by extending this linear section back to N = 0.

Figure 3.1 illustrates a typical multisegment model profile, showing the two linear segments from h_0 to h_2 and subsequent parabolic segments up to height h_J. In the absence of information at frequencies above the last read off the ionogram, f_J, the maximum electron density was initially taken to be N_J.

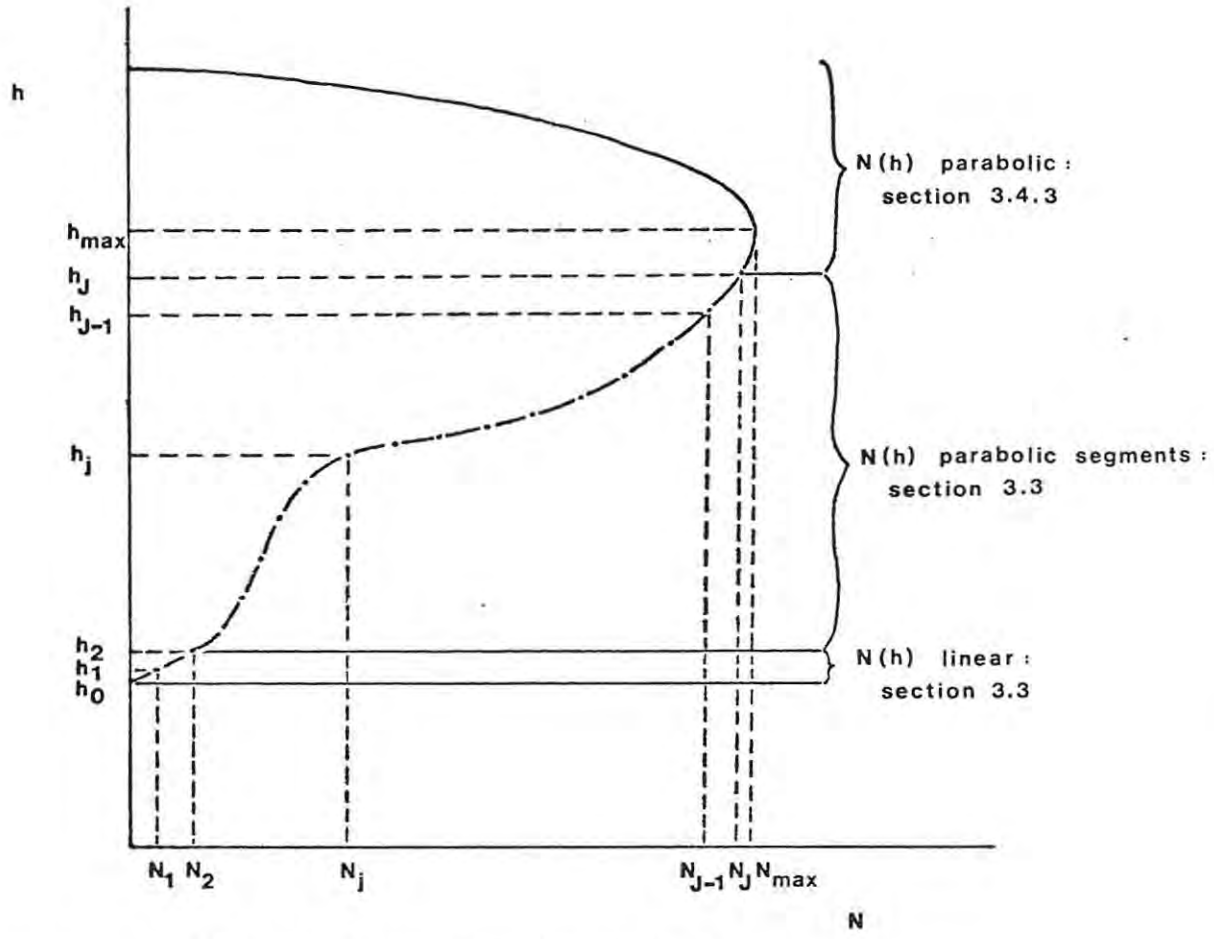

F 3.1 MODEL ELECTRON DENSITY PROFILE

3.4. Discussion of the model.

Titheridge (1975) has examined the relative accuracy of N(h) profiles derived from ionograms by similar methods to that of 3.3. The main weaknesses of the model, as presented, are: the D region is poorly defined and the base is too high; the profile is always monotonic; the maximum electron density and corresponding height are underestimated.

3.4.1. The D region.

This is defined by the first two points from the ionogram. In the limit of zero frequency, the true and virtual heights of reflection are equal, and thus the lower the minimum frequency, the better the initial approximation $h_1 = h'_1$. On the ionograms used, f_1 was at best about 1 MHz.

Various methods of improving the base and D region calculations have been proposed. The use of double interpolation, as suggested by Smith (1970), could make the lowest segment parabolic; Titheridge (1959) and Danilkin et al. (1975) used data from the extraordinary trace of the ionogram to estimate the base.

Comparison of experimental and synthesized vertical ionograms indicated that the effect of the poorly defined D region is negligible at frequencies above about 2,5 MHz as, at these frequencies, the overall time spent by a ray in the region of low electron density is small compared to its total delay time.

3.4.2. Monotonic profile.

A discontinuity at the E region of the ionogram indicates the presence of a "valley" in the actual profile (section 2.7.1). Because of the nature of the calculation of 3.3, this would not be reproduced in the model profile and the true heights corresponding to electron densities greater than those of the E region would be underestimated.

Points from the extraordinary trace can be used to calculate a profile for the valley region (Titheridge, 1959; Danilkin et al. 1975), but if ionograms with continuous ordinary traces are chosen to be converted to profiles, the problem does not arise.

3.4.3. Maximum electron density.

Theoretically, virtual height tends asymptotically to infinity as the ray frequency approaches f_oF2, the vertical penetration frequency of the F2 layer for the ordinary mode (sections 2.7.1, 2.7.2). In practice, at virtual heights above 400 km to 600 km, the ionogram trace disappears due to noise and heavy absorption (section 2.9.2). Thus N_J and h_J, corresponding to the last point obtained from the ionogram,

are less than N_{max} and h_{max}, the true maximum electron density and the height at which it occurs.

Piggott (1976) has suggested that, since it is possible to estimate f_oF2 with an accuracy better than 0,1 MHz on most of the ionograms which were used, N_{max} can be reliably calculated. A value for h_{max} can also be obtained by assuming a parabolic shape for this part of the F2 region.

Then, at $h>h_J$, N is given by

$$N(h) = ah^2 + bh + c \qquad ...(3.4)$$

The coefficients a, b and c can be calculated by applying the condition $\frac{dN}{dh} = 0$ at N_{max} and specifying that the parabola also passes through the last two previously determined points of the profile. They are given by

$$a = \frac{N_{J-1} - N_J}{h^2_{J-1} - h^2_J} - \frac{b}{h_{J-1} + h_J} \qquad ...(3.5)$$

$$b = \left(-q - (q^2 - 4pr)^{\frac{1}{2}} \right) /(2p) \qquad ...(3.6)$$

$$c = N_{max} - b^2/(2a) \qquad ...(3.7)$$

where $p = (h_{J-1} - h_J)^4$

$$q = (h_{J-1} - h_J)^2 \left(h_{J-1} (N_J - N_{max}) + h_J (N_{J-1} - N_{max})\right)$$

$$r = (N_{J-1} - N_J) \left(h_J (N_{J-1} - N_{max})^2 - h_{J-1}(N_J - N_{max})^2\right)$$

and the height of maximum electron density is $h_{max} = -b/(2a)$.

This part of the profile, extending from h_J to h_{max}, is also shown in figure 3.1. The parabolic region implicitly extending above h_{max} is not a realistic representation of the topside ionosphere, but a model of this region was not required since rays which are reflected back to earth do not reach the topside.

3.5. Variation of the ionosphere over long distances.

No latitudinal or longitudinal gradients in electron density, such as must exist in the actual ionosphere for the N(h) profiles to vary from place to place, are included in the type of model described in 3.3. This is a reasonable assumption for ray tracing over short distances, for which the N(h) profiles or vertical ionograms at the two endpoints of the transmission path are very similar. Such models are spherically stratified since N depends only on the radial position co-ordinate $r = h+r_e$, where r_e is the radius of the (spherical) earth.

The problem of modelling the ionosphere over distances of thousands of kilometers, with significantly different N(h) profiles at the endpoints, has been approached in various ways. A single profile, representative of conditions over the transmission path, can be used (Rush and Edwards, 1975). Effective profiles for particular transmission paths have been derived from oblique ionograms by, for example, Gething (1969) and Smith (1970); George (1970) discussed the physical significance of this type of profile. Kuriki et al. (1974) used profiles from ionospheric stations situated near the geographic midpoint of each "hop" of a ray (section 5.3.5).

When the ionosphere model includes latitudinal and/or longitudinal gradients, it is said to be tilted. Methods of incorporating realistic gradients include interpolation between the values of different profiles specified at separate points on the earth's surface (Rush et al., 1974; Lee and Nisbet, 1975), or multiplication of a single profile by a suitable function of latitude and longitude (Fiszleiber et al., 1975). In the present work, linear interpolation between N(h) profiles at the endpoints of the transmission path was used. Since the expressions for N and its partial derivatives become very cumbersome if distance along the great circle between the endpoints is taken as the controlling parameter for the interpolation, it was more convenient to use either latitude or longitude. In this case the difference in latitude between the endpoints (Grahamstown and SANAE, section 7.1) is probably more significant - conveniently, also, great circle path distance is nearly linearly related

to latitude between these stations.

Equations for two latitude dependent models are derived in 3.5.1. and 3.5.2.

3.5.1. First latitude dependent model.

$N_1(h)$ and $N_2(h)$ are electron density profiles from stations 1 and 2, at latitudes θ_1 and θ_2 respectively. $N(h,\theta)$ is the electron density at height h and latitude θ and is defined to be a linear interpolation between $N_1(h)$ and $N_2(h)$. If $\Delta\theta = \theta_2 - \theta_1$

$$N(h,\theta) = N_1(h)\ (\theta_2-\theta)\ /\Delta\theta\ + N_2(h)\ (\theta-\theta_1)/\ \Delta\theta \quad ...(3.8)$$

N now has partial derivatives with respect to height and latitude, given by

$$\frac{\partial N}{\partial h} = \frac{dN_1}{dh}\ (\theta_2-\theta)\ /\Delta\theta\ + \frac{dN_2}{dh}\ (\theta-\theta_1)\ /\ \Delta\theta \quad ...(3.9)$$

$$\frac{\partial N}{\partial \theta} = \left(N_2(h) - N_1(h)\right)\ /\ \Delta\theta \quad ...(3.10)$$

With this model the base of the ionosphere is the lower of the base heights h_{01} and h_{02} of the two profiles; it is not latitude dependent.

The profiles $N_1(h)$ (SANAE) and $N_2(h)$ (Grahamstown), and the variation of N with h at three equally spaced intermediate latitudes, are shown in figure 7.6.

3.5.2. Second latitude dependent model.

It is probably more realistic to interpolate between electron densities in physically similar parts of the ionosphere. It is now assumed that the base height h_0 and height h_{max} of maximum electron density vary linearly between the values at the two stations; h_0 and h_{max} at latitude θ are then given by

$$h_0(\theta) = h_{01}\ (\theta_2-\theta)\ /\Delta\theta\ + h_{02}\ (\theta-\theta_1)\ /\Delta\theta \quad ...(3.11)$$

$$h_{max}(\theta) = h_{m1}\ (\theta_2-\theta)\ /\Delta\theta\ + h_{m2}\ (\theta-\theta_1)/\Delta\theta \quad ...(3.12)$$

where h_{m1} and h_{m2} are the heights of maximum electron density at stations 1 and 2 respectively.

Using the difference between h_0 and h_{max} as a scaling factor, height h at latitude θ corresponds to heights h_1 at θ_1 and h_2 at θ_2, where

$$h_i(h,\theta) = \left\{ \frac{h - h_0(\theta)}{h_{max}(\theta) - h_0(\theta)} \right\} (h_{mi} - h_{0i}) + h_{0i}, \quad i=1,2 \qquad \ldots(3.13)$$

The electron density $N(h, \theta)$ is a linear interpolation between $N_1(h_1)$ and $N_2(h_2)$:

$$N(h,\theta) = N_1(h_1)\ (\theta_2-\theta)\ /\Delta\theta + N_2(h_2)\ (\theta-\theta_1)\ /\ \Delta\theta \qquad \ldots(3.14)$$

Defining the following parameters,

$$\begin{aligned} p &= \theta_2 - \theta \\ q &= \theta - \theta_1 \\ r &= h_{m_1} - h_{0_1} \\ s &= h_{m_2} - h_{0_2} \\ t &= (\theta_2-\theta)\ (h_{m_1} - h_{0_1}) \\ u &= (\theta-\theta_1)\ (h_{m_2} - h_{0_2} \\ v &= h\Delta\theta - h_{0_1}p - h_{0_2}q \\ w &= h_{0_1}\ h_{m_2} - h_{0_2}\ h_{m_1} \end{aligned} \qquad \ldots(3.15)$$

the partial derivatives of N become

$$\frac{\partial N}{\partial h} = \frac{dN_1}{dh}\bigg|_{h_1} \frac{t}{t+u} + \frac{dN_2}{dh}\bigg|_{h_2} \frac{u}{t+u} \qquad \ldots(3.16)$$

$$\frac{\partial N}{\partial \theta} = \frac{N_2(h_2) - N_1(h_1)}{\Delta\theta} + \frac{dN_1}{dh}\bigg|_{h_1} \frac{tw}{(t+u)^2} + \frac{dN_2}{dh}\bigg|_{h_2} \frac{uw}{(t+u)^2} \qquad \ldots(3.17)$$

This model is illustrated, for the same data as figure 7.6, in figure 7.7.

3.6. Selection criteria for ionograms in the present work.

All that was required to test the effectiveness of the ray tracing program in reproducing vertical results was a suitable vertical ionogram. For short distance oblique work on the Alice - Grahamstown transmission path (Chapter 6), a vertical ionogram from either station, to set up the ionosphere model, and an almost simultaneous oblique ionogram for comparison with ray tracing results, were required. On the long distance SANAE - Grahamstown path (Chapter 7), simultaneous vertical ionograms from both endpoint stations and an oblique ionogram were needed.

In view of the points raised in the foregoing sections, it will be seen that some ionograms are more suitable than others for conversion into electron density profiles. Oblique records from an undisturbed ionosphere are also preferable for comparison with ray tracing results. Criteria for the selection of ideal sets of ionograms, together with references to appropriate sections, are listed in table 3.1. Ionograms from relatively stable times of day were chosen in order to minimise the effect of the 5 minute delay between the recording of vertical and oblique ionograms.

In practice, it was impossible to fulfil all the requirements of table 3.1 for the SANAE - Grahamstown work. Many excellent oblique and Grahamstown vertical ionograms exist, but most of the SANAE vertical records have high minimum frequencies and show almost no E region due to absorption and various technical factors. As a compromise, SANAE vertical ionograms with any visible E regions were selected and Grahamstown vertical and oblique records for corresponding dates and times were examined to find ionograms which fulfilled most of the requirements.

Table 3.1: Selection criteria for ionograms.

TYPE OF IONOGRAM	REQUIREMENT	REASON
Vertical and short distance oblique	Low minimum frequency and flat, horizontal E region.	Better definition of base and D region (3.4.1).
	No sporadic E, spread F, or extra ripples in trace.	Stable ionosphere with relatively simple N(h) profile.
	Continuous ordinary and, if possible, extraordinary traces.	N(h) profile is truly monotonic (3.4.2).
	Well defined F region up to at least 400km.	Better definition of h_{max} and N_{max} (3.4.3).
Long distance oblique	Smooth, continuous trace.	Stable ionosphere.
	Clearly defined nose frequency.	Complicated modes of propagation unlikely (7.2).
	High ray section discernible and minimum frequency low.	Indicative of propagation in most of F region and possibly in E region (7.4.3).

CHAPTER 4

THE GEOMAGNETIC FIELD MODEL

4.1. Introduction.

The external magnetic field must be defined as a function of the position co-ordinates for use in the ray tracing equations (section 2.8.1).

The earth's magnetic field is discussed briefly in 4.2. A dipole approximation to the actual field was used and this is described in 4.3.

4.2. The geomagnetic field.

The earth has a magnetic field resembling that which would be produced by a dipole at the centre with its axis close to, but not aligned with, the rotation axis (Davies, 1965, p.19). Its direction undergoes a slow change known as the secular variation (Cook, 1973, pp.225-6), but provided that data from the correct epoch are used, this need not be considered. There is also a rapidly varying time dependent part of the field, but its contribution to the total is only about 1% of that of the main field (Cook, 1973, pp. 208,221).

Like all vector fields, the geomagnetic field at a point can be specified by three independent parameters. Seven standard magnetic elements are in common use: the total field strength F (sometimes T), the vertical and horizontal components Z and H of the field, the inclination (or dip) I between the field and the horizontal direction, the declination D between the horizontal component and the geographic meridian, and the north-south and east-west components of H known as Y and X (Chapman and Bartels, 1951, pp. 1,2). The magnetic elements X,Y and Z are not the same as the

ionospheric parameters with the same symbols. The elements F,I and D are an example of an independent set.

Two relationships between various elements, which will be used later, are (Davies, 1965, p.21)

$$\tan I = Z/H \qquad \ldots(4.1)$$

$$F^2 = Z^2 + H^2 \qquad \ldots(4.2)$$

World charts of various elements, for example Kolesova et al. (1974), show that the geomagnetic field is more complicated than that of a dipole, and accurate models of the field are usually obtained by spherical harmonic expansions (Cook, 1973, pp. 217-23; Jensen and Cain, 1962). Dipole models with no time variation were, however, considered adequate for the present work, and in addition have the advantage of being relatively simple to program.

4.3. The dipole approximation to the geomagnetic field.

The equations of a northward-pointing dipole magnetic field, in geophysical polar co-ordinates (section 2.8.2) referred to the axis of the dipole, are

$$B_r = -2B_0 (r_e/r)^3 \sin\theta = -Z \qquad \ldots(4.3a)$$

$$B_\theta = B_0 (r_e/r)^3 \cos\theta = H \qquad \ldots(4.3b)$$

$$B_\phi = 0 \qquad \ldots(4.3c)$$

where B_r, B_θ, B_ϕ are the three components of the vector $\vec{B}$ at a point (r,θ,ϕ)

B_0 is the magnitude of the vector $\vec{B}$ at the equator at the surface of the (spherical) earth

r is radial distance from the origin

r_e is the radius of the earth

θ is measured northwards from the equatorial plane

ϕ is measured westwards from some zero meridian.

The dipole axis defines a system of geomagnetic co-ordinates, which is not necessarily the same as the usual geographic system referred to the earth's rotation axis, although both

systems are considered to have their origin at the centre of the earth. When the two are identical, the dipole is said to be untilted. Initially the ray tracing program used such a model, with $B_0 = 2{,}93 \times 10^{-5}$T.

There are two ways of incorporating a tilted dipole: either by expressing the magnetic field equations in terms of the geographic system (Cook, 1973, p. 185), or by ray tracing in magnetic co-ordinates (Jones and Stephenson, 1975). The latter approach was used. A set of transformation equations between the two systems was therefore required; these are given in 4.3.1. The methods by which various models were obtained are outlined in 4.3.2 and the models are summarised in 4.3.3.

4.3.1. Transformation equations.

Geographic latitude and longitude are denoted by θ and ϕ , geomagnetic co-ordinates by θ_m and ϕ_m, as illustrated in figure 4.1 for a point P on the surface of the earth. Also shown are the geographic north pole, N, and the geomagnetic north pole, M, which has (geographic) latitude Θ and longitude Φ . The zero meridian in the magnetic system is defined by the great circle passing through M and N.

The geomagnetic co-ordinate system is obtained by a three-dimensional rotation of the geographic one; extending the method of Hutchins (Hollis et al., 1974, Appendix 5A) , the transformation equations are

$$\theta_m = \arcsin \left[\sin\theta \sin\Theta + \cos\theta \cos\Theta \cos(\phi-\Phi)\right] \quad \ldots (4.4)$$

$$\phi_m = \arctan_2 \left\{ \frac{\cos\theta \sin(\phi-\Phi)}{\cos\theta \sin\Theta \cos(\phi-\Phi) - \sin\theta \cos\Theta} \right\} \quad \cdots (4.5)$$

while the inverse transformation is given by

$$\theta = \arcsin \left[\sin\theta_m \sin\Theta - \cos\theta_m \cos\Theta \cos\phi_m\right] \quad \ldots (4.6)$$

$$\phi = \arctan_2 \left\{ \frac{\cos\theta_m \sin\phi_m}{\cos\theta_m \sin\Theta \cos\phi_m + \sin\theta_m \cos\Theta} \right\} \quad \ldots (4.7)$$

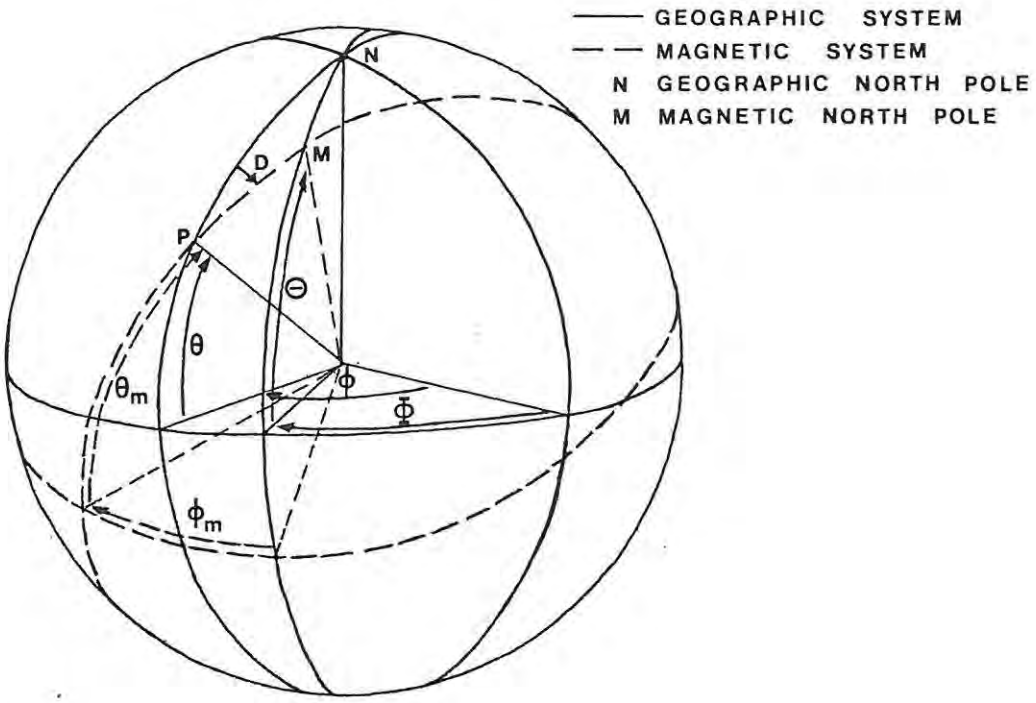

F 4.1 GEOGRAPHIC AND GEOMAGNETIC COORDINATES

The function arc $\tan_2$ is defined as

$$\text{arc } \tan_2 (s/t) = \text{arc } \tan (s/t), \quad t \geq 0 \qquad \ldots (4.8)$$

$$= \text{arc } \tan (s/t) + \pi \, \text{sgn } (s), \quad t < 0$$

in radians, and the function sgn or signum is +1 for positive and -1 for negative arguments (Bracewell, 1965,p.61).

The magnetic field model is thus completely defined if the latitude and longitude, Θ and Φ, of the magnetic north pole, and the magnitude of the field at the geomagnetic equator at the surface of the earth, B_0 are known. The determining of these parameters is the subject of the following section.

4.3.2. The tilted dipole models.

It is possible to calculate the defining parameters of the dipole which would produce the same measured field at a point $P(r,\theta,\phi)$ as does the actual field. The inclination I is related to magnetic latitude θ_m, and by (4.1) and (4.3)

$$\theta_m = \text{arc tan } (\tfrac{1}{2} \tan I) \qquad \ldots(4.9)$$

By applying the spherical cosine rule in the spherical triangle MNP of figure 4.1

$$\Theta = \text{arc sin } \theta \left(\sin \theta \sin \theta_m + \cos\theta \cos \theta_m \cos D\right) \qquad \ldots(4.10)$$

$$\Phi = \phi - \text{arc cos} \left\{ \frac{\sin \theta_m - \sin \theta \sin \Theta}{\cos\theta \cos\Theta} \right\} \qquad \ldots(4.11)$$

The total field F is the magnitude of $\vec{B}$ at point P and hence, from (4.2) and (4.3)

$$B_0 = F(r/r_e)^3 \left(3 \sin^2\theta + 1 \right)^{\frac{1}{2}} \qquad \ldots(4.12)$$

The data used to calculate the best-fit dipole field parameters for Grahamstown and SANAE listed in table 4.1 were taken from Kolesova et al. (1974), and charts for South Africa published by the Magnetic Observatory (1972).

Table 4.1: Best-fit dipoles for Grahamstown and SANAE.

Station	Θ (°N)	Φ (°W)	B_0 ($\times 10^{-5}$ T)
Grahamstown	66,90	109,24	1,80
SANAE	62,86	32,75	2,74

A model for the region of the transmission path between these two stations was obtained in the following manner. The values of Θ and Φ for all the stations listed by Barish and Roederer (1969) were calculated, and averages were obtained from all the stations (N-S in table 4.2) and from those in the northern (N) and southern (S) hemispheres separately.

The inclinations and declinations for selected South African, Antarctic, and southern Atlantic stations were then calculated according to each of the three tilted dipole models and compared with the values given by Barish and Roederer (1969). Table 4.2 lists the co-ordinates of the magnetic north pole, Θ and Φ, as well as the r.m.s. errors in inclination and declination, ΔI and ΔD, for the various models; the results for an untilted (U) dipole are included for comparison.

Table 4.2: r.m.s. errors in inclination and declination over the southern Atlantic region.

Model	Θ (°N)		Φ (°W)		Δ I (°)	Δ D (°)
U	90,00		0,00		42,16	23,39
N	81,57	5,11	99,43	36,94	21,34	19,57
N-S	78,83	7,25	91,87	6,56	16,51	17,82
S	70,35	6,30	68,55	30,01	13,25	15,56

By using combinations of Θ and Φ intermediate between the means for the best-fit SANAE and Grahamstown models and those of model S, either ΔI or ΔD could be reduced at the expense of increasing the other, and it was decided to use the values of model S when tracing rays from SANAE to Grahamstown.

The value of $B_0 = 2,37 \times 10^{-5}$ T, which was adopted for this model, gave minimum differences between the calculated and actual field strength simultaneously at Grahamstown and SANAE.

4.3.3. Summary of the models.

Early work (Chapter 6) was done using an untilted dipole magnetic field with an equatorial earth surface magnetic field B_0 of $2,93 \times 10^{-5}$T.

More sophisticated tilted models with the magnetic north pole at latitude Θ and longitude Φ were later introduced. Dipole fields which reproduce the measured values of magnetic elements at Grahamstown and SANAE, and are therefore suitable

for ray tracing in the vicinities of these stations, were obtained; their defining parameters are listed in table 4.1. The magnetic field model which was used for tracing rays between these stations (Chapter 7) was obtained by averaging over data from stations in the southern hemisphere. Its defining parameters are Θ = 70,35°N, Φ = 68,55°W, and B_0 = 2,37 x 10^{-5}T.

CHAPTER 5

THE RAY TRACING PROGRAM

5.1. Introduction.

The program was written by Dr. P.D. Terry of the Rhodes University Applied Mathematics Department and was modified by the author. It is written in ICL FORTRAN IV and is suitable for tracing rays in the frequency range 1 - 30 MHz.

A general description of the program is provided in 5.2, and followed by a discussion of the adaptations made in 5.3. The Rhodes ray tracing program is compared with others in 5.4.

5.2. General description.

The program solves Haselgrove's equations in geophysical spherical polar co-ordinates to find the ray paths; phase and delay time, and hence virtual height and virtual path, are also calculated. The ray tracing equations are used in a form (Terry, 1974) similar to that given by Haselgrove and Haselgrove (1960) for cartesian co-ordinates. Using the symbols defined in section 2.8 and the terms

$$Y_i = \frac{eB_i}{2\pi mf}$$

$$Y^2 = \sum_i Y_i^2$$

$$\rho^2 = \sum_i \rho_i^2$$

$$\vec{Y}.\vec{\rho} = \sum_i Y_i \rho_i$$

the equations for the ray path, delay time τ, and phase p become

$$\frac{dx_i}{d\sigma} = \frac{1}{h_i}\left(J\rho_i + KY_i\right) \qquad \ldots(5.1)$$

$$\frac{d\rho_i}{d\sigma} = \frac{1}{h_i}\left\{\frac{L\partial X}{\partial x_i} + \sum_k (MY_k - K\rho_k)\frac{\partial Y_i}{\partial x_k} - \sum_k \frac{dx_k}{d\sigma}\left(\rho_i\frac{\partial h_i}{\partial x_k} - \rho_k\frac{\partial h_k}{\partial x_i}\right)\right\}$$

$$\ldots(5.2)$$

$$\frac{d\tau}{d\sigma} = \frac{-1}{c} \left(P\eta + Q + 2LX + MY^2 - K\vec{Y}.\vec{\rho}\right) \quad ..(5.3)$$

$$\frac{dp}{d\sigma} = J\rho^2 + K\vec{Y}.\vec{\rho} \quad ..(5.4)$$

where i,k =r,θ,ϕ and the integration variable has been changed from s to

$$\sigma = -4\,(a+b)\,s/X \quad ..(5.5)$$

Other quantities used in equations (5.1) - (5.5) are

$$a = (1-X)\{(1-X)^2 - Y^2\}$$
$$b = (X-1)\,(1 - X - Y^2)\,\rho^2 + \tfrac{1}{2} XY^2\rho^2 - \tfrac{1}{2} X\,(\vec{Y}.\vec{\rho})^2$$
$$\eta = (\rho^2 - 1)/X$$
$$J = 2\{2\,(1-X-Y^2)\,(\eta+1) + (\vec{Y}.\vec{\rho})^2 - Y^2\}$$
$$K = 2\,(\rho^2 - 1)(\vec{Y}.\vec{\rho})$$
$$L = \{(\rho^2 - 1) - (\vec{Y}.\vec{\rho})^2 - 2(1-2X) + Y^2\}\eta - 2 + 3X$$
$$M = 2(\rho^2 - 1)\,(\eta + 1)$$
$$P = \eta\{-4\,(1 - X)^2 + 2Y^2\,(2 - X)\}$$
$$Q = 2Y^2 - 4(1-X)^2 - 2(\vec{Y}.\vec{\rho})^2$$

The program uses a predictor - corrector - modifier technique (Hamming, 1962, p.206), started off with a modified Runge-Kutta method (Gill, 1951), to integrate equations (5.1) - (5.4). The phase refractive index μ is defined by the collisionless Appleton-Hartree equation (2.1) in the vector notation, biquadratic form used by Haselgrove and Haselgrove (1960). At each point on the ray path, μ can be calculated either as $(\Sigma_i \rho_i^2)^{\frac{1}{2}}$ or from the quadratic. This extra degree of freedom can be used as a check on the stability of the equations (Yabroff, 1966). The ray tracing equations are used only within the ionosphere, that is, where the electron density is greater than zero. The rectilinear sections of the ray path in free space are determined by simple trigonometry.

Input data for each ray consist of its initial position, initial wave normal direction, frequency, mode, integration step size, and parameters controlling various program options. The initial position and direction are specified by height h above the earth, latitude θ , longtitude ϕ, and the take-off angles α to the vertical and β counter-clockwise from the magnetic meridian. Standard output for a ray consists of the position and direction co-ordinates, delay time, phase, phase refractive index and various other parameters, printed out at specified height intervals; graphs of ray paths are optional.

The amount of computer "mill time" taken to trace a ray depends on the machine itself and on factors such as the amount of numerical integration performed, the degree of sophistication of the ionosphere model, and the output required. Typical mill times on the Rhodes ICL 1902-T computer were 5 - 10 seconds for vertical ($\alpha=0°$) rays in the frequency range 1 - 7 MHz, and 0,5 - 3 minutes for a single hop (section 5.3.5) of an oblique ray in the frequency range 10 - 20 MHz, with $70° \leqslant \alpha \leqslant 90°$.

5.3. Adaptation of the program.

While minor alterations were made to various subroutines, the main changes were the addition of a homing feature, a complete revision of the subroutines concerned with the electron density model, provision of an option to change the integration step size, incorporation of a tilted dipole geomagnetic field model, and extensions to allow for more than one "hop" per ray.

5.3.1. The homing feature.

The ray tracing equations can only be used to find the path of a ray given the initial position and direction. An additional homing procedure was therefore incorporated into the program to calculate the take-off angles required to send rays to a given point on the earth's surface. This was especially necessary for short distance oblique rays, which have complicated three-dimensional paths in an

anisotropic ionosphere.

The program solves the simultaneous equations

$$f(\alpha,\beta) = \theta(\alpha,\beta) - \theta_e \quad \ldots(5.6)$$

$$g(\alpha,\beta) = \phi(\alpha,\beta) - \phi_e \quad \ldots(5.7)$$

where $\theta(\alpha,\beta)$ and $\phi(\alpha,\beta)$ are the co-ordinates of the endpoint of a ray with take-off angles α and β, and θ_e and ϕ_e are the co-ordinates of the desired endpoint. The numerical method of solution which was used was formulated by Terry (1971); it is outlined below. Programming details have been discussed by the author (Lambert, 1974).

$f(\alpha,\beta)$ is a function of two variables and hence $f(\alpha,\beta)= 0$ is the equation of a curve in the α-β plane. Similarly, $g(\alpha,\beta) = 0$ defines another curve and where the two intersect, f and g are simultaneously zero. If (α_i,β_i), $i = 1,2,3$, are three approximations to the solution, (α,β), then the functions $f(\alpha,\beta)$ and $g(\alpha,\beta)$ can be approximated, in the region of the solution, by planes through the points (f_i,α_i,β_i) and $(g_i,\alpha_i,\beta_i,)$ respectively, where $f_i = f(\alpha_i,\beta_i)$, $g_i = g(\alpha_i,\beta_i)$. Their lines of intersection with the α-β plane are approximations to the curves $f(\alpha,\beta)=0$ and $g(\alpha,\beta) = 0$; the point of intersection of the lines is thus an improved approximation to the solution. The process is iterative, each new pair of values (α,β) replacing the previous (α_3,β_3) to generate a fresh approximation.

The program uses the input values of α and β for a ray as α_1 and β_1, and generates (α_2,β_2) and (α_3,β_3) as the other two vertices of an equilateral triangle in the α-β plane, with the side length specified as an input parameter. The iterations cease either when $|f(\alpha,\beta)|$ and $|g(\alpha,\beta)|$ are simultaneously less than a predetermined "convergence criterion", or when the number of iterations exceeds an allowed maximum.

5.3.2 Electron density model.

A subroutine, NHPR, which is based on a program written by A.W.V. Poole, is called at the beginning of the program. It calculates and stores the layer parameters of up to two electron density models at present, via the methods outlined in section 3.3. Another subroutine, PROFILE, is called by the integration subroutines to evaluate electron density, plasma frequency, and the ionospheric parameter X and its partial derivatives for use in equations (5.1) - (5.4).

Three versions of PROFILE are currently available, in which:

(i) electron density is a function only of height on each hop of a ray;

(ii) electron density varies with height and latitude as described in 3.5.1;

(iii) electron density varies with height and latitude as described in 3.5.2.

Different profiles or the same profile can be used on each hop of a ray with version (i).

5.3.3. The integration step size.

The choice of an integration step size for a set of differential equations depends to a certain extent on the requirements of the user. In general, the smaller the size, the more accurate is the process and the less prone to instabilities, whereas the larger the size, the less computer time is required. Ideally, the integration algorithm should determine and continuously modify its own step size, but this is very time consuming and really only necessary for highly unstable equations. Since the differential equations are reasonably stable and computer time is an important consideration in ray tracing, the step size is supplied by the user and was held constant throughout the tracing of a ray in the original version of the program.

Optimum step sizes were determined for the present work for a range of frequencies and take-off angles to the vertical (α), by tracing sets of rays with identical input data except for the step size, which was varied until a further decrease produced no further change in accuracy (as measured by the constancy of the co-ordinates of the endpoint and the delay time, to four significant figures). As a general rule, larger step sizes could be used for greater values of α and higher frequencies. It was also found that a considerable saving of computer time could be effected on long distance oblique rays, with little loss of accuracy, by further increasing the step size provided that a smaller step size was used to start the integration at the base of the ionosphere.

After consultation with P.D. Terry, the program was altered so that the step size can be increased by an empirical factor (20 for rays with $\alpha \lesssim 70°$) once the ray is more than 3 km into the ionosphere, but only if the difference between the predicted and corrected values of all the quantities being integrated is less than 1% of the corrected value.

5.3.4. Tilted dipole magnetic field.

The geomagnetic field model is set up at the beginning of the program by reading in the geographic latitude θ and longitude Φ of the magnetic north pole, and the equatorial electron gyrofrequency at the surface of the earth, f_{H0}. The program transforms the initial position co-ordinates of a ray into those of the geomagnetic system before starting the ray tracing, and transforms back to the geographic system whenever printed or graphical output is required.

5.3.5. Multi-hop propagation.

A feature of high frequency radio propagation is the ability of radio rays to travel between a transmitter and a receiver along paths involving intermediate reflections off the surface of the earth. Each earth to ionosphere to earth section of a ray path is termed a "hop". The program was adapted for multi-hop propagation by assuming that the ray undergoes specular reflection at the surface of the earth (Kelso, 1964, p.211). The user specifies the number of hops required.

5.4. Comparison with other ray tracing programs.

Detailed descriptions and listings of programs by Croft and Gregory (1963), Curtis (1972), and Jones and Stephenson (1975) were available. The principal features of these and of the Rhodes program (Terry and Lambert) can be seen in table 5.1, which is arranged roughly in order of increasing complexity.

Croft and Gregory used a method which is not "ray tracing" in the usual sense of the term. The program is fast, simple, and of limited applicability.

Curtis' program is less complicated than the Rhodes program, with the exception of the signal-loss calculation. Examples of electron density model subroutines are provided; provision is made for the inclusion of a sporadic E layer.

The program of Jones and Stephenson is very versatile. Several versions of the subroutines for the magnetic field model (including a spherical harmonic type), electron density profile, and collision frequency model are provided; subroutines for ionospheric tilts and irregularities are also included. Frequency shifts due to time variation of the ionosphere can be calculated.

With the exception of the homing feature, the Rhodes program is less sophisticated than that of Jones and Stephenson, but was entirely adequate for the present work. The main improvement which could be made to it would be to include a signal-loss calculation.

Table 5.1: Principal features of four ray tracing programs.

FEATURES \ AUTHORS	Croft and Gregory	Curtis	Terry and Lambert	Jones and Stephenson
Ray tracing method	Snell's Law in layers of constant electron density	Equations derived by program author from Fermat's Principle	Haselgrove's equations (section 5.2)	Haselgrove's equations plus Hamiltonian equation for time
Ray paths	2-D	2-D	3-D	3-D
Geomagnetic field	none	none	dipole	various
Number of hops	one	not more than five	any	any
Signal-loss calculation	none	electron collisions and spatial dispersion	none	electron collisions
Wave polarization calculation	no	no	no	yes
Homing feature	no	no	yes	no
Depature of ionosphere model from spherical stratification	tilts in plane of propatation	tilts in plane of propagation	latitude dependence	various

CHAPTER 6

VERTICAL AND SHORT DISTANCE RAY TRACING

6.1. Introduction.

The results of early work with the ray tracing program are presented in this chapter. The data consisted of vertical ionograms from Grahamstown (33,290°S; 26,527°E) and short distance oblique ionograms transmitted at Alice (32,875°S; 26,864°E) and received at Grahamstown. General features of the ionograms are discussed in 6.2.

Since the ray tracing program calculates the virtual height or path of a ray, ionograms can be synthesized from values obtained for a range of frequencies. The program had been adapted to use multisegment electron density profiles calculated from vertical ionograms, and one of the aims was to determine how effectively ray tracing through these profiles could reproduce the original ionograms. Also of interest was how closely synthesized oblique ionograms agreed with experimental ones, and what data was required for optimum agreement. Synthesized and experimental ionograms are compared in 6.3. Vertical and oblique incidence ray paths are discussed in 6.4 and interpreted in terms of the electron density profile and the geomagnetic field.

In the initial stages of the project, the untilted dipole model of the geomagnetic field was the only one programmed. Some improved results, obtained subsequently by using the tilted dipole equivalent to the actual geomagnetic field at Grahamstown, are also included in this chapter.

6.2. The data.

Vertical ionograms recorded during the day at Grahamstown usually show a broad maximum in virtual height at the F1 layer critical frequency; the E region may, in some cases, be split into E1 and E2 layers, which is indicated by two sharp maxima closely spaced in frequency (Al'pert, 1963, p.23).

Table 6.1: Critical frequencies of experimental and synthesized ionograms.

Identification	Critical frequencies (MHz)	Experimental ionogram (MHz)	Synthesized ionogram (MHz)	
10:00 SAST (vertical)	f_oE1	3,00 ± 0,02	3,00 ± 0,20	
	f_oE2	3,20 ± 0,02	3,25 ± 0,05	
	f_oF1	4,20 ± 0,02	4,20 ± 0,05	
	f_oF2	6,70 ± 0,05	6,70 ± 0,00	
	f_xF1	4,70 ± 0,02	4,80 ± 0,05	tilted 4,70
	f_xF2	7,15 ± 0,05	7,25 ± 0,02	tilted 7,05
			10:00	10:05
10:05 SAST (oblique)	f_oE	3,00 ± 0,02	3,05 ± 0,02	3,05 ± 0,02
	f_oF2	6,70 ± 0,10	> 6,50	6,70 ± 0,10
	f_xF2	7,10 ± 0,05	> 7,10	> 7,10
10:15 SAST (vertical)	f_oE1	3,00 ± 0,02	3,00 ± 0,02	
	f_oE2	3,25 ± 0,02	3,30 ± 0,05	
	f_oF1	4,20 ± 0,02	4,20 ± 0,05	
	f_oF2	6,50 ± 0,05	6,50 ± 0,00	
	f_xF1	4,60 ± 0,02	4,80 ± 0,05	
	f_xF2	6,80 ± 0,10	7,05 ± 0,02	
			10:15	10:20
10:20 SAST (oblique)	f_oE1	3,05 ± 0,02	3,05 ± 0,02	3,10 ± 0,02
	f_oE2	3,25 ± 0,02	3,30 ± 0,02	3,35 ± 0,05
	f_oF1	4,20 ± 0,02	4,25 ± 0,02	4,30 ± 0,05
	f_oF2	6,40 ± 0,05	6,40 ± 0,10	6,40 ± 0,10
	f_xE	3,60 ± 0,02	3,90 ± 0,05	3,90 ± 0,05
	f_xF1	4,70 ± 0,02	4,80 ± 0,05	4,80 ± 0,05
	f_xF2	6,90 ± 0,05	7,00 ± 0,05	> 6,80

Oblique Alice - Grahamstown ionograms closely resemble vertical ionograms. They were recorded with ½P' (where P' is the virtual path) on the vertical axis, as the same format was used for both vertical and oblique ionograms. The ½P'(f) curves were single-valued on the records studied and, theoretically, the distance between the two stations, 64 km, is not sufficient to produce features such as a nose frequency (section 2.7.3).

Two vertical ionograms and the immediately following oblique ionograms, which satisfied most of the criteria of table 3.1, were selected from the Grahamstown records. They are represented by solid curves in figures 6.1 - 6.4. The uncertainty in virtual height h' or ½P' due to the thickness of the traces was 5 - 10 km.

6.3. Comparison of experimental and synthesized ionograms.

Standard terminology, f_{mode}REGION, is used for critical frequencies in the following sections. Those of the experimental vertical and oblique ionograms, together with the corresponding values for synthesized ionograms obtained by tracing rays through various electron density or N(h) profiles, are listed in table 6.1. In the "experimental" column, the errors represent the uncertainty in reading the frequencies of maxima and asymptotes of the h'(f) curves. Those in the "synthesized" column arise because the ionograms are built up from discrete points. The convergence criterion, which was used in the homing feature of the program to direct the oblique rays to a specific destination, was 0,03° (section 5.3.1).

6.3.1. Vertical ionogram - 10:00 SAST.

The experimental ionograms are represented by solid curves, the synthesized ones by dotted curves, in figures 6.1B (ordinary) and 6.1C (extraordinary). The N(h) profile in figure 6.1A, which was used for the ray tracing, was obtained from the experimental ordinary ionogram.

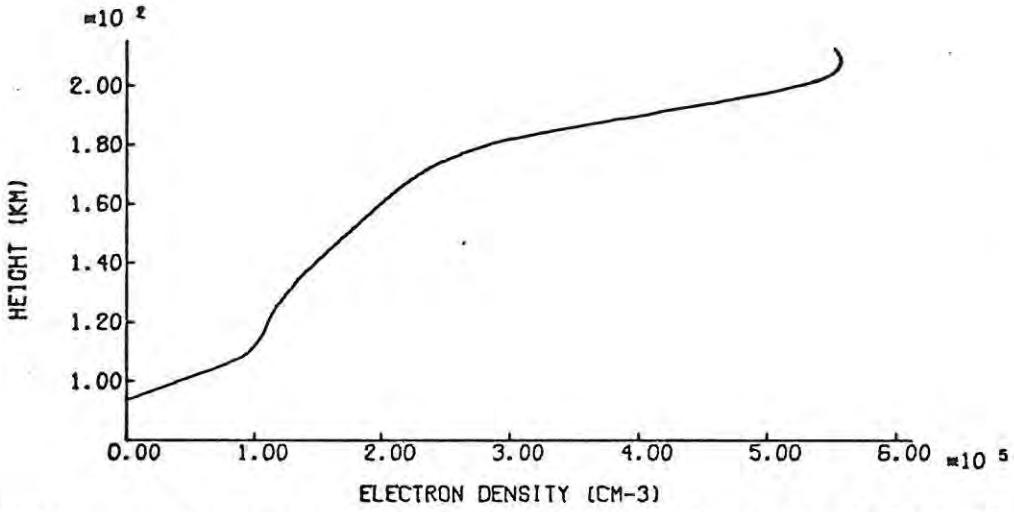

F 6.1A GRAHAMSTOWN N(h) PROFILE DAY 210 1974 10:00 SAST

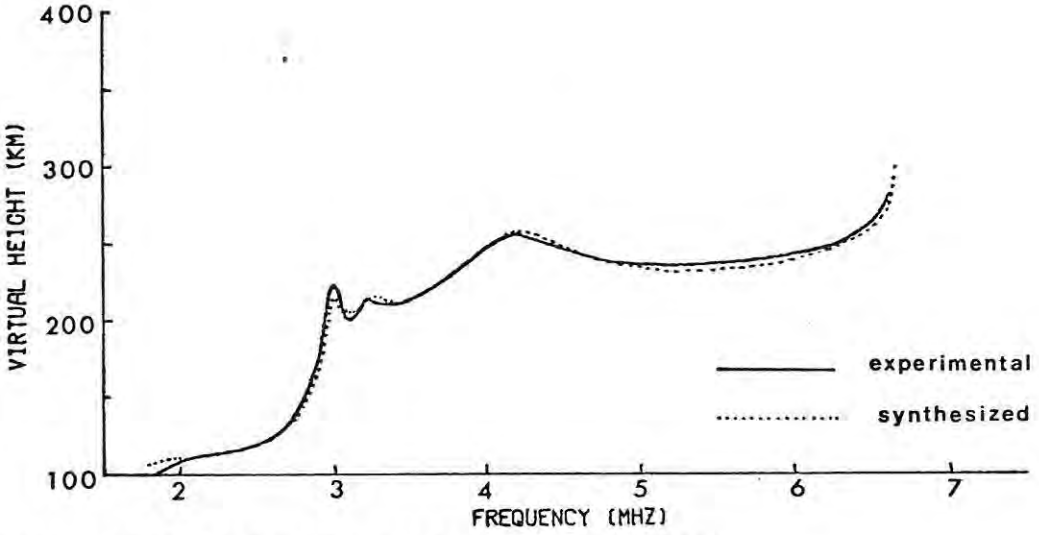

F 6.1B GTN. ORDINARY VERTICAL IONOGRAM

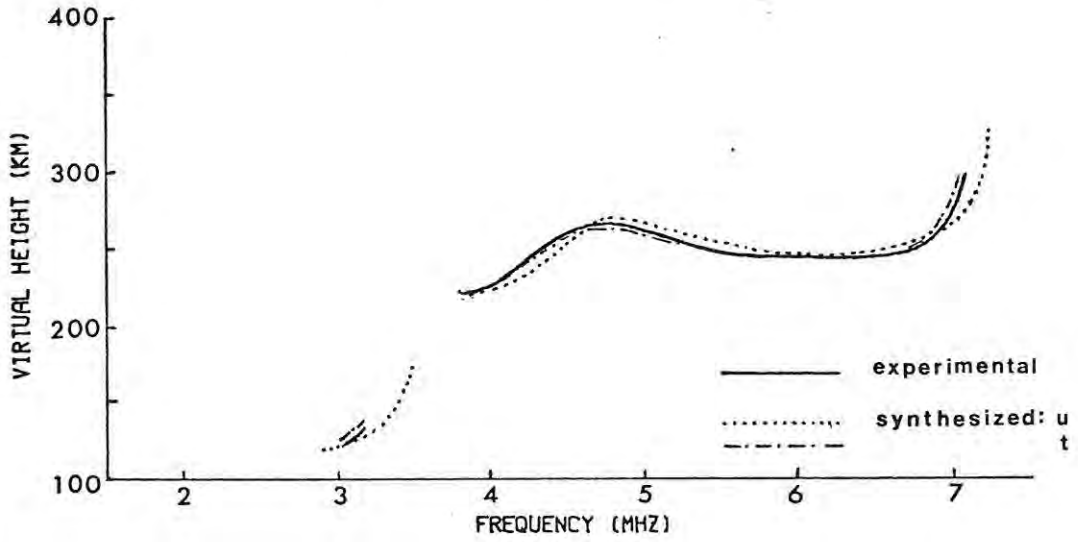

F 6.1C GTN. EXTRAORDINARY VERTICAL IONOGRAM

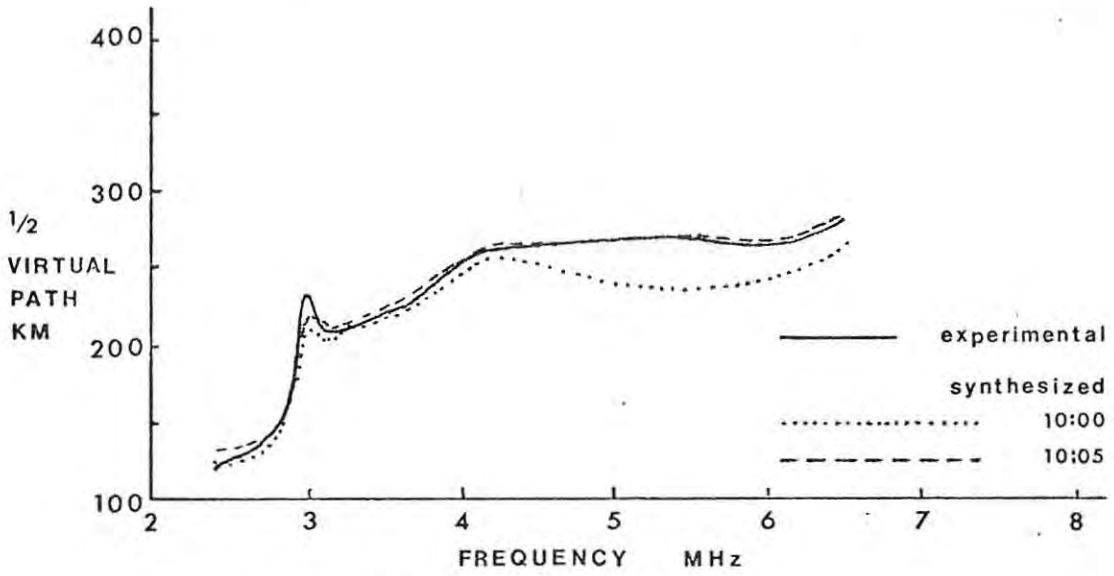

A ORDINARY

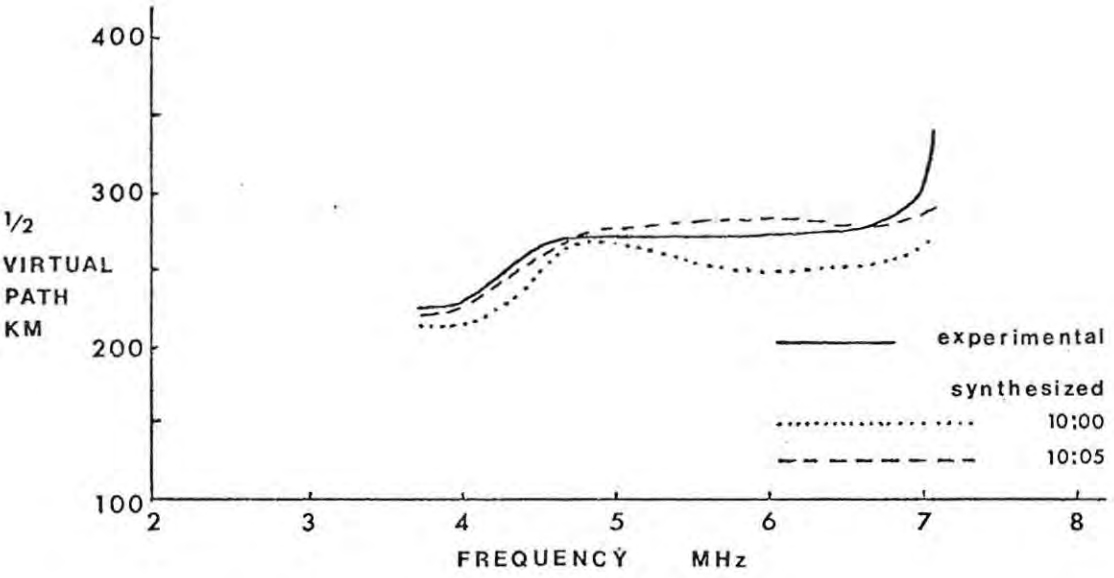

B EXTRAORDINARY

F 6.2 ALICE – GRAHAMSTOWN OBLIQUE IONOGRAM
DAY 210 1974 10:05 SAST

The ordinary critical frequencies are reproduced on the synthesized ionogram (the apparent shift in f_oE2 is probably due to broadening of the E peaks); the agreement in virtual height h' is good except at the low frequency end (section 3.4.1) and in the E region of figure 6.1B. The r.m.s. error in h' is 4 km. f_xF1 and f_xF2 are both shifted upwards on the synthesized ionogram of figure 6.1C, but the basic shape of the experimental curve is retained. No comparison of the E regions was attempted as this was blank on the experimental record. The r.m.s. error in h' is 9 km.

6.3.2. Oblique ionogram - 10:05 SAST.

The dotted ordinary and extraordinary ionograms in figures 6.2A and 6.2B were synthesized using the N(h) profile for 10:00 SAST (figure 6.1A). The fit in the F region is poor. The experimental ionograms, represented by the solid curves, level off to a nearly constant value of ½P' over a frequency range of approximately 1,5MHz, whereas the synthesized ionograms have clear F1 maxima. The E peak is lowered, and a spurious E2 peak is introduced, in figure 6.2A. From the shape of the synthesized extraordinary curve in figure 6.2B, it appears that f_xF2 is overestimated.

That the poor agreement in the F region is due to temporal changes in the N(h) profile between the recording of the vertical ionogram at 10:00 SAST and the oblique at 10:05 SAST, rather than the ray tracing process, is indicated by the improved agreement between the experimental (solid) ionograms and the dashed curves. The latter were obtained using a non-rigorously derived N(h) profile for 10:05 SAST. At the suggestion of Gledhill (1975), it was calculated from the experimental oblique ionogram of figure 6.2A by the methods of section 3.3, which strictly apply only to vertical incidence; because of the relatively short distance between Alice and Grahamstown, oblique rays, particularly

at higher frequencies, are assumed to be close enough to the vertical to make the approximation a reasonable one. In figure 6.2A f_oE1 for the dashed curve is high, and the low frequency end differs from that of the solid curve, but the high frequency fit is good. In figure 6.2B, it appears that f_xF2 of the dashed curve is high. The r.m.s. errors in ½P' are 7 km and 13 km for the ordinary and extraordinary ionograms respectively.

6.3.3. Vertical ionogram - 10:15 SAST.

As before, solid curves represent the experimental and dotted curves the synthesized ionograms in figures 6.3B and 6.3C. The N(h) profile of figure 6.3A, used for ray tracing,was derived from the experimental curve in figure 6.3B.

The critical frequencies of the ordinary ionograms match, and except in the E1, E2 and lower F2 regions, the agreement in virtual height is good; the r.m.s. error is 8km. f_xF1 and f_xF2 are shifted upwards, and the r.m.s. error in h' is 12 km on the extraordinary curves.

6.3.4. Oblique ionogram - 10:20 SAST.

The dotted ionograms in figures 6.4A and 6.4B, synthesized with the N(h) profile for 10:15 SAST (figure 6.3A), agree reasonably with the experimental (solid) ionograms. With the exception of f_oE1, the critical frequencies of the ordinary and extraordinary synthesized ionograms are slightly high ; the r.m.s. errors in ½P' are 13 km and 12 km respectively.

The dashed curves in figures 6.4. show ionograms synthesized with an approximate profile for 10:20 SAST, obtained as described in 6.3.2. All the critical frequencies are high. The r.m.s. error in ½P' is reduced to 10 km on the ordinary, but increased to 18 km on the extraordinary, ionograms. This is the same order of error as that obtained with the more rigorous 10:15 SAST profile, which indicates that the ionosphere could not have changed significantly during the 10-minute interval required for recording the vertical and

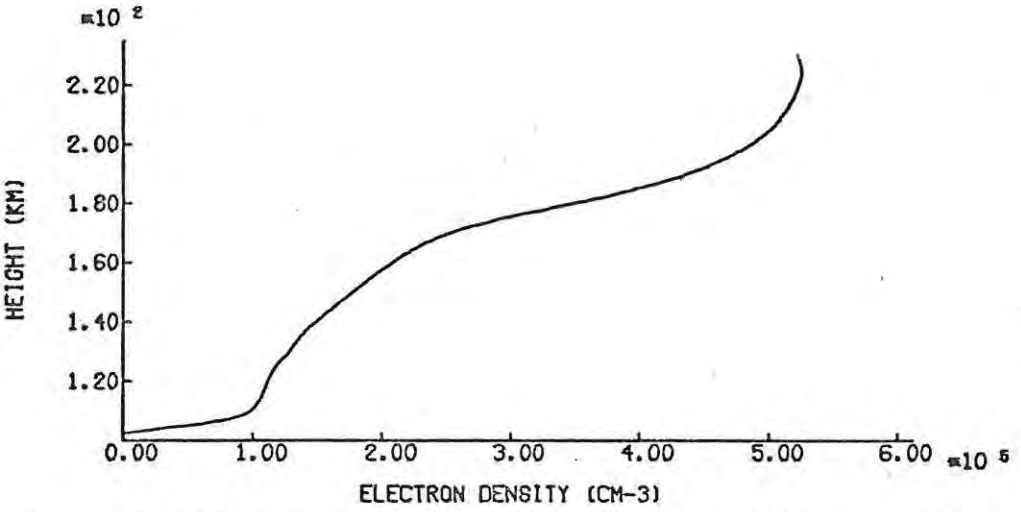

F 6.3A GRAHAMSTOWN N(h) PROFILE DAY 210 1974 10:15 SAST

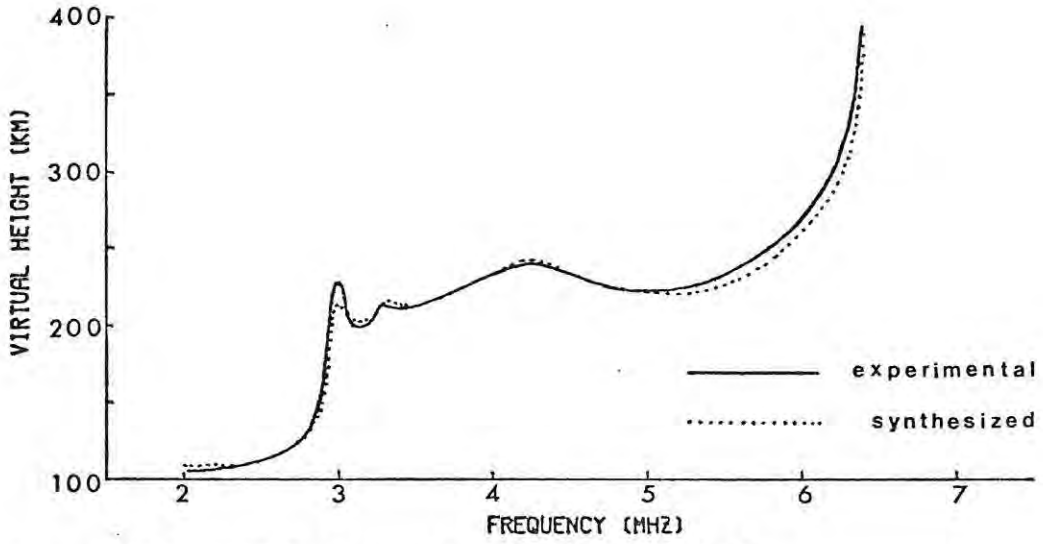

F 6.3B GTN. ORDINARY VERTICAL IONOGRAM

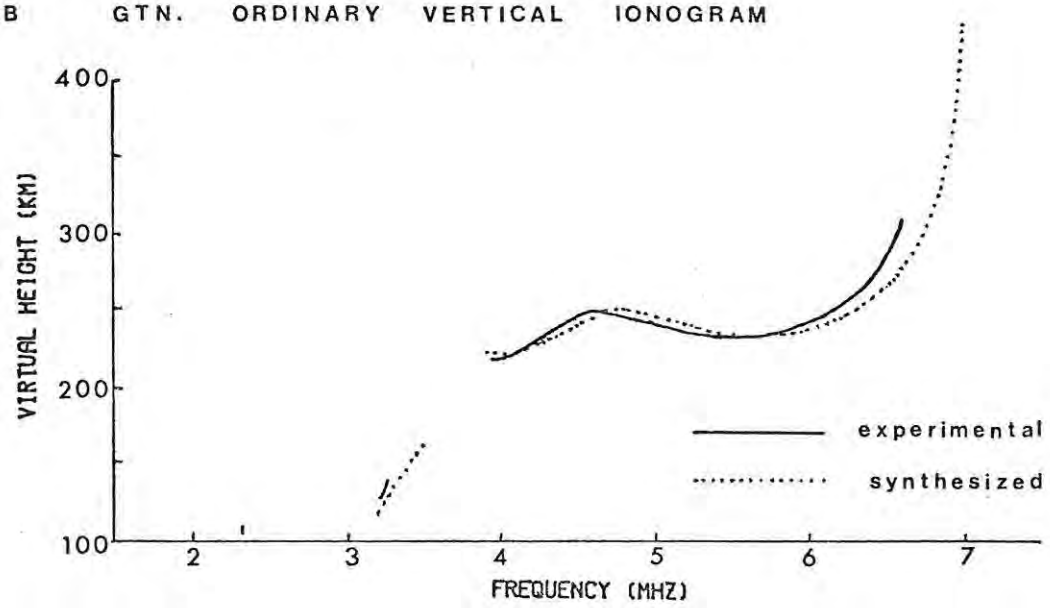

F 6.3C GTN. EXTRAORDINARY VERTICAL IONOGRAM

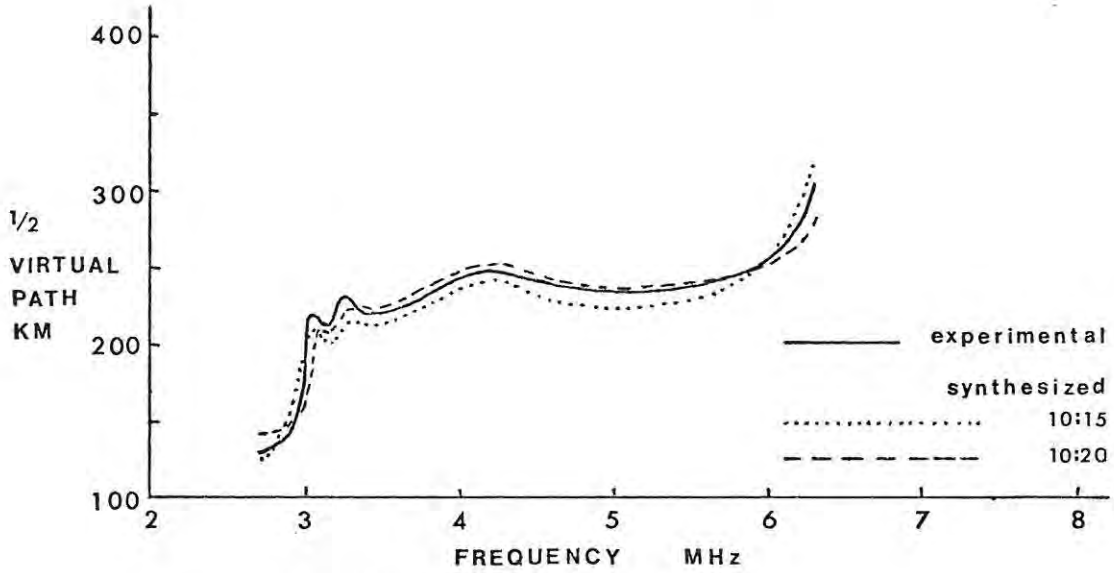

A ORDINARY

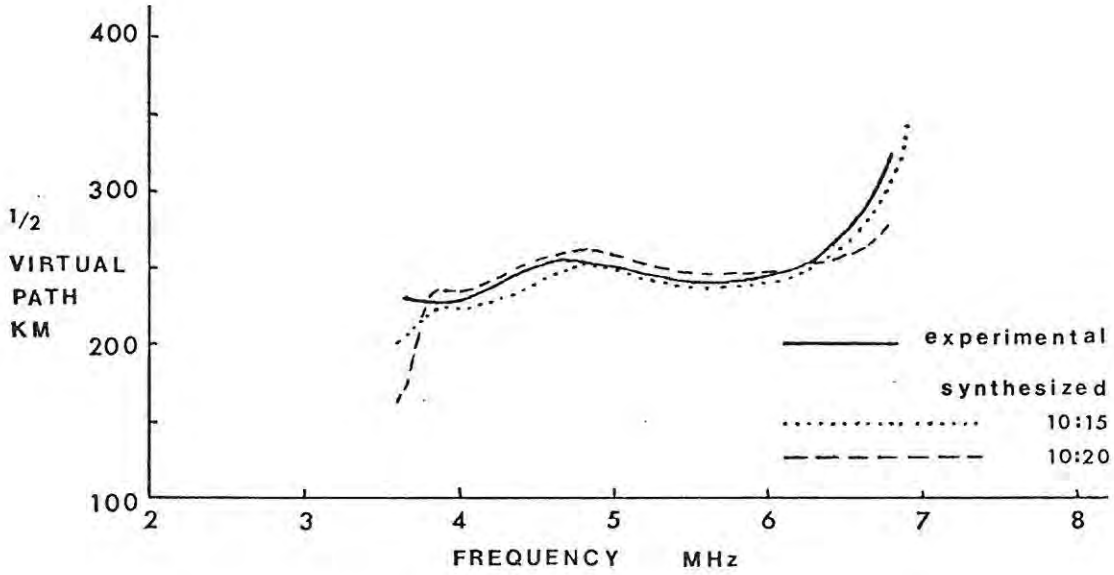

B EXTRAORDINARY

F 6.4 ALICE - GRAHAMSTOWN OBLIQUE IONOGRAM
DAY 210 1974 10:20 SAST

oblique ionograms.

6.3.5. Discussion and conclusions.

The results of 6.3.1 and 6.3.3 for vertical ionograms show that the synthesized ordinary ionograms agree quite well with the experimental traces, from which the N(h) profiles were derived. The discrepancies between the synthesized and experimental extraordinary ionograms can be explained in terms of the geomagnetic field model.

From (2.17), the approximate relationship between the vertical penetration frequencies is

$$\Delta f = f_x F_2 - f_o F_2 \simeq \tfrac{1}{2} f_H \qquad \ldots(6.1)$$

where f_H is the gyrofrequency at the height of maximum electron density. According to the untilted dipole model (section 4.3), $\tfrac{1}{2} f_H$ = 0,52MHz 200km above Grahamstown, and in both 6.3.1 and 6.3.2, Δf = 0,55 ±0,02MHz.

After the program had been suitably adjusted (section 5.3.4), rays at the frequencies used in synthesizing the ionograms of figures 6.1B and 6.1C were re-traced with the equivalent tilted dipole field for the vicinity of Grahamstown (section 4.3.2). The extraordinary ionogram synthesized in this way is shown by the chained curve (t = tilted dipole) in figure 6.1C; in figure 6.1B the ordinary curve is now indistinguishable from the experimental (solid) ionogram except at the lowest frequencies, where it coincides with the dotted curve. The r.m.s. errors in h' are reduced to 3 km on both the ordinary and extra-ordinary ionograms. The ordinary critical frequencies are unchanged, being independent of the magnetic field, but there is a noticeable improvement in the extraordinary ionogram and now Δf = 0,35 ± 0,02MHz. According to the equivalent dipole model, which has the same value of f_H = 0,82MHz at 0km at Grahamstown as that established by the Rhodes group, $\tfrac{1}{2} f_H$ = 0,37MHz at 200km.

In figure 6.1C, f_xF2 (chained) is actually less than the experimental value. A limited survey of Grahamstown vertical ionograms considered for use in this and the following chapter showed that the experimental frequency differences scatter about a mean, and that $\Delta f = 0{,}40 \pm 0{,}05$MHz. The author doubts whether better agreement between experimental and synthesized vertical ionograms could be obtained without taking into account measured values of the geomagnetic field obtained simultaneously with the ionograms.

Time did not allow all the work to be repeated, but it is expected that the trends described above would also apply to 6.3.2 - 6.3.4.

The oblique ionograms, allowing for the fact that the magnetic field model was only a moderately good approximation, were also quite accurately reproduced by ray tracing, provided that the correct N(h) profile was used - relatively minor changes in the E or F1 regions of the ionosphere, which probably would not affect the shape of an oblique ionogram with a greater transmitter-receiver separation, show up clearly on Alice - Grahamstown ionograms. Unless the oblique ionogram differs markedly from the preceding vertical one, it is probably best to use the N(h) profile rigorously derived from the vertical ionogram for oblique ray tracing.

The most significant difference between the oblique and vertical ionograms synthesized with identical N(h) profiles and geomagnetic field models (which would correspond to an experimental situation where oblique and vertical ionograms were received simultaneously) was that f_oE1, f_oE2, f_oF1, f_xE(probably) and f_xF1 were all about 0,5MHz higher on the oblique ionograms. f_oF2 and f_xF2 appeared to be the same, presumably because oblique rays reflecting near the height of maximum electron density are nearly vertically incident on the ionosphere (ray tracing showed that the angle of incidence, α, may be as little as 5°). These observations also explain why, when approximate profiles derived from oblique ordinary traces were used, critical

frequencies were shifted upwards even on the ordinary synthesized oblique ionograms.

6.4. Ray paths.

6.4.1. Vertical rays.

The paths of vertical rays from Grahamstown, at frequencies separated by 0,5MHz intervals, are plotted in figure 6.5. The N(h) profile was that of figure 6.1A, so the virtual heights of the rays correspond to points on the dotted ionograms of figures 6.1B and 6.1C. The base height and height of maximum electron density are 94km and 208km respectively for this model. On the scale of the figure, 1mm for 1km, the effects of the curvature of the earth are not noticeable.

According to program output, the longitude remains constant along the ray paths. Geographic and geomagnetic co-ordinates are identical with an untilted dipole field, and the ray paths are therefore shown to be confined to the plane of the magnetic meridian. As can be seen in figure 6.5, the ordinary rays, denoted O, are deflected south towards the nearer magnetic pole, and the extra-ordinary, or X, rays are deflected north towards the magnetic equator (section 2.5.2).

Ordinary rays reflect at greater heights than extra-ordinary rays at the same frequency. If $f_o(h)$ is the frequency of the ordinary ray which reflects at a certain height h, then, since the reflection condition is X = 1,

$$f_o(h) = f_N(h) \qquad \ldots (6.2)$$

where f_N is the plasma frequency, from (2.2), $f_N \propto N^{\frac{1}{2}}$. The reflection condition X = 1 - Y applies to the extraordinary mode at frequencies above the electron gyrofrequency f_H. It can be shown that the frequency $f_x(h)$ of the extraordinary ray reflecting at the same height is approximately given by

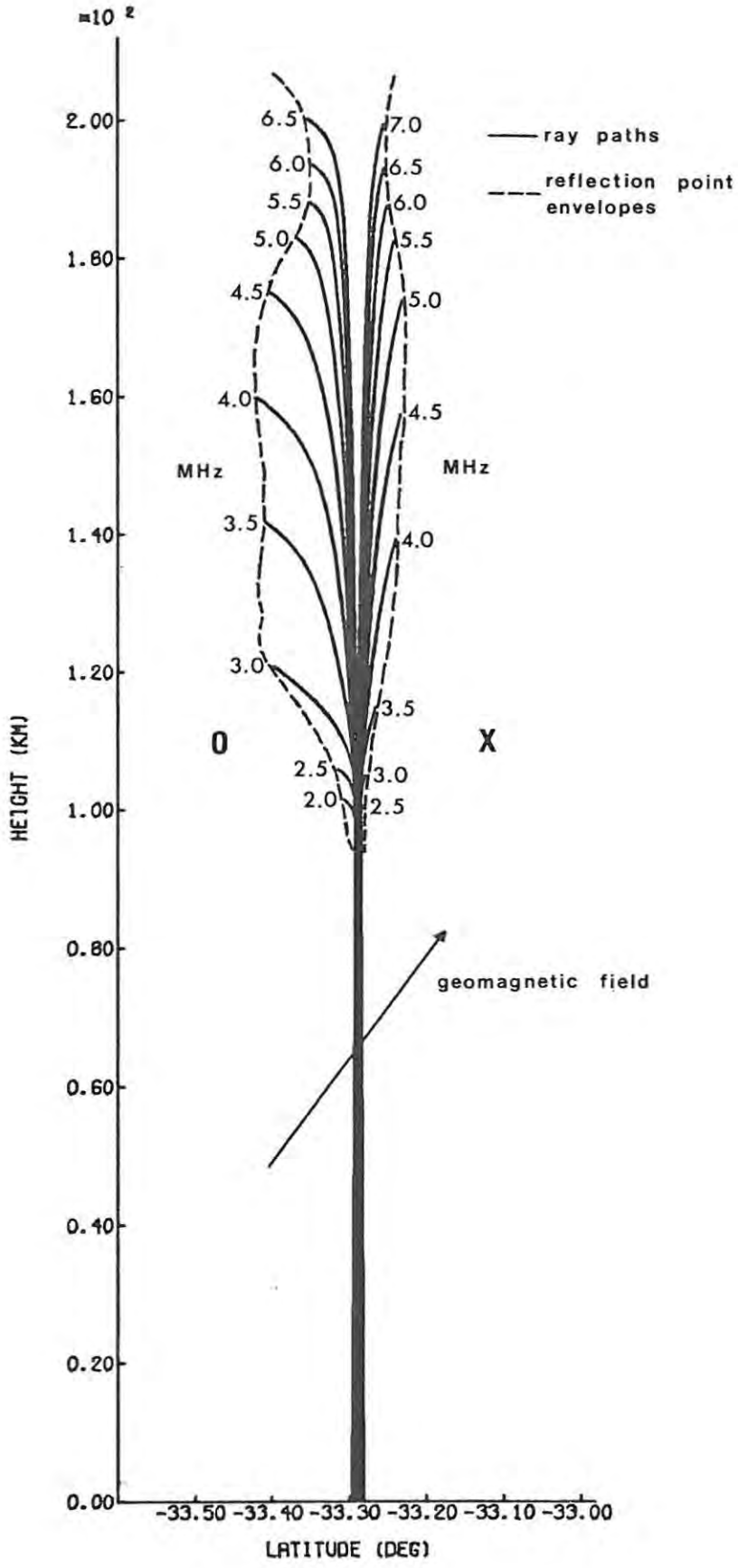

F 6.5 VERTICAL RAY PATHS AT GRAHAMSTOWN DAY 210 1974

$$f_x(h) \simeq f_N(h) + \tfrac{1}{2} f_H(h) \qquad \ldots(6.3)$$

when f_x, $f_N >> f_H$. Equations (6.2) and (6.3) explain why extraordinary rays in figure 6.5 reflect at about the same heights as ordinary rays 0,5MHz lower in frequency - according to the geomagnetic field model, $\frac{1}{2}f_H$ falls from 0,54 MHz at 100 km to 0,52MHz at 200 km.

It is convenient to define the lateral deviation of a ray vertically incident on the ionosphere as the horizontal distance between the reflection and transmission points. The lateral deviation of the ordinary rays is consistently greater than that of the extraordinary rays (section 2.5.2).

The magnetic dip at Grahamstown, independent of height because the field model is a dipole, is, according to the untilted model, -52,7° where the minus sign indicates that the field vector points above the horizontal. The ordinary rays in figure 6.5 appear to be perpendicular to the field at reflection; calculations using program output confirm this to an accuracy of 0,2°. The extraordinary rays are not parallel to the field at reflection but, according to calculations, are angled at about 20° to the vertical. From Budden (1961), p.247, it can be shown that the angle, ξ, between the vertical and the extraordinary ray direction at reflection (measured positive clockwise from the vertical axis) is given by

$$\xi = -\arctan\left\{\frac{\sin I \cos I}{(4\cos^2 I + \sin^4 I)^{\frac{1}{2}}}\right\} \qquad \ldots(6.4)$$

where I is the magnetic dip (sections 4.2, 4.3.2). According to the untilted model, ξ = 19,4°.

The dashed envelopes in figure 6.5 show the variation of reflection height and latitude with ray frequency for the two modes. They resemble the ionograms of figures 6.1B and 6.1C in that lateral deviation, like virtual height, has maxima at certain frequencies. These occur because the ray is most deviated from the direction of the wave

normal, which here is vertical, in regions where the plasma frequency is comparable with the ordinary ray or associated extraordinary ray frequency. Where $\frac{dN}{dh}$ is small, this is the case over a relatively large height range, and a correspondingly large lateral deviation results. The reflection points of ordinary rays in figure 6.5 are up to 15km, and those of extraordinary rays up to 7km, horizontally away from Grahamstown.

The paths of rays influenced by the actual geomagnetic field would be similar to those illustrated in figure 6.5. They remain in the plane of the magnetic meridian which is angled 24° west of the geographic meridian at Grahamstown. The electron gyrofrequency at 0km being 0,82MHz, extraordinary rays reflect at about the same height as ordinary rays 0,4MHz lower in frequency, which implies that they would actually reflect a few km higher than those shown in figure 6.5. The magnetic dip at Grahamstown is -65,6° and extraordinary rays, making an angle ξ= 18° to the vertical at reflection, would have slightly steeper paths as well. Ordinary rays, with ξ = -65,6° at reflection, would bend closer to the horizontal than those shown in figure 6.5.

The shape of the envelope of reflection points depends on the magnetic field in the vicinity of the transmitter and on the N(h) profile of the ionosphere overhead. The smaller the field strength, the less distorted are the refractive index surfaces from the spherical and hence the less are rays of both modes deviated from the vertical. With ordinary propagation, the greater $|I|$, the magnitude of the magnetic dip, the greater is $|\xi|$ and hence the lateral deviation (except in the case of longitudinal propagation). From equation (6.4), $|\xi|$ and hence the lateral deviation of the extraordinary rays attains a maximum at $|I| = 55°$. At Grahamstown f_H is less than, and $|I|$ greater than, the values predicted by the untilted model. The above factors reinforce in the case of the extraordinary and almost cancel with the ordinary rays - according to program output,

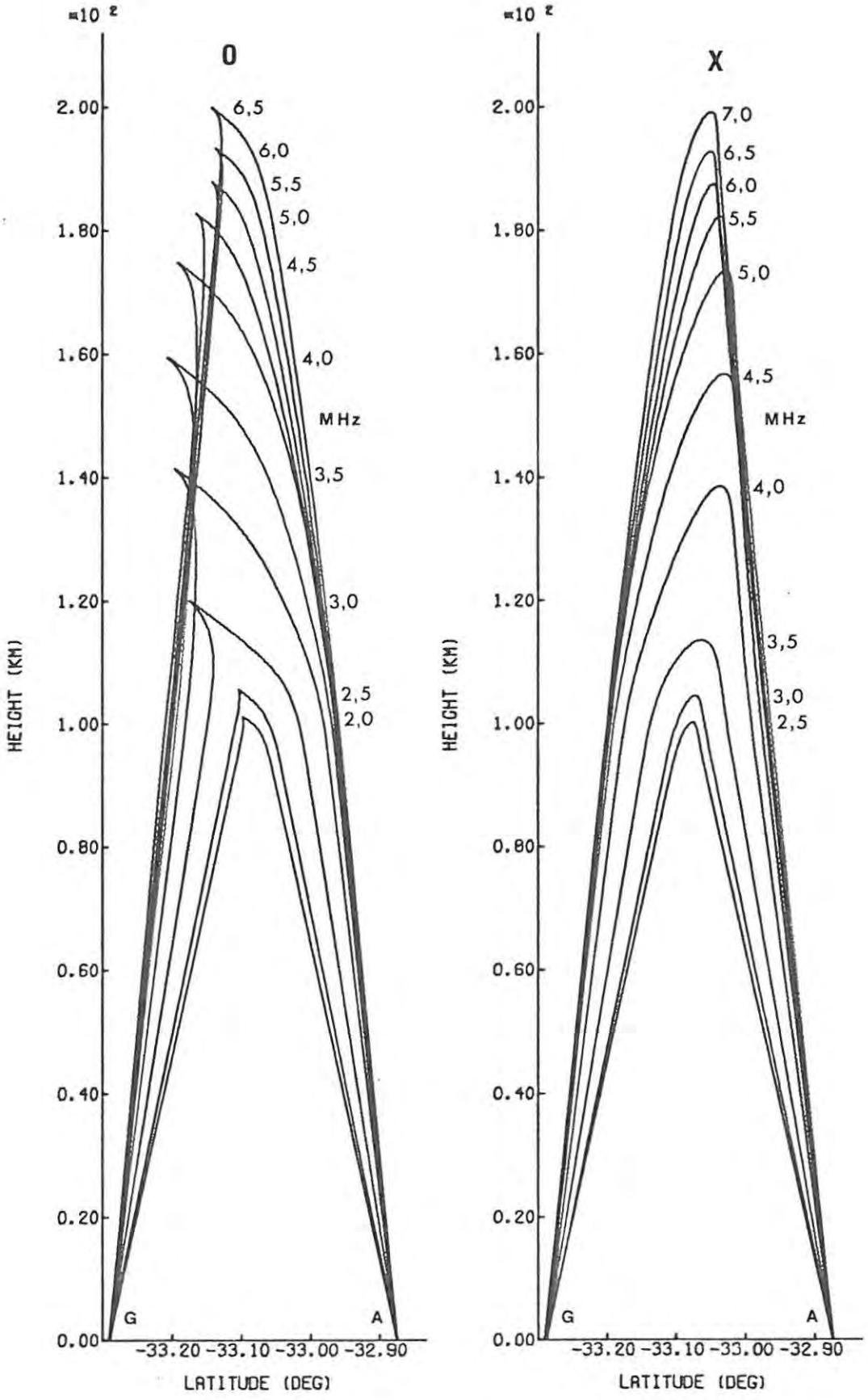

F 6.6 ALICE- GRAHAMSTOWN OBLIQUE RAY PATHS DAY 210 1974

rays re-traced with the equivalent tilted model and the same N(h) profile reflect up to 13km (ordinary) and 4 km (extraordinary) away from Grahamstown.

6.4.2. Oblique rays.

Height versus latitude graphs of oblique rays, traced through the same N(h) profile and at the same frequencies as those in figure 6.5, are plotted in figure 6.6. The ordinary (O) and extraordinary (X) rays are shown on separate axes for clarity. The scale is again 1mm for 1km. These graphs are the projections of three-dimensional figures on to the h-θ plane; since the geomagnetic field model is an untilted dipole, it is also the magnetic meridian plane.

Both sets of ray paths are asymmetric, with the ordinary rays reflecting south and the extraordinary rays north of the mean latitude for Grahamstown and Alice. In this projection it appears that the ordinary rays have sharp "spitzes". Decreased heights of reflection compared with those of vertical rays of the same mode and frequency, corresponding to reflection below the levels X = 1 and X = 1-Y (section 2.5.2), are discernible only on the extraordinary paths. The variation of the latitude at reflection with frequency is similar to, but less pronounced than, that indicated by the reflection point envelopes on the vertical graphs in figure 6.5.

Latitude versus longitude graphs, or ground plans, of selected ray paths are shown in figure 6.7 to a slightly expanded scale. The geographic convention of positive east has been used in the figure. The deflections of the reflection points northward and southward from the great circle through Grahamstown and Alice can clearly be seen. The oblique rays, at these and other frequencies, reflect along approximately the same (magnetic) longitude, to within 0,01° according to program output. The linear sections of the graphs are the projections of the ray

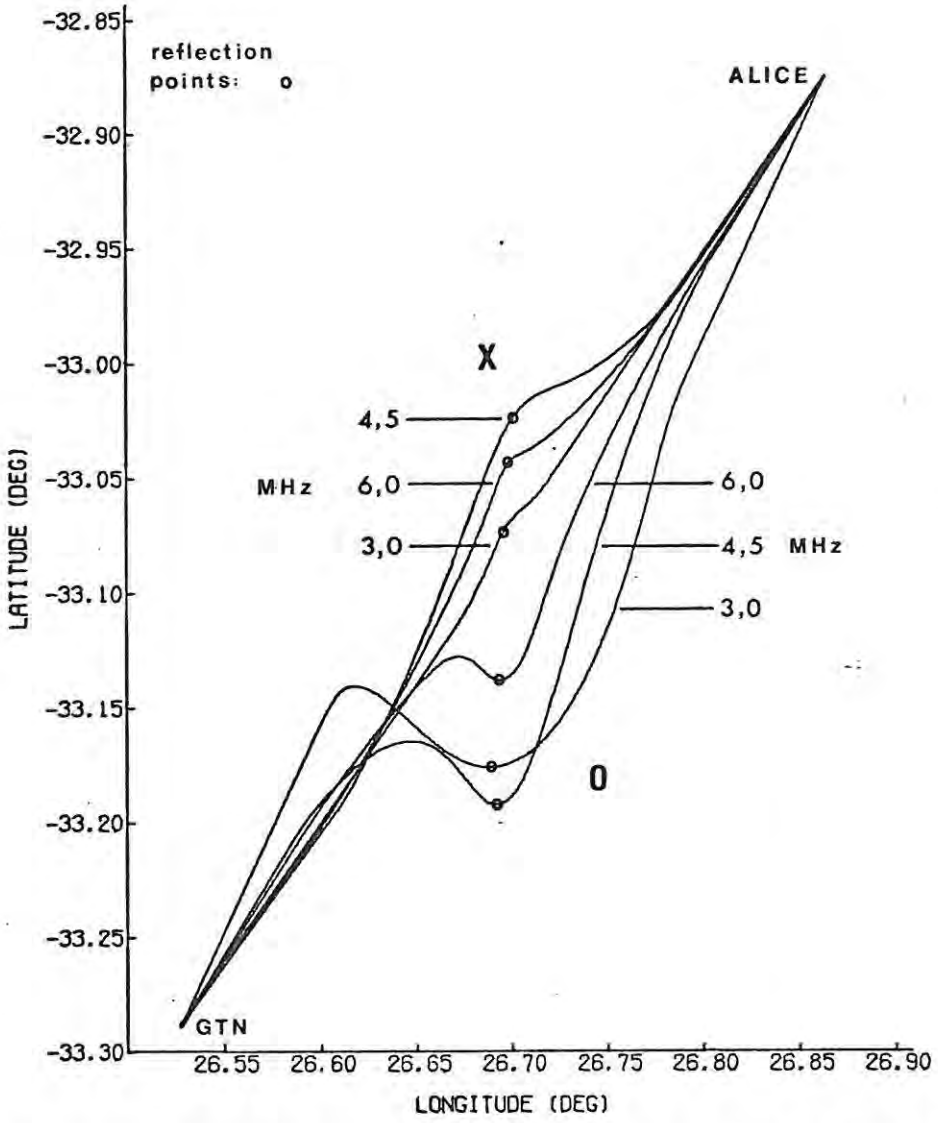

F 6.7 ALICE - GRAHAMSTOWN RAY PATH GROUND PLANS DAY 210 1974

paths in the region of free space below the ionosphere. The two linear sections for each ray are parallel, implying that the planes of incidence and of exit are parallel, to within 0,4°. All the extraordinary rays have very similar values of the take-off angle to the magnetic meridian, β . The ordinary rays are considerably more distorted from the no-field shape and their take-off angles β are frequency dependent.

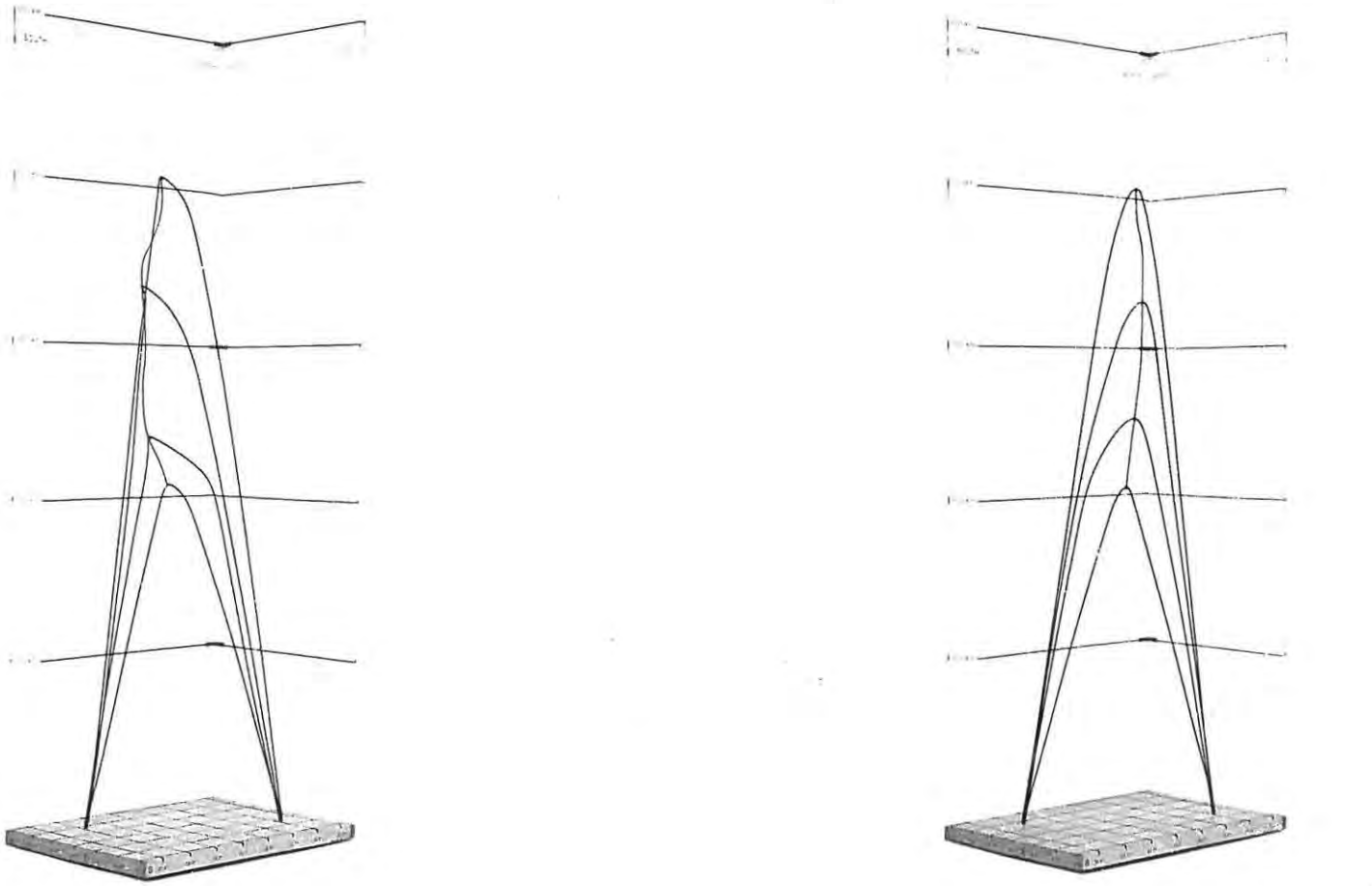

A ORDINARY B EXTRAORDINARY

F 6.8 3-D MODELS OF ALICE-GRAHAMSTOWN OBLIQUE RAY PATHS AND REFLECTION POINT ENVELOPES

The wire scale models of ray paths shown in the photographs, figures 6.8A and 6.8B,were constructed with the help of Mike Gaylard and members of the Physics Workshop staff. The base of the framework represents the earth's surface, flat because the curvature is negligible over the distances involved, with a grid of lines of latitude and longitude at 0,1° intervals. Heights on the vertical sides are marked out at 50km intervals. In the photographs Grahamstown is on the left. Rays which reflect fairly low in the ionosphere, and in the E, F1, and F2 regions,are represented - the frequencies are 2,5; 3,0; 4,2; 6,5 MHz and 3,0; 3,7; 4,7; 7,0 MHz for the ordinary and extraordinary models respectively. The twisted, three-dimensional nature of the oblique ray paths is clearly evident; as can be deduced by considering the projections of ordinary rays in figures 6.6 and 6.7, the ordinary rays are everywhere smooth curves which do become horizontal at reflection.

The paths of oblique rays in the presence of the actual geomagnetic field would be fundamentally similar to those discussed above. Reflection could be expected to take place along the same magnetic longitude, which implies that the reflection points for ordinary and extraordinary rays are respectively south-east and north-west of those shown in figure 6.7. On the basis of the discussion in 6.4.1, the extraordinary rays at the frequencies shown in figure 6.6 probably reflect at greater heights under the influence of the actual field.

6.4.3. Summary.

Ray paths, obtained by ray tracing with an untilted dipole model of the geomagnetic field, have been examined. Features of the paths have been related to properties of the ionosphere and geomagnetic field models, and deductions have been made about the paths of vertical rays at Grahamstown and short distance oblique rays between Alice and Grahamstown, in actual conditions.

CHAPTER 7

LONG DISTANCE RAY TRACING

7.1. Introduction.

Oblique ionograms transmitted from SANAE, Antarctica (70,309° S; 2,356° W) have been recorded at Grahamstown, South Africa (33,290° S; 26,527° E) since March, 1975. Ray tracing results indicate that the lowest mode of propagation is likely to be the two-hop mode (section 7.2).

Oblique ionograms synthesized by tracing rays through various ionosphere models are compared with selected experimental records in 7.3. The validity of the different models is discussed.

Some of the main features of actual oblique two-hop ray paths at frequencies recorded on the oblique ionograms are deduced in 7.4 from the paths of rays traced through the different ionosphere models.

7.2. Lowest mode of propagation.

Oblique SANAE-Grahamstown records frequently show several distinct traces of decreasing nose frequency and increasing mean virtual path in the region of the nose. These are caused by multi-hop propagation, each trace corresponding to rays making a certain number of hops from transmitter to receiver (section 5.3.5). The higher the number of hops, the greater is the virtual path and the smaller the nose frequency due to the shorter mean distance along the earth covered per hop (section 2.7.3).

By reducing simultaneous sets of multi-hop traces on oblique ionograms to equivalent vertical ionograms, assuming no magnetic field, and by finding the hop numbers which gave

self-consistent results, Rash and Poole (1975) inferred that the lowest mode of propagation on this transmission path was probably two-hop.

Ray tracing supports this conclusion. The greatest possible take-off angle α is 90° and the curvature of the earth results in three types of path for such rays, which leave the transmitter tangentially to the earth:

(i) the ray is reflected from the ionosphere back to a receiver on the earth;
(ii) above a certain frequency, the ray is reflected but only attains a perigee, not returning to the earth (this can also occur for angles $\alpha < 90°$ in certain cases);
(iii) at higher frequencies the ray penetrates the ionosphere.

With the ionosphere models described in 7.3, the maximum single hop propagation distance proved to be about 80% of the great circle distance between Grahamstown and SANAE, thus confirming that single hop propagation is unlikely under normal conditions.

Faint traces which could be due to the single hop mode have been observed on certain ionograms. A thick, highly ionized F region and a height of maximum electron density greater than 270km along most of the path might allow single hop propagation. It would be interesting to convert vertical ionograms corresponding to such oblique ionograms to electron density profiles.

Time did not permit any modes higher than the two-hop, or modes involving internal reflections in the ionosphere (Kelso, 1964, pp. 211-3; Davies 1965, pp. 182-3) to be studied.

7.3. Ionosphere models and oblique ionograms.

The aim of the project was to determine how accurately individual oblique ionograms could be reproduced, using available data, and thus to provide a basis for understanding their main features. In optimum cases, the data consisted of sets comprising a Grahamstown vertical ionogram, a SANAE vertical ionogram, and a SANAE-Grahamstown oblique ionogram (section 3.6), and the assumption was made that the ionosphere did not change significantly during the 10-minute period spanned by the recording of the ionograms. There are no other ionospheric stations in the South Atlantic near the great circle through SANAE and Grahamstown. Information about the ionosphere over this 4470 km transmission path could thus be found, in the form of electron density or N(h) profiles for specific places, only at the two endpoints.

A number of different ionosphere models was used. Oblique ionograms were first synthesized by tracing rays through spherically stratified models in which the ionosphere over the transmission path was represented by the Grahamstown or SANAE N(h) profiles. Next, the SANAE profile was used on the first and the Grahamstown profile on the second hop. Although,with this model, the profiles differed during the two hops, on each hop the ray was still being traced through a spherically stratified ionosphere. An "effective" N(h) profile, intended to represent conditions over the whole transmission path, was the next model. Finally two tilted, latitude dependent electron density models, for which the theory was developed in 3.5.1. and 3.5.2, were used.

The geomagnetic field model for all the work in this chapter was the tilted dipole model for the South Atlantic region (sections 4.3.2, 4.3.3).

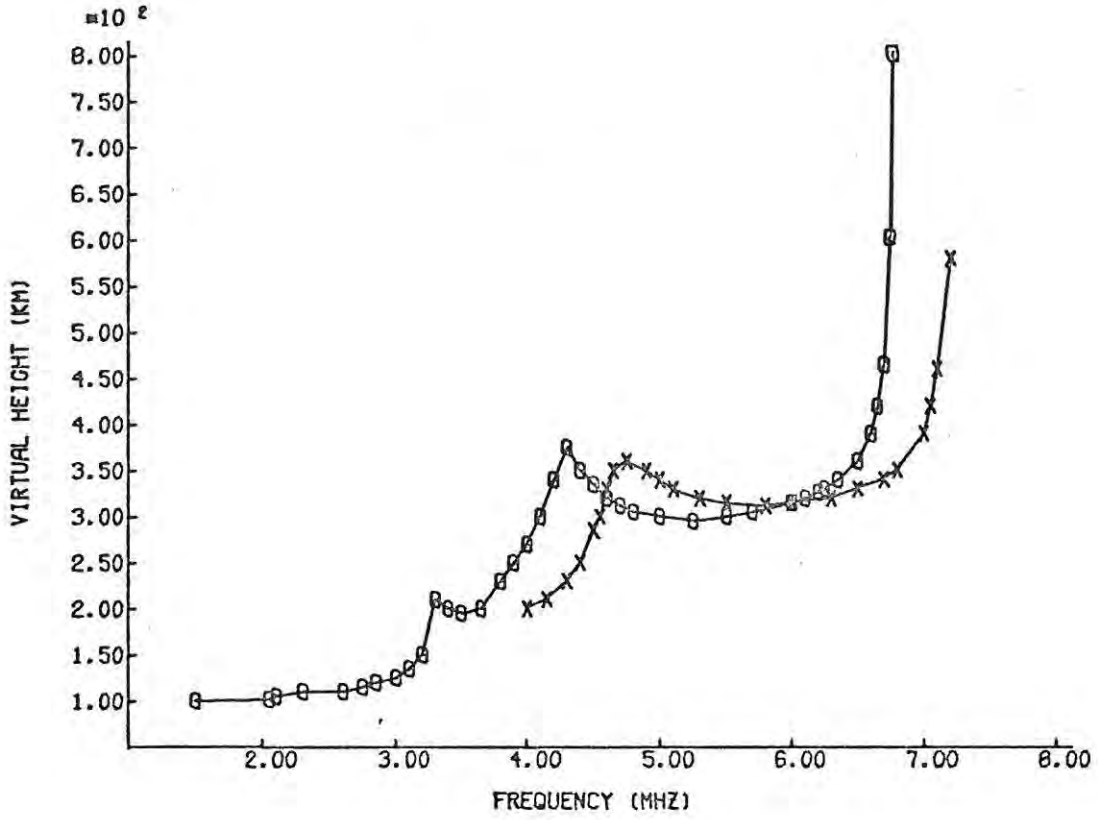

F 7.1A GRAHAMSTOWN VERTICAL IONOGRAM DAY 72 1975 14:00 SAST

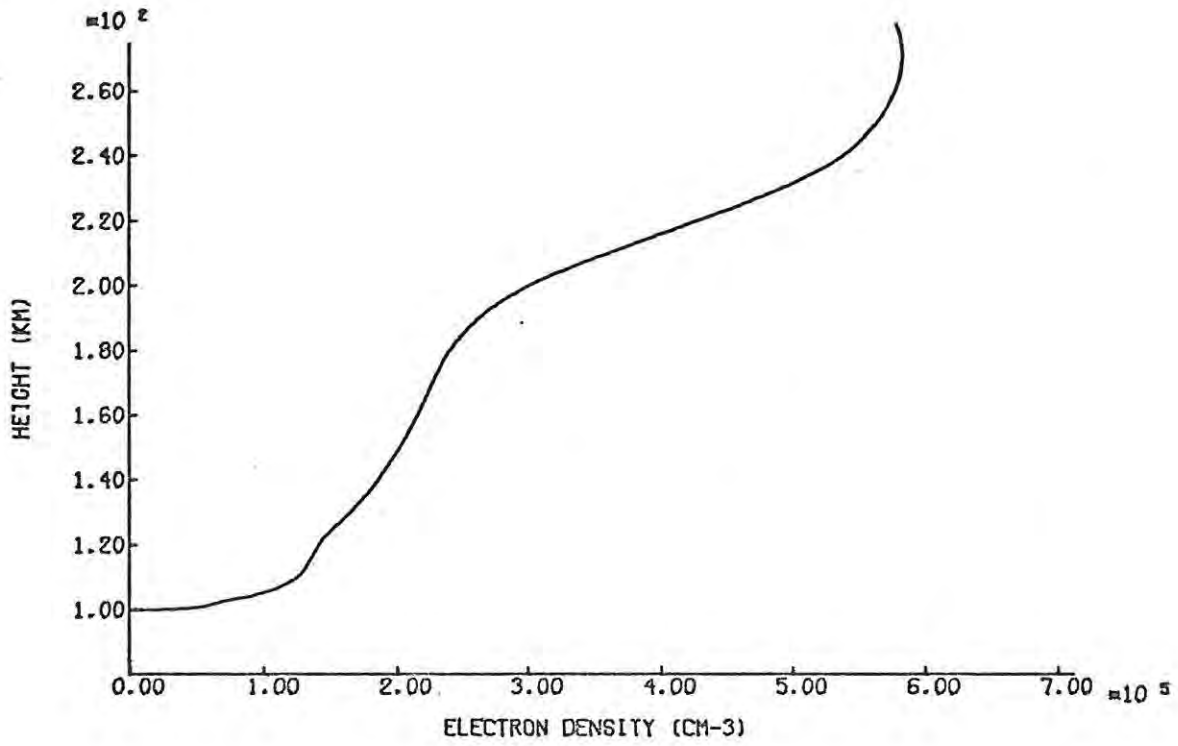

F 7.1B GRAHAMSTOWN N(h) PROFILE

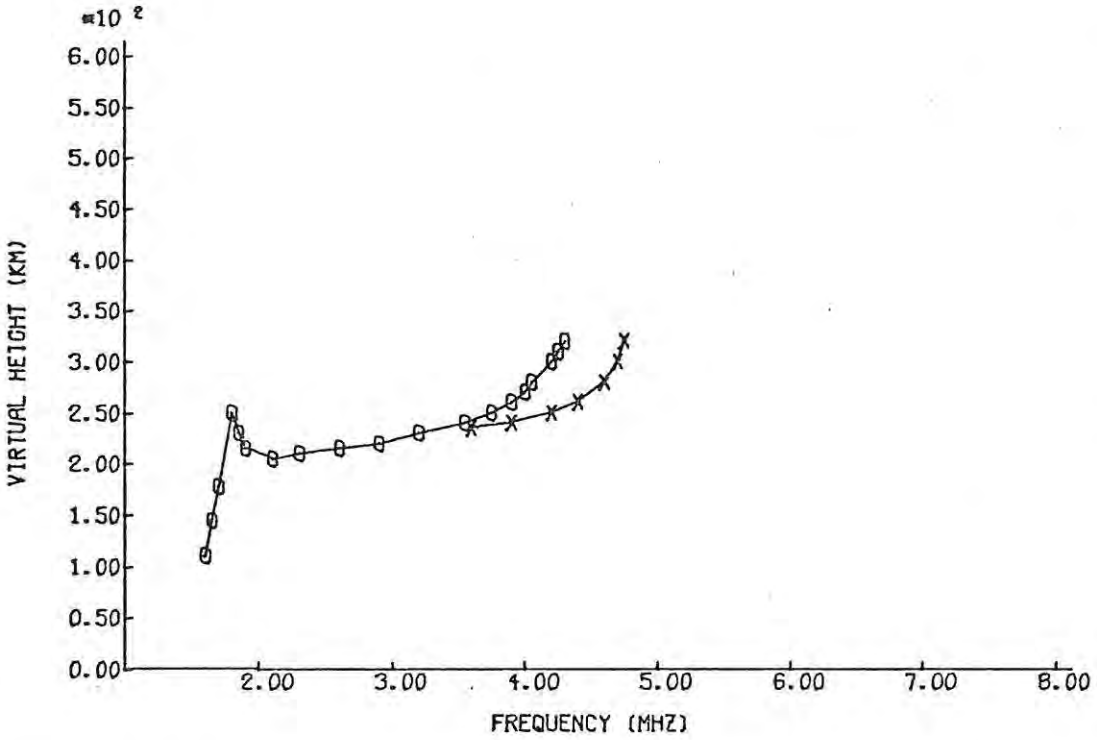

F 7.2A SANAE VERTICAL IONOGRAM DAY 232 1975 9:00 UT

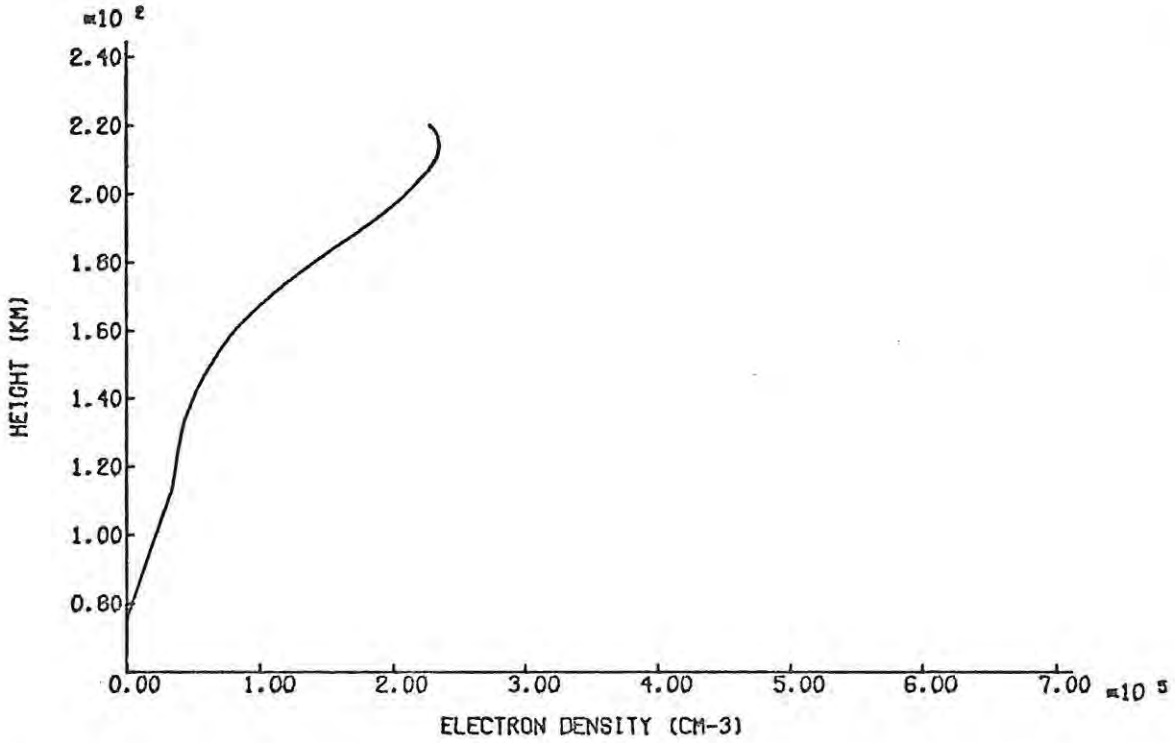

F 7.2B SANAE N(h) PROFILE

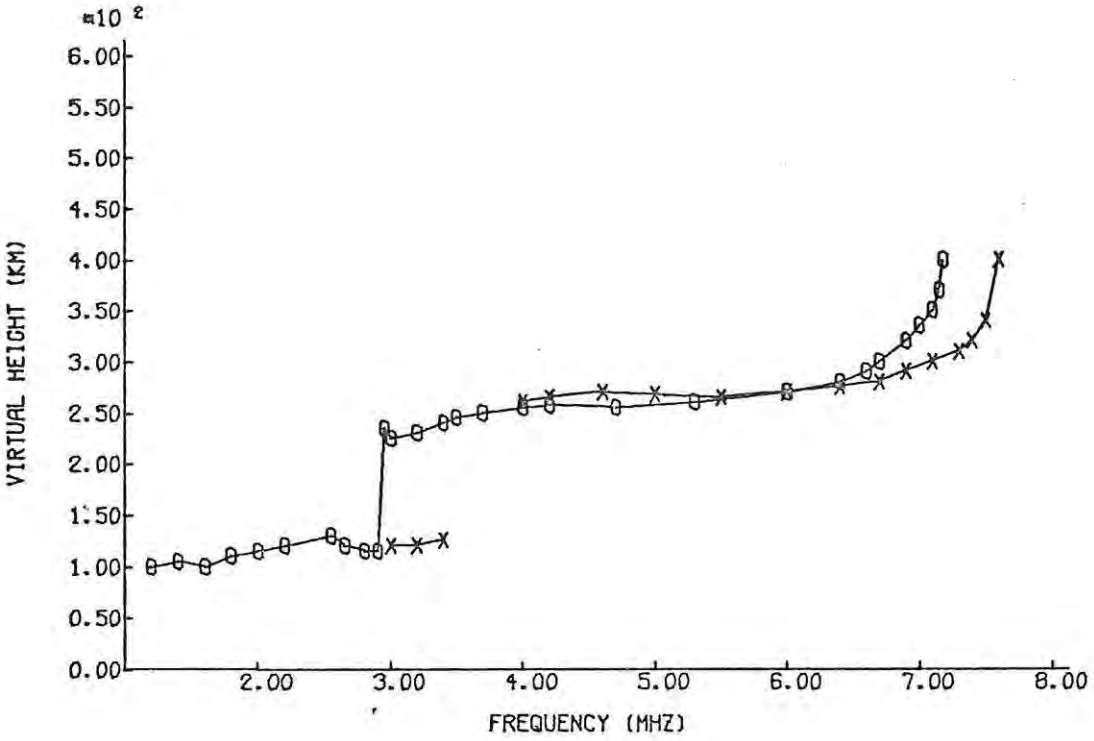

F 7.3A GRAHAMSTOWN VERTICAL IONOGRAM DAY 222 1975 15:45 SAST

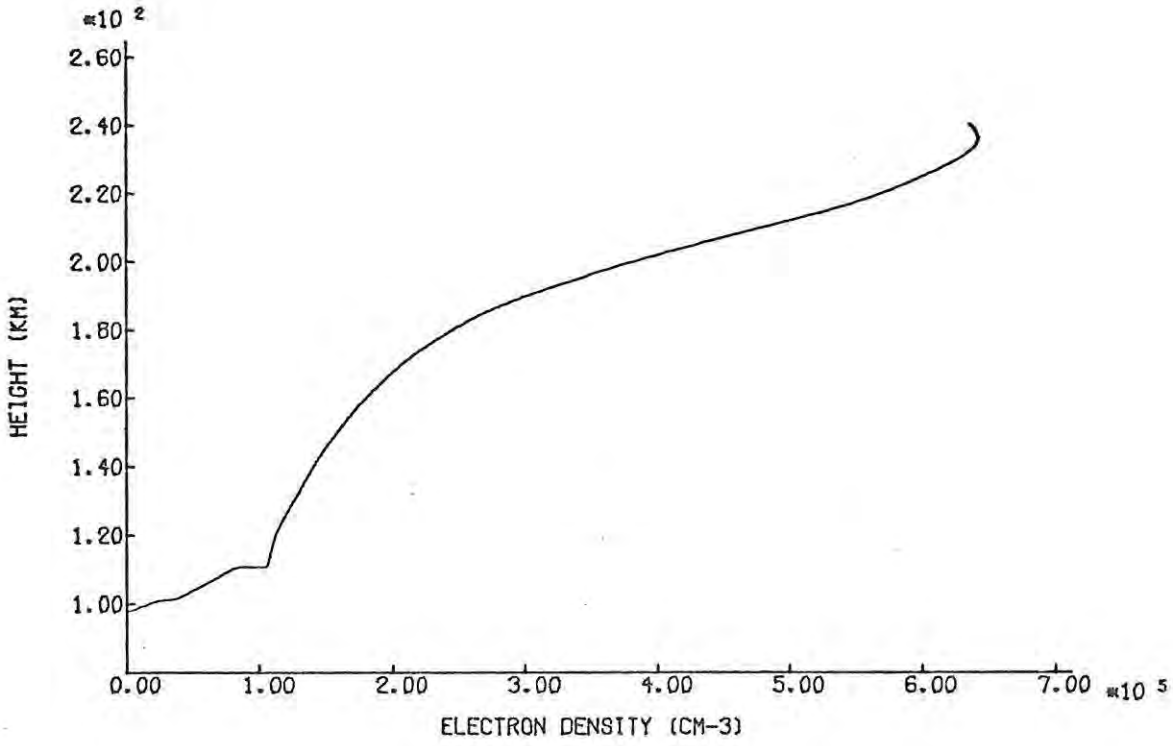

F 7.3B GRAHAMSTOWN N(h) PROFILE

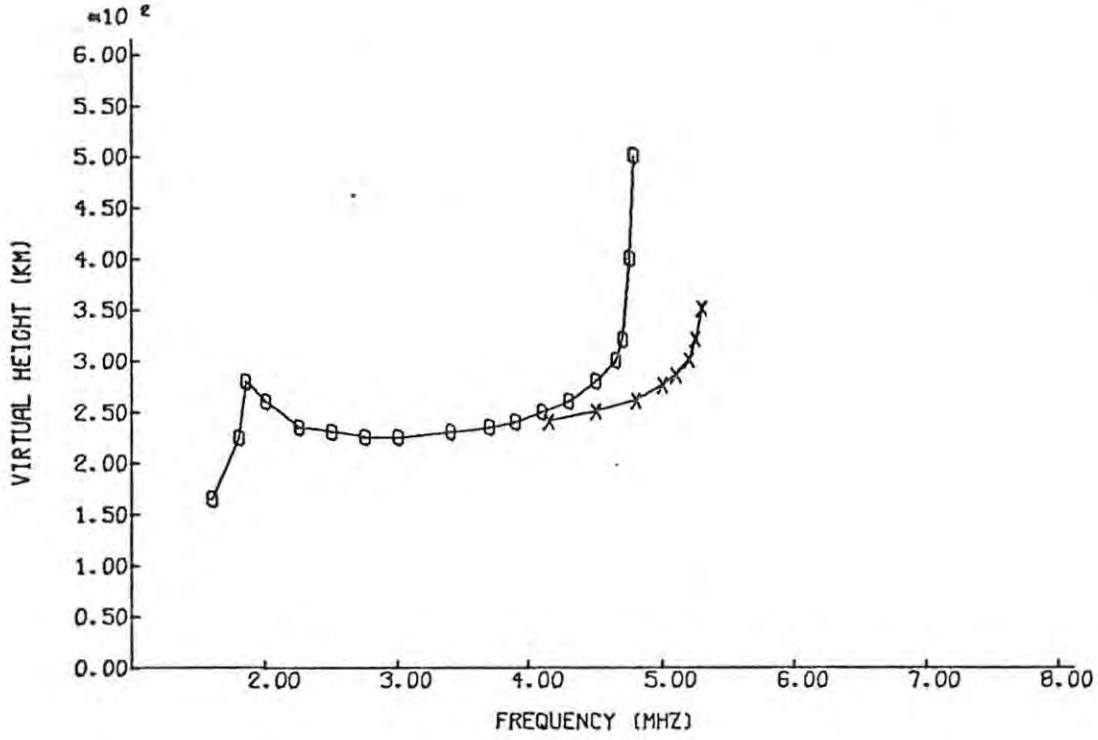

F 7.4A SANAE VERTICAL IONOGRAM DAY 222 1975 13:45 UT

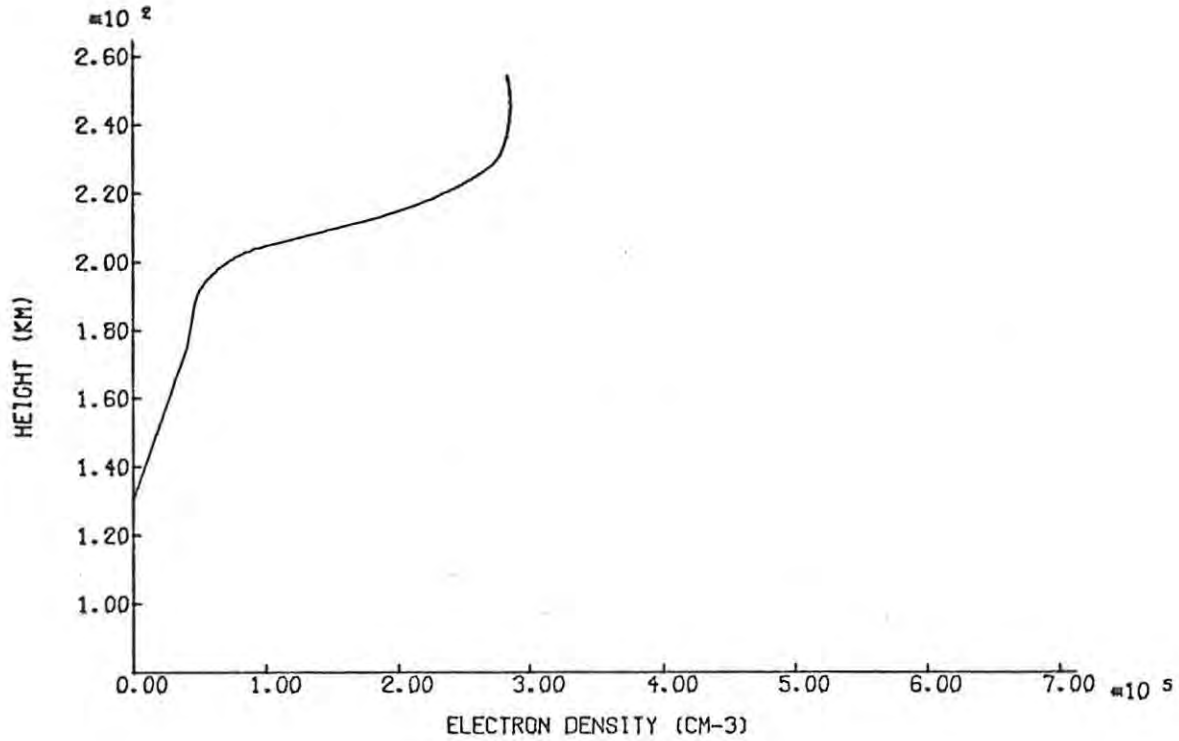

F 7.4B SANAE N(h) PROFILE

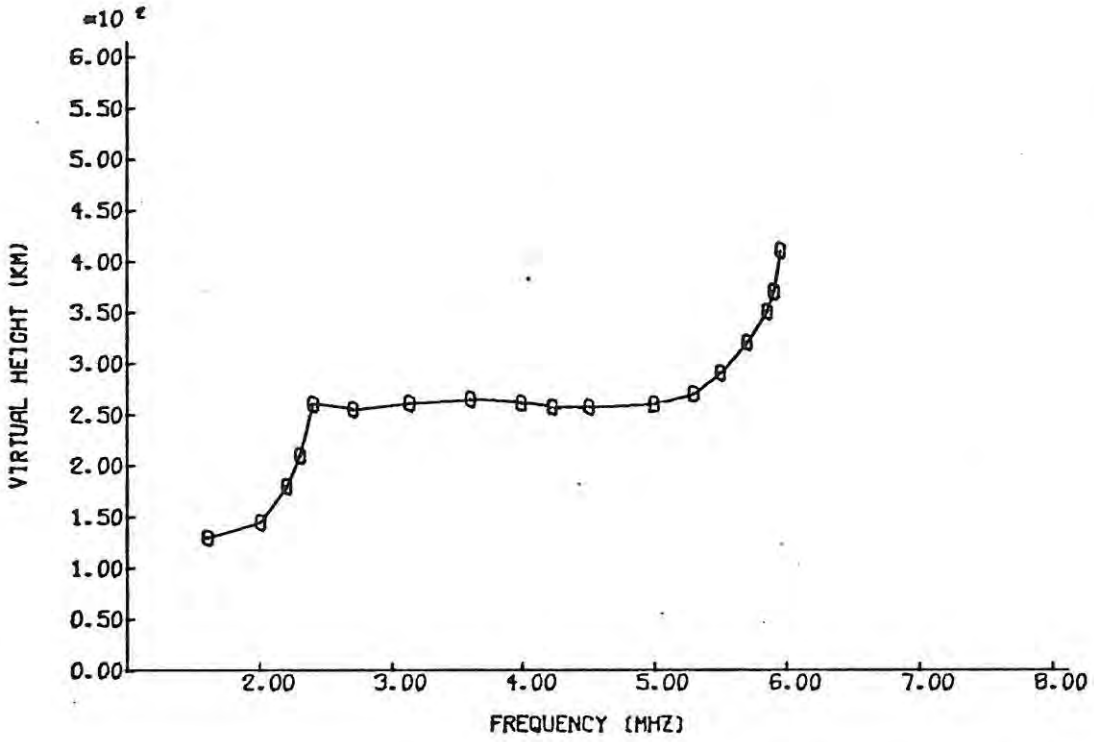

F 7.5A EQUIVALENT VERTICAL IONOGRAM DAY 222 1975 15:50 SAST

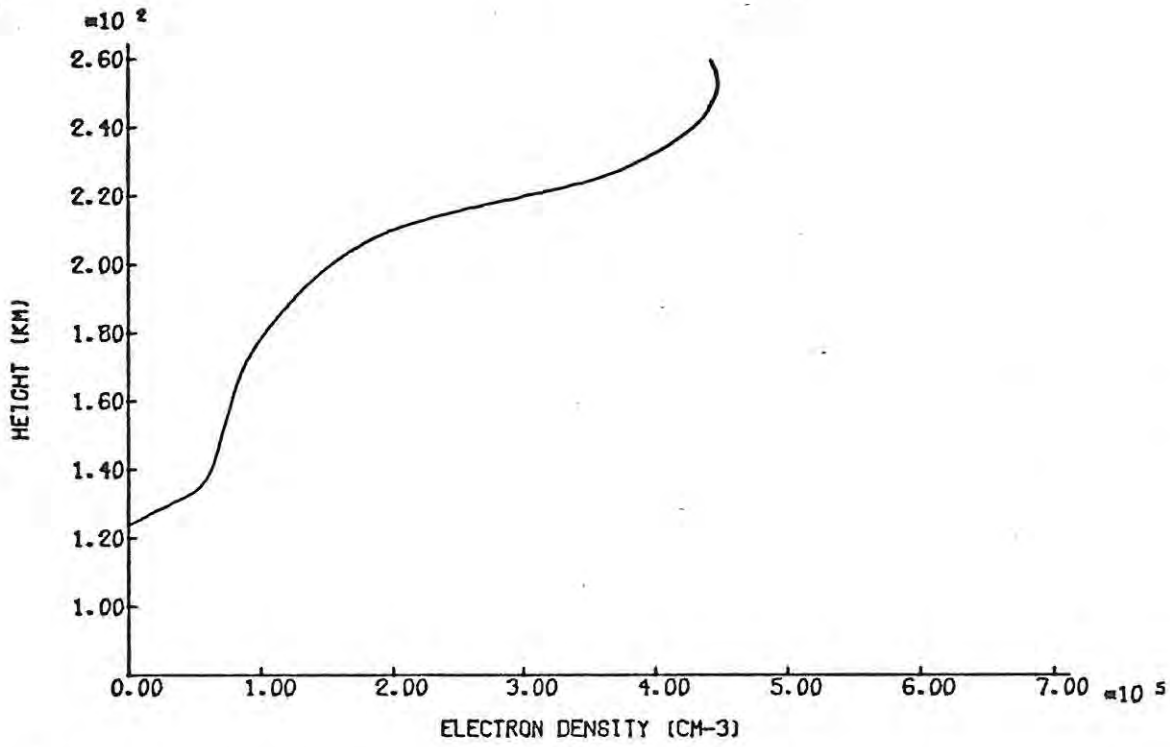

F 7.5B EFFECTIVE N(h) PROFILE MODEL

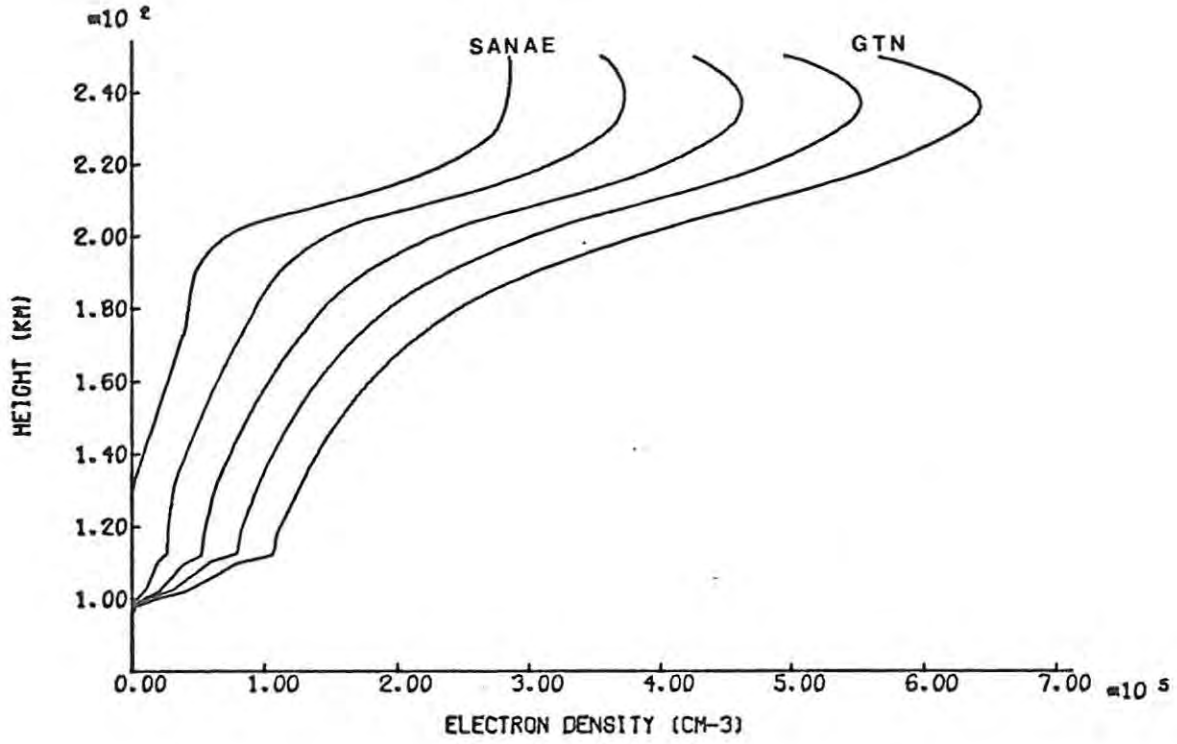

F 7.6 FIRST LATITUDE DEPENDENT MODEL

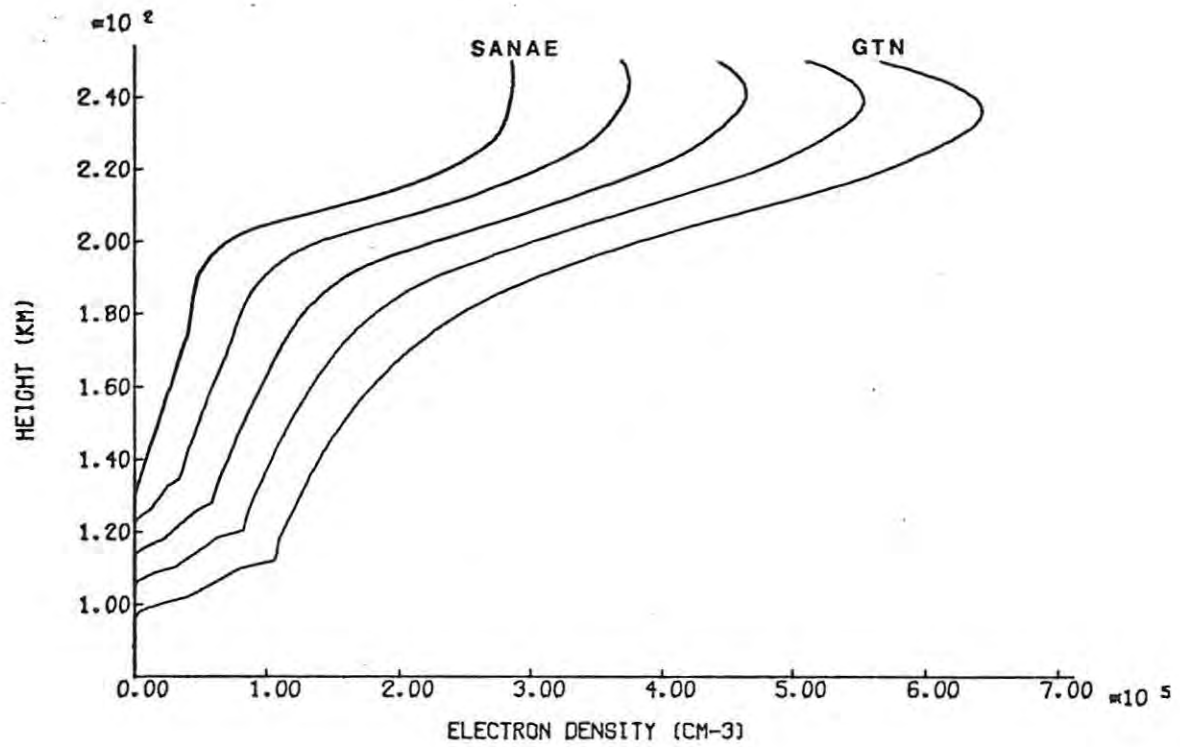

F 7.7 SECOND LATITUDE DEPENDENT MODEL

Some general points about the experimental oblique ionograms and the ray tracing are presented in 7.3.1. Ionograms synthesized using the different models are compared with experimental records in 7.3.2, and a discussion of the results follows in 7.3.3.

7.3.1. The oblique ionograms.

Experimentally recorded ionograms are represented by solid curves in figures 7.8 - 7.13. Higher modes (three-, four- and five-hop) which appeared on the ionograms of days 222 and 232 have not been included.

The finite thickness of the ionogram traces was typically 10km on nearly horizontal parts of the low ray curves and 20km on the high ray sections, with a width of 0,4MHz at the nose frequency. (These terms have been defined in section 2.7.3). No separation of ordinary and extra-ordinary traces was observable on these particular ionograms, and, except where otherwise indicated, only ordinary ionograms have been synthesized.

Virtual path P' on oblique ionograms recorded at Grahamstown is expressed with respect to an arbitrary origin. The true values of P' on an ionogram are obtained by adding a constant called the offset, for a particular date and time, to the recorded values, thus effectively translating the virtual path origin to its true position. The method by which the offsets are obtained has been described by Rash (1976).

Minimum frequencies for oblique ionograms near midday are usually between 10 MHz and 12 MHz. High ray sections of the ionograms are usually discernible only over a frequency range from 0,5 MHz to 3 MHz below the nose frequency, and not back to the vertical penetration frequency as predicted in section 2.7.3, figure 2.4A. This is probably due to strong absorption of the signal (Kelso, 1964, p.221).

Table 7.1: Comparison of features of synthesized and experimental oblique ionograms.

Model description	N_{max} ($\times 10^5$ cm^{-3})	f_{expt} (MHz)	f_{synth} (MHz)	Δf (MHz)	% error
a. GTN, day 72, 14:00 SAST	5,82	14,6	18,80	4,20	29
b. SAN, day 232, 9:00 UT	2,35	16,8	13,90	-2,90	17
c. GTN, day 222, 15:45 SAST	6,43	18,8	21,20	2,40	11
d. SAN, day 222, 13:45 UT	2,86	18,8	15,10	-3,70	20
e. Two-profile, c and d	-	18,8	15,45	-2,35	18
f. Effective profile, day 222, 15:50 SAST	4,47	18,8	18,00 o 18,25 x	-0,80 o -0,55 x	4,3 o 2,9 x
g. 1st Latitude dependent, c and d	-	18,8	18,07	-0,73	4,0
h. 2nd Latitude dependent, c and d	-	18,8	17,90	-0,90	4,8

A corresponding phenomenon was noticed with the ray tracing: there was a practical limit, dependent on the ionosphere model, to the frequency range below the nose frequency over which high rays could be traced. This is not connected with absorption, but is numerical in nature. The reason for it is not clearly understood. No lower limit on the low ray frequencies was found. In figures 7.8 - 7.10 lower frequencies have not been traced because the nose region was thought to be the most important and, ray tracing being very time consuming, it was decided rather to improve the ionosphere model than to continue work on an inadequate model.

The r.m.s. error in virtual path on the synthesized ionograms is approximately 10 - 15 km, due to over- or undershooting of Grahamstown and errors associated with the integration of equations (5.1) - (5.4).

7.3.2. Comparison of synthesized and experimental ionograms.

The maximum electron densities, N_{max}, of the various ionosphere models, the nose frequencies of experimental and synthesized ionograms, f_{expt} and f_{synth} respectively, the difference $\Delta f = f_{synth} - f_{expt}$, and this difference expressed as a percentage of the experimental nose frequency, are listed in table 7.1.

The Grahamstown profile models (a and c).

The results of two-hop ray tracing through Grahamstown electron density profiles, models a and c in table 7.1, are shown as chained curves in figures 7.8 and 7.10. The experimental oblique ionogram for day 72, 1975, 14:05 SAST of figure 7.8 was one of the first recorded that was also preceded by a good vertical ionogram. That for day 222, 1975, 15:50 SAST in figure 7.10 was selected later because good vertical ionograms for the

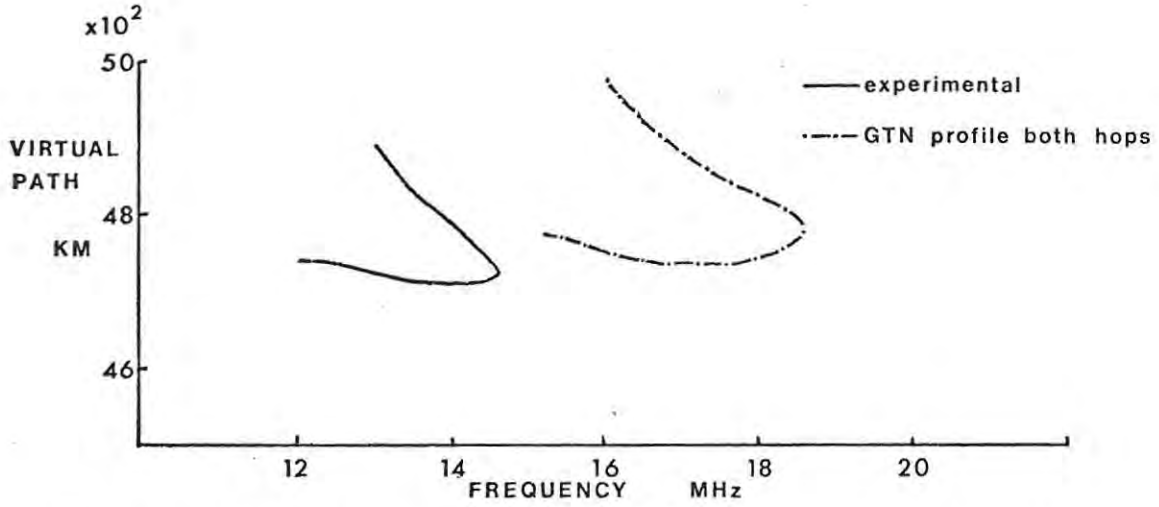

F 7.8 SANAE–GTN OBLIQUE IONOGRAM DAY 72 1975 14:05 SAST

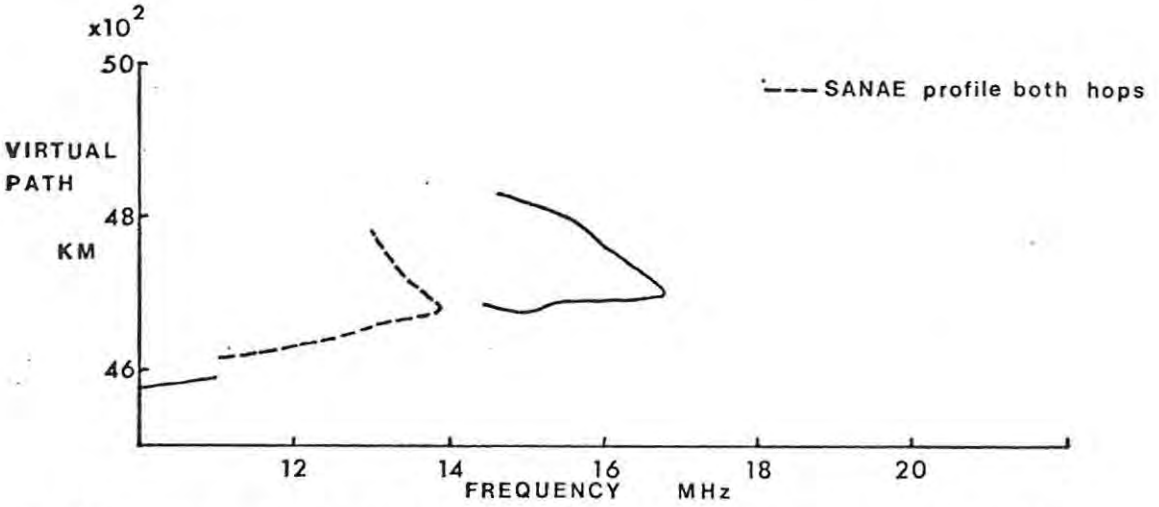

F 7.9 SANAE–GTN OBLIQUE IONOGRAM DAY 232 1975 11:05 SAST

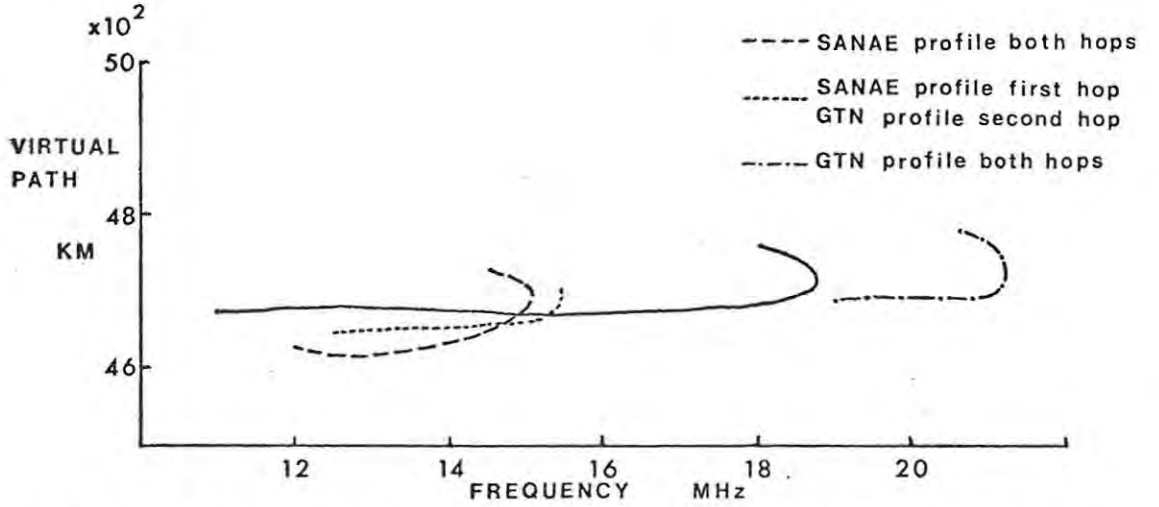

F 7.10 SANAE–GTN OBLIQUE IONOGRAM DAY 222 1975 15:50 SAST

same time existed for both Grahamstown and SANAE. These vertical ionograms and the N(h) profiles derived from them are illustrated in figures 7.1 and 7.3.

As can be seen from figures 7.8 and 7.10 and from table 7.1, the nose frequencies are overestimated with the Grahamstown models. This implies that the electron densities of the F region are in excess of their effective values over the transmission path.

The virtual path values on the high ray sections of the experimental ionogram in figure 7.8 increase more rapidly with decreasing frequency, over the range recorded, than those in figure 7.10, which seem to be levelling off. This "open" or "closed" appearance of the ionograms near the nose is roughly reproduced by the chained curves, as are the downward slope of the low ray section towards the nose in figure 7.8, indicating that there must have been considerable retardation in the F1 region over much of the actual transmission path, and the nearly horizontal low ray section in figure 7.10.

The virtual path agreement in figure 7.10 is good. The virtual path positioning of the experimental ionogram in figure 7.8 is uncertain, since this ionogram was recorded before the procedure for obtaining offsets had been instituted. The offset was estimated from values for later ionograms; the error in position is thus of the order of 100 km, compared with 0,5 km on the other experimental ionograms of figures 7.9 - 7.13.

The SANAE profile models (b and d).

The SANAE records were unfortunately blank on day 72, 1975, so that no comparison between the results of model a and of a corresponding SANAE profile was possible. Scanning records from later in 1975, it was found that the oblique ionogram for day 232, 11:05 SAST, shown in figure 7.9, was associated with a reasonable SANAE vertical

ionogram. This, together with the N(h) profile, is shown in figures 7.2A and 7.2B. Work on this set of data was, however, discontinued after an oblique ionogram had been synthesized with the SANAE profile, because the corresponding Grahamstown ionogram appeared disturbed and unstable. The ripples and gap on the oblique ionogram may also be indicative of a disturbed ionosphere. The SANAE vertical ionogram and corresponding N(h) profile for day 222, 1975, 13:45 UT are shown in figures 7.4A and 7.4B.

Ionograms synthesized using the SANAE profiles, models b and d, are indicated by dashed curves in figures 7.9 and 7.10. Together with table 7.1, the figures show that the nose frequencies are underestimated, which implies that the electron densities of the F region are low compared to their effective values over the transmission path.

The virtual paths agree reasonably in figure 7.9, and the upward slope of the low ray section towards the nose frequency and the open appearance are also reproduced in the synthesized ionogram. In figure 7.10 the closed shape is reproduced, but the low ray section is too curved and the values of virtual path are low.

The two-profile model (e).

The Grahamstown and SANAE N(h) profiles having proved to have respectively too high and too low values of maximum electron density, as evidence by the over- and underestimated nose frequencies of the chained and dashed ionograms in figure 7.10, a crude attempt was made to vary the electron density profile between the two endpoints. The SANAE profile (day 222, 9:00 UT, figure 7.4B) was used on the first and the corresponding Grahamstown profile (day 222, 11:00 SAST, figure 7.3B) on

the second hop of each ray. Part of an ionogram synthesized with this model is shown by the dotted curve in figure 7.10.

Low rays were traced up to the nose frequency which, although higher than that obtained using the SANAE profile on both hops, is still considerably underestimated (table 7.1). The nose region appears to be rounded and the low ray curve is flatter, with better agreement in virtual path, than that obtained with the SANAE profile. In general the dotted two-profile curve bears a marked resemblance to the dashed SANAE profile curve, which indicates that the SANAE end is more influential in the two-profile model, causing the high frequencies to be lost before the rays reach the greater electron densities of the Grahamstown end where they could be reflected.

The model also proved so prone to program instabilities at the smaller take-off angles required for high rays (section 2.7.3), that it was abandoned for lack of time.

The effective profile model (f).

Since the two-profile model had not proved very successful, it was decided to trace rays through a spherically stratified, single N(h) profile model representative of overall conditions over the transmission path. Since there were no vertical data from the region of the path midpoint, the following approach was adopted. Points from all the modes (two-, three-, four- and five-hop) of the experimental oblique ionogram of day 222, 15:50 SAST were reduced to points on equivalent vertical ionograms via equations (2.20) and (2.22), neglecting the geomagnetic field but correcting for the curvature of the earth. Most of the F region of a vertical ionogram was obtained in this way. f_oE and f_oF2 were taken as the means of the values on the SANAE and Grahamstown vertical ionograms of figures 7.4A and 7.3A, because of the scarcity of points in these regions. The composite vertical ionogram and the corresponding "effective" N(h) profile for the transmission path are shown in figures 7.5A and 7.5B.

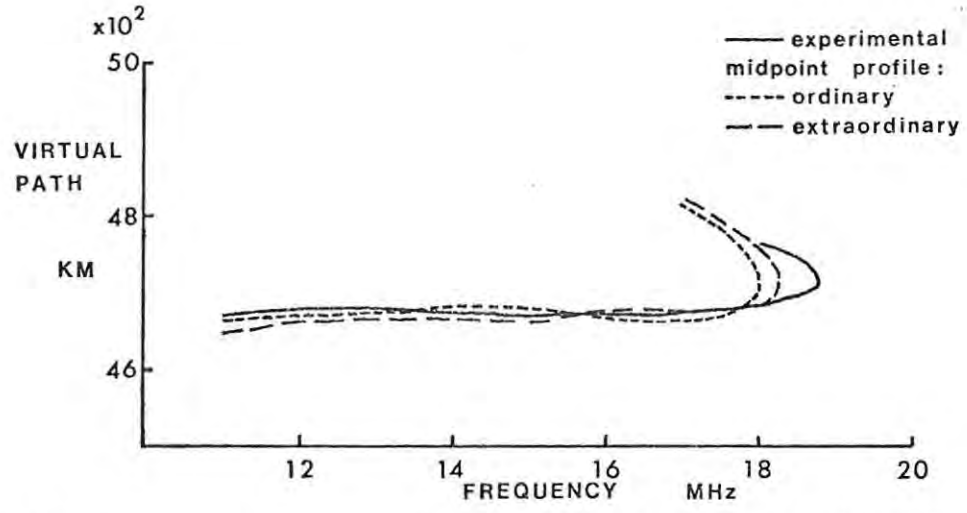

F 7.11 SANAE-GTN IONOGRAM DAY 222 1975 15:50 SAST

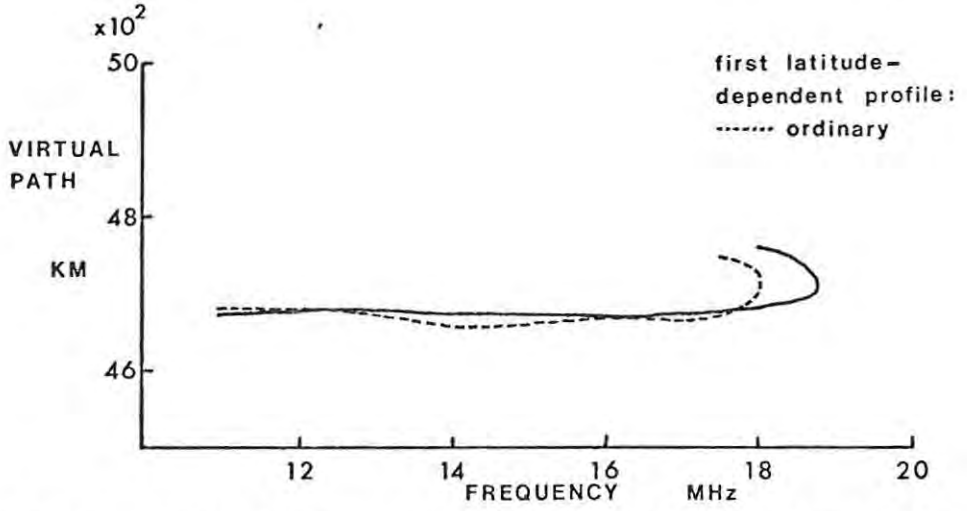

F 7.12 SANAE-GTN IONOGRAM DAY 222 1975 15:50 SAST

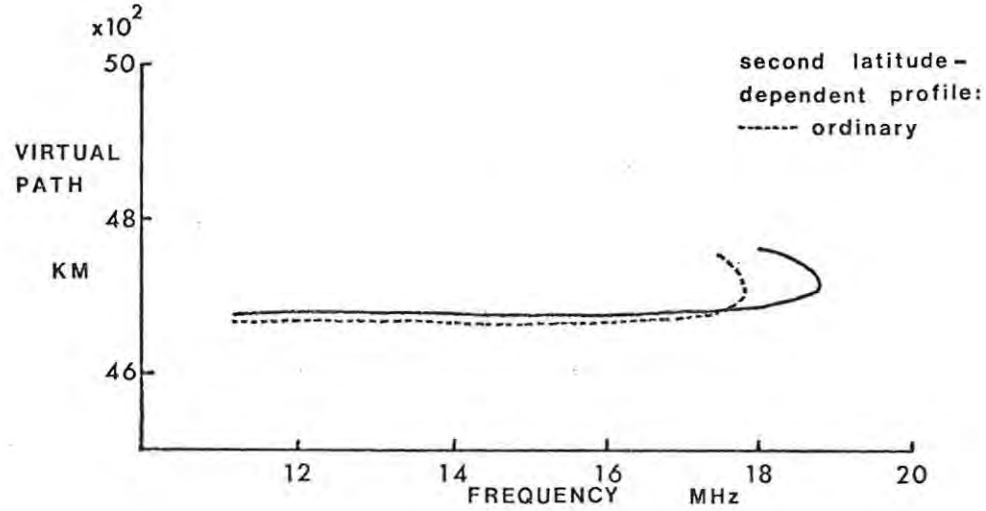

F 7.13 SANAE-GTN IONOGRAM DAY 222 1975 15:50 SAST

The ordinary oblique ionogram which was obtained by tracing rays through this profile is shown by the dotted curve in figure 7.11. The nose frequency, although underestimated, is much closer to the experimental value than that obtained with models c, d and e (table 7.1), indicating that important sections of the F region and the maximum electron density are reasonably well represented by this model. The flat low ray section is reproduced but the nose region is more open than that of the experimental ionogram.

Since a model which gave reasonable agreement in nose frequency had been obtained, the extraordinary ionogram was also synthesized. This is indicated by the dashed curve in figure 7.11. Its appearance is very similar to that of the ordinary curve. The largest differences in the values of virtual path for the two modes occur near the nose frequency on the high ray sections of the ionograms, and the extraordinary nose frequency exceeds that of the ordinary mode by 0,25 MHz. This result is in agreement with Davies (1965), pp. 180-1, for single hop propagation approximately transverse to the geomagnetic field, over a distance of 2250 km. Similar results for appropriately oriented rays have also been obtained by Kopka and Möller (1968), with single hop ray tracing over 2000 km.

The first latitude dependent model (g).

Figure 7.6 illustrates the variation of electron density N with height and latitude as described by equation (3.8), when the N(h) profiles at Grahamstown and SANAE are those of day 222, 15:45 SAST and 13:45 UT, shown in figures 7.3B and 7.4B respectively. The variation of electron density with height is shown for the two endpoints and the intermediate latitudes 61,05°S; 51,80°S and 42,54°S. The electron density model is a linear interpolation with latitude between values at the endpoints at the same height.

The dotted curve in figure 7.12 represents the ordinary ionogram synthesized by tracing rays with this model. The nose frequency, still underestimated, is close to that obtained with the previous model (table 7.1). The shape of the nose region is well reproduced; there are some ripples in the low ray section which may be due to the definition of the model. The values of virtual path agree well with those of the experimental ionogram.

The second latitude dependent model (h).

According to this model, the interpolation is between electron densities at related heights at the endpoints. Figure 7.7 shows the variation of electron density with height according to equation (3.14), for the same endpoint profiles and at the same latitudes as those used in figure 7.6.

The ordinary ionogram synthesized with this model is shown by the dotted curve in figure 7.13. The nose frequency is similar to but slightly lower than those of the previous two models (f and g), and analysis of the electron density versus height curves of figures 7.6 and 7.7 reveals that the second model (h) does predict lower electron densities than the first (g) at heights between 210 km and 240 km. The difference, up to 1×10^4 cm^{-3}, is small compared to typical electron densities of 2×10^5 cm^{-3} to 7×10^5 cm^{-3} in the F region.

The low ray part of the ionogram is free from ripples, possibly indicating that this is a better model of the lower regions of the ionosphere. The nose region is slightly more open than that on both the experimental ionogram and that synthesized with the first latitude dependent model (g).

7.3.3. Discussion of the results.

Grahamstown and SANAE type spherically stratified electron density models were shown to result in over- and underestimated values respectively for oblique nose frequencies. This result was to be expected, since the ionosphere changes over the transmission path and the two endpoints probably have the profiles with the highest and lowest values respectively of maximum electron density under normal conditions.

The two-profile model was a crude attempt to represent the gradation in the properties of the ionosphere between Grahamstown and SANAE. The nose frequency according to this model was little greater than that obtained using the SANAE profile on both hops. This implies that the properties must change fairly rapidly, moving away from SANAE, in order that the higher frequencies are not lost. It appears that it is the N(h) profile in the vicinity of the first ionospheric reflection point, only slightly modified by that near the second, which controls the nose frequency of an oblique ionogram.

Improved results were obtained by using an effective N(h) profile which was fairly representative of ionospheric conditions over the transmission path. The nose frequency was still underestimated, which implies that the maximum electron density of the model is too low or, possibly, that the F2 region is too thick (see below).

The two tilted, latitude dependent electron density models appear to make the best use of the data. Good agreement with the experimental ionogram was obtained without any intermediate calculations (such as were required for the previous model). The two models also produced very similar values of nose frequency and virtual path. This is in agreement with Rush and Edwards (1975), who showed that subtly different

models of the F2 region based on the same parameters caused differences in propagation characteristics which are less than those associated with a 10% uncertainty in specifying the parameters. They concluded that their results, obtained with a spherically stratified model, should also be applicable to models having non-vertical gradients in electron density.

The relationship between the ionosphere model and the shape of the oblique ionogram is complicated. Möller (1964), while extensively discussing oblique propagation, makes no specific reference to this topic. A thin F or F2 region, which would produce a vertical ionogram in which virtual height h' rises rapidly with increasing frequency f near penetration, can be expected to result in a closed shape for the nose region of an equivalent oblique ionogram, obtained via equations (2.20) and (2.22) or graphically by means of transmission curves (Davies, 1965 pp. 165,-6). Application of the latter method also shows that, for the same vertical penetration frequency and hence maximum electron density, the thinner the ionospheric layer (and consequently the more steep the h'(f) curve), the higher is the nose frequency of the equivalent oblique ionogram.

The ionograms synthesized with models a,b,c,d and f conform to this approximate rule to varying degrees; other factors are probably also influential. An attempt to investigate the differing shapes of the experimental ionograms of day 72, 14:05 SAST, day 232, 11:05 SAST and day 222, 15:50 SAST, by converting them to equivalent vertical ionograms and comparing F2 regions, proved inconclusive.

It is of interest that the two latitude dependent models (g and h), and the effective profile model (f) which also relied partly upon a crude linear interpolation between data at the endpoints, all gave low values for the nose frequency of the particular experimental ionogram used.

The difference between the experimental nose frequency and that obtained by ray tracing through one of the above models could be

(i) within the error inherent in setting up the N(h) profiles and in the ray tracing procedure, or

(ii) indicative of a non-linear gradation in the properties of the ionosphere between SANAE and Grahamstown, or

(iii) due to temporal changes in the ionosphere during the interval of the recording of the vertical and oblique ionograms.

Without analysing more records, it is not really possible to say which of the above is most influential.

7.4. Oblique ray paths.

A ray path in a spherically stratified ionosphere with no external magnetic field would be planar, following the great circle route between SANAE and Grahamstown, according to 2.7.3, and the two hops would each have precisely the same shape.

The influence of the geomagnetic field and the various ionosphere models will be discussed in an attempt to draw conclusions about the paths of actual rays on the SANAE - Grahamstown transmission path.

7.4.1. Ground plans of the ray paths.

The ground plans of rays traced through spherically stratified ionosphere models were effectively great circles at frequencies equal to and above 11 MHz, which was the lowest used. The rays were all sent off along the great circle bearing of Grahamstown at SANAE and maximum deviation from the great circle was approximately 4 km with, for example, the effective electron density profile. Over the distance 4470 km, therefore, the geomagnetic field does not cause rays in the frequency range 10 - 30 MHz to deviate significantly from the great circle route between the transmitter and the receiver.

Rays traced from SANAE to Grahamstown through the two latitude dependent models required take-off angles (β) slightly north of the great circle bearing. This northward deviation was of negligible magnitude with the first model (g) but just noticeable with the second (h); it increased with increasing height of reflection of the rays, being at most 0,7°. This observation can most easily be explained using the flat earth, ionospheric mirror model of Kelso (1964), pp. 211-3. Because of the latitude gradient, the mirror is tilted, sloping downwards towards the north. A ray transmitted at SANAE, in the vertical plane containing SANAE and Grahamstown, reflects off the mirror. The incident and reflected rays and the normal to the mirror, which has both southward and vertically downward components, are coplanar. Therefore the ray returns to earth consistently south of Grahamstown and, to reach it, must be transmitted in a more northerly direction to compensate.

The maximum deviation of the ground plans from the great circle should occur at the ground reflection points (section 7.4.5), and here, with the second model (h), it was found to be approximately 14km.

7.4.2. The dependence of ray paths on the take-off angle α.

Since the ground plans are effectively great circles, and at these latitudes distance along the great circle is nearly linearly related to latitude, it is convenient to illustrate the dependence of ray endpoints on the take-off angle to the vertical, α , by graphs of final latitude versus α .

Figure 7.14 shows some of these graphs, for ordinary and extraordinary two-hop rays at 16, 17 and 18 MHz, traced from SANAE in the direction of Grahamstown through the effective electron density profile (model f). The dashed line represents the latitude of Grahamstown, and where the solid curves intersect this line, a ray of that mode, frequency and angle α will reach Grahamstown.

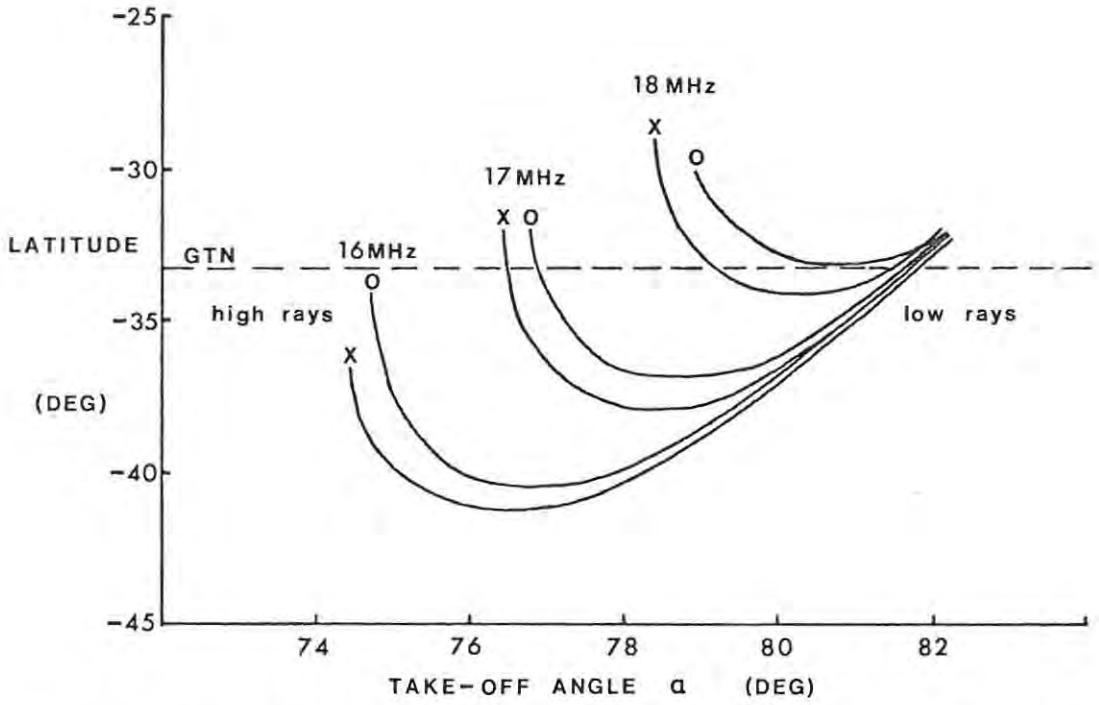

F 7.14 VARIATION OF RAY ENDPOINT LATITUDE WITH TAKE-OFF ANGLE

There is an obvious similarity to figure 2.4B: a furthest south, or "skip", latitude, and a minimum value of α below which rays penetrate the ionosphere, can be identified for each curve. The ordinary nose frequency is 18MHz as the dashed line is tangent to the curve for this mode and frequency. At and below 17MHz, low rays which reach Grahamstown all have α approximately 81,5°; the extraordinary low ray α's exceed the ordinary by about 0,1° at the same frequency. The angles of the high rays are more frequency dependent, increasing by about 2° per 1MHz over this range. Ordinary and extraordinary high ray curves are also quite distinct, and rays of the latter mode which reach Grahamstown have α about 0,5° less than the former at the same frequency. Extraordinary skip latitudes are further south than those of the ordinary mode at the same frequency; the extraordinary nose frequency, whose curve is not shown, is greater than 18MHz.

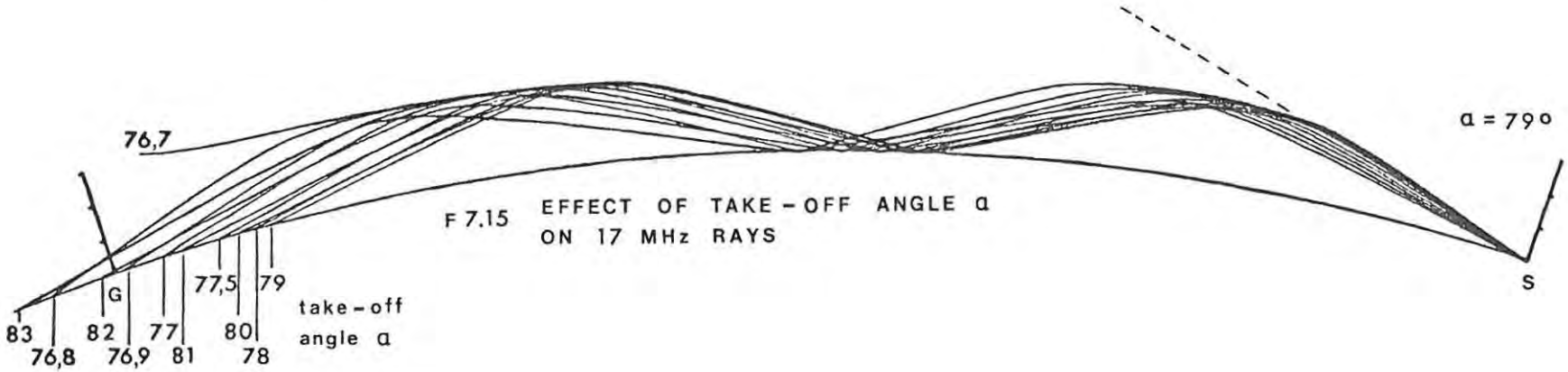

F 7.15 EFFECT OF TAKE-OFF ANGLE α ON 17 MHz RAYS

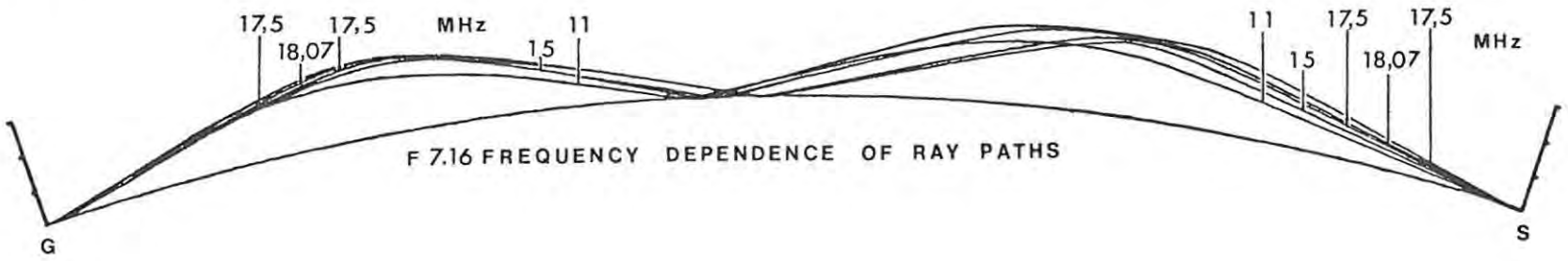

F 7.16 FREQUENCY DEPENDENCE OF RAY PATHS

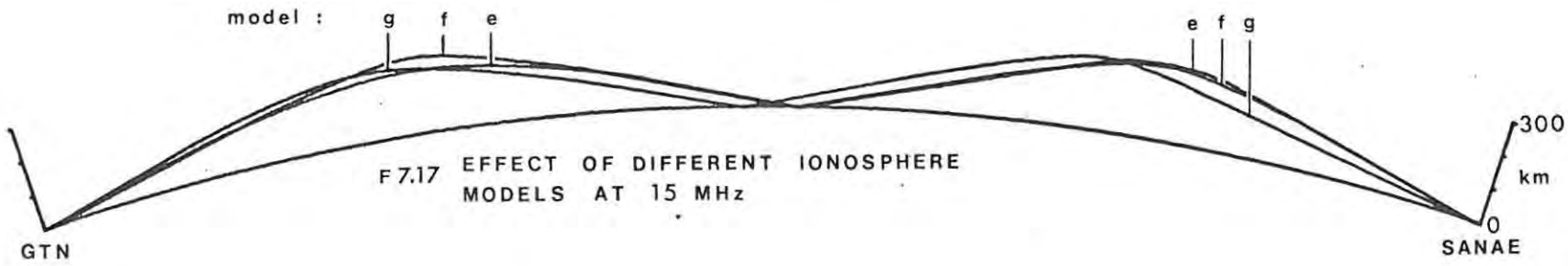

F 7.17 EFFECT OF DIFFERENT IONOSPHERE MODELS AT 15 MHz

A selection of rays whose endpoints formed part of the data for figure 7.14 is shown in figure 7.15. Here height is plotted against latitude. The ray with $\alpha = 76,7°$ penetrates the ionosphere (on the second hop), rays with $76,8° \leqslant \alpha \leqslant 78°$ are high rays and those with $79° \leqslant \alpha \leqslant 83°$ are low rays - the skip angle (section 2.7.3) for this set, according to figure 7.14, was 78,6°. The height marker at the latitude of Grahamstown in figure 7.15 corresponds to the dashed line in figure 7.14.

7.4.3 Reflection heights of the rays.

The reflection height, or height at which a ray becomes horizontal, depends on the ionosphere model and the mode and frequency of the ray. General trends are illustrated in figure 7.16, which shows ordinary rays traced from SANAE to Grahamstown through the first latitude dependent ionosphere model (g), at frequencies 11; 15; 17,5 and 18 MHz (the nose frequency). The reflection heights increase with frequency on both hops for the low rays and increase with decreasing frequency for the high rays, only one of which (17,5MHz) is shown.

Table 7.2: Reflection heights for rays at the nose frequency.

Model	Height of maximum electron density (km).		Height of reflection (km).		Difference (km).	
	1st hop	2nd hop	1st hop	2nd hop	1st hop	2nd hop
a	272	272	229	230	43	42
b	214	214	197	198	17	16
c	236	236	216	217	20	19
d	246	246	224	225	22	21
e	246	236	229	184	17	52
f	252	252	228o	228o	24o	24o
			227x	227x	25x	25x
g	238(variable)	236	228	212	10	24
h	243	238	227	211	16	27

In terms of actual heights, the lowest frequency (11MHz) low rays traced were found to reflect low in the F region between 150km and 190km according to the model. Rays at the nose frequency reflect from 10km to 43km below the height of maximum electron density, depending on the thickness of the F or F2 region, as shown in table 7.2; this is a wider variation than the 25 - 30 km below the maximum found by Rush et al. (1974). The entries for models g and h in the table were calculated using the latitudes at which the rays reflect, and are included only as a guide. High rays have been traced to within 8 km of the height of maximum electron density.

Rays of different modes and the same frequency differ in their reflection heights: low extraordinary rays reflect beneath low ordinary rays, and conversely high extraordinary rays reflect above high ordinary rays, by 1 - 3 km in both cases.

The reflection heights are not the same on the two hops of a ray. The effect of the geomagnetic field is noticeable when the ionosphere model is spherically stratified. If h_1 is the reflection height on the first (SANAE) and h_2 on the second (Grahamstown) hop, then $h_1 < h_2$ for the ordinary mode and $h_1 > h_2$ for the extraordinary. The difference, $\Delta h = h_1 - h_2$, is plotted against frequency for rays traced through the effective profile (model f) in figure 7.18. The dotted and dashed curves apply to the ordinary and extraordinary modes respectively. The magnitude of Δh varies between 0,1 km and 2 km: for low rays, it decreases to a roughly constant value from low through medium frequencies and increases again towards the nose frequency; at the frequencies traced, Δh decreases with increasing frequency on the high rays.

The effect of the overall increase in electron density from SANAE to Grahamstown is to give the first (SANAE) hop the greater reflection height, as a ray must travel further into the ionosphere to reach electron densities comparable with those occurring at lower heights nearer

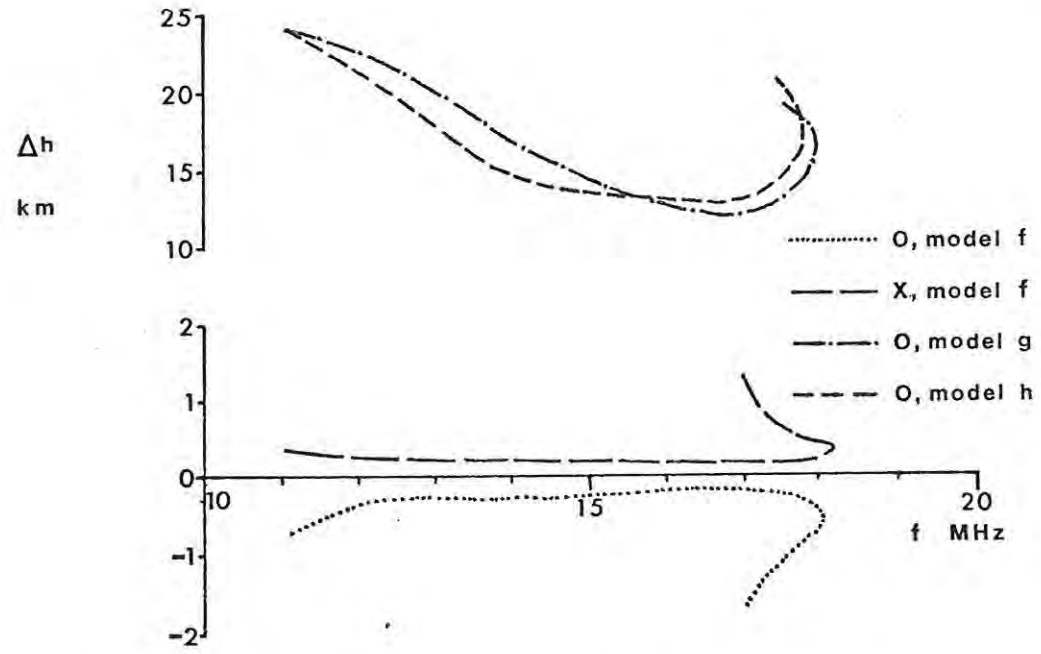

F 7.18 DIFFERENCE BETWEEN FIRST AND SECOND HOP REFLECTION HEIGHTS

Grahamstown. The diagrams of two-hop ray paths presented by Kuriki et al. (1974) similarly show that, where maximum electron densities differ significantly, the hop having the profile with the smaller maximum density has the greater reflection height. Using the two-profile model (e), the difference Δh was typically 45km. Values which are intuitively more satisfactory, ranging from 11km to 25km, were obtained with the first and second latitude dependent models (g and h). These are also represented in figure 7.18, by chained and broken curves respectively. Δh is greatest for the low frequency low rays, but increases with decreasing frequency on the high rays at the frequencies traced.

In figure 7.17 the path of an ordinary low ray at 15MHz is shown in the two-profile (e), effective profile (f), and first latitude dependent (g) ionosphere models; the dependence on the ionosphere model of the reflection heights and of their relationship on the first and second hops is noticeable.

7.4.4 Shapes of the ray paths.

The ray paths on each hop are nearly symmetrical about a vertical line through the reflection point, in a spherically stratified ionosphere, since the effects of the magnetic field are small at high frequencies. With such ionospheric models (a,b,c,d and f), the acute angles between the wave normal and the vertical at the surface of the earth are the same, for upgoing and downgoing rays on both hops, to within 0,1°.

This relationship no longer holds when the ionosphere is tilted. With the first latitude dependent model (g), the angle to the vertical for the upgoing ray exceeds that of the downgoing ray by 4,0° ± 1,0° on the first (SANAE) hop and by 2,0° ± 0,3° on the second, averaging over all the frequencies traced.

High rays, as shown in figures 7.15 and 7.16, spend more of their total path length deep in the ionosphere and are more flattened in appearance than the relatively pointed low rays.

7.4.5. Ground reflection points.

The rays all reflect off the surface of the earth (or sea) to begin their second hop at approximately the geographic midpoint of the path when spherically stratified ionosphere models are used. These ground reflection points, for ordinary rays and the effective model (f), are depicted in figure 7.19; only high rays (identified by frequency followed by the letter h) at 17 MHz and 17,5 MHz (near the nose frequency) are noticeably further south than the other frequencies which are not individually identified.

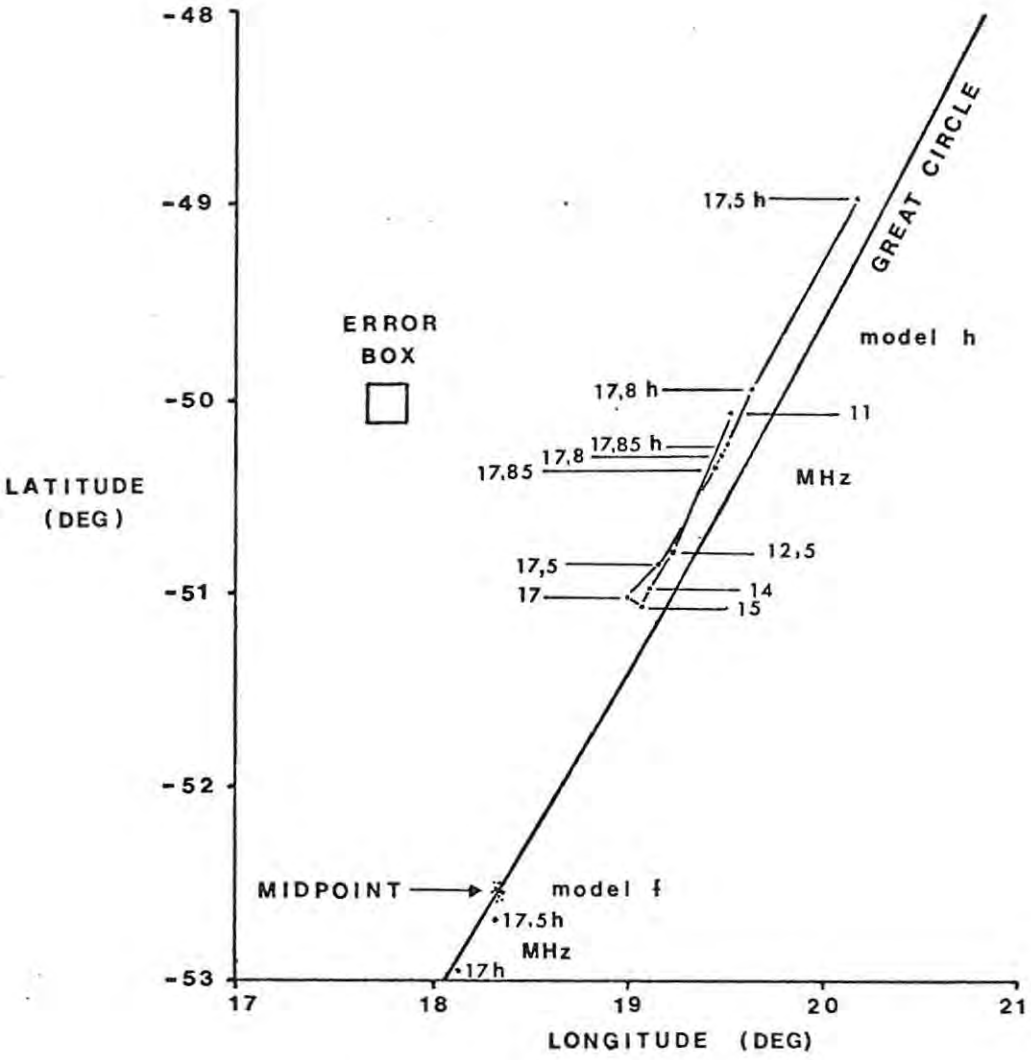

F 7.19 GROUND REFLECTION POINT POSITIONS

The tilted ionosphere models have the effect of shifting the ground reflection points north-east of the geographic midpoint (which can be seen in figure 7.17), and of separating the reflection points of the different frequencies. Figure 7.19 also shows the ground reflection points of high and low ordinary rays at various frequencies when the second latitude dependent model (h) was used. The low rays just below the nose frequency, at 15 MHz and 17 MHz, reflect furthest south, and about 170 km away from the geographic midpoint. The reflection points for this model in figure 7.19 are spread out over a distance of about 250 km.

The probable maximum error in the points, for both models, is taken as half the allowed maximum error at the endpoint (Grahamstown), which was 0,2° for this data. The error box with sides of 0,1° thus indicates that each of the points in figure 7.19 lies somewhere within such an area.

7.4.6. Main features of actual ray paths.

The following conclusions can tentatively be drawn about the behaviour of rays reaching Grahamstown from SANAE, at frequencies observed on oblique ionograms recorded during the daytime:

(i) the ground plans effectively follow the great circle route from SANAE to Grahamstown;

(ii) rays at most of the observable frequencies have been reflected in the F region above about 150 km;

(iii) the influence of ionospheric tilts on reflection heights of the hops is greater than that of the geomagnetic field so that the reflection heights decrease towards Grahamstown;

(iv) in a tilted ionosphere the ground reflection points of two-hop rays are closer to Grahamstown than to SANAE and are spread out according to frequency.

CHAPTER 8

C O N C L U S I O N

The ionosphere models for this project were derived from vertical ionograms. It was possible to reproduce the original ordinary and extraordinary traces closely by tracing vertical rays through such electron density profiles, with the geomagnetic field taken as a tilted dipole equivalent to the actual field at the transmitter.

The results of Chapter 6 show that the ionosphere can be considered as spherically stratified for short distance oblique propagation between Alice and Grahamstown. The ordinary and extraordinary oblique ionograms closely resemble vertical ones recorded at Grahamstown, and can be reasonably reproduced by ray tracing, although the basic minimum error appears to be greater than that for vertical propagation. Vertical and oblique ray paths calculated by the ray tracing program have been studied in detail and related to properties of the ionosphere and the geomagnetic field.

It has been shown, in Chapter 7, that the two-hop mode is, under normal circumstances, the first received for long distance propagation between SANAE and Grahamstown. The best agreement between synthesized and experimental oblique ionograms was obtained with a simple, tilted ionospheric model in which it was assumed that the ionosphere varied linearly with latitude between the electron density profiles at Grahamstown and SANAE. The geomagnetic field does discernibly affect the ray paths, but effects arising from ionospheric tilts are more significant.

The ray tracing program could be improved in some ways; the problem of low frequency "high" rays should be investigated, and a signal-loss calculation could usefully be included. Suggestions for future use of the program include application to higher modes of propagation and modes which involve internal reflections in the ionosphere, testing of detailed explanations of normal and abnormal

ionosphere models, and perhaps application to travelling disturbances.

Ionospheric data at present being gathered on the voyage of the supply ship RSA to and from SANAE may enable a more realistic model of the gradation in ionospheric properties over the South Atlantic Ocean to be formulated for use with the ray tracing program.

LITERATURE CITED

Al'pert, Ya. L. (1963). Radio Wave Propagation and the Ionosphere. Consultants Bureau Enterprises, New York.

Barish, F.D. and Roederer, J.G. (1969). "Conjugate intersects to selected geophysical stations". STP Notes No. 4 (May), 91-109.

Bracewell, R. (1965). The Fourier Transform and its Applications. McGraw-Hill, New York.

Budden, K.G. (1961). Radio Waves in the Ionosphere. Cambridge University Press.

Budden, K.G. and Terry, P.D. (1971). "Radio ray tracing in complex space". Proc. R. Soc. A 321, 275-301.

Chapman, S. and Bartels, J. (1951). Geomagnetism. Oxford University Press.

Cook, A.H. (1973). Physics of the Earth and Planets. Wiley, New York.

Croft, T.A. and Gregory, L. (1963). A Fast, Versatile Ray-Tracing Program for IBM 7090 Digital Computers. Report SEL-63-107, Stanford Electronics Laboratories, Stanford, California.

Curtis, A.R. (1972). A Two-Dimensional Ray-Tracing Program. Report 034/72, AWRE, Aldermaston, Berkshire, England.

Danilkin, N.P., Denisenko, P.F. and Sotskiy, V.V. (1975). "Computation of ionospheric N(h) profiles by quadratic programming". Geomagn. & Aeron. (USA) 15, 292-3.

Davies, K. (1965). Ionospheric Radio Propagation. Monograph 80, Natl. Bur. Stand., U.S. Dept. of Commerce.

Fiszlieber, F.,de Feraudy, H. and Cerisier, J.C. (1975). "Influence of horizontal density gradients on the propagation of VLF waves through the ionosphere". J. Atmos. & Terr. Phys. 37, 1525-34.

George, P.L. (1970). "True height analysis of oblique incidence HF radio wave data". J. Atmos. & Terr. Phys. 32, 905-16.

Gething, P.J.D. (1969). "The calculation of electron density profiles from oblique ionograms". J. Atmos. & Terr. Phys. 31, 347-54.

Gill, S. (1951). "A process for the step-by-step integration of differential equations in an automatic digital computing machine". Proc. Camb. Philos. Soc. 47, 96-108.

Gledhill, J.A. (1975). Private Communication.

Hamming, R.W. (1962). Numerical Methods for Scientists and Engineers. McGraw-Hill, New York.

Haselgrove, C.B. and Haselgrove, J., (1960). "Twisted ray paths in the ionosphere". Proc. Phys. Soc. 75, 357-63.

Haselgrove, J., (1955). "Ray theory and a new method for ray tracing". Phys. Soc. Conf. Ionosph., 355-64.

Hollis, J.S., Lyon, T.J. and Clayton, L. (1970). Microwave Antenna Measurements. Scientific-Atlanta, Atlanta, Georgia.

Jensen, D.C. and Cain, J.C. (1962). "An interim geomagnetic field". J. Geophys. Res. 67, 3568-9.

Jones, R.M. and Stephenson, J.J. (1975). A Versatile Three-Dimensional Ray Tracing Computer Program for Radio Waves in the Ionosphere. OT Report 75-76, Office of Telecommunications, U.S. Dept. of Commerce.

Kelso, J.M. (1964). Radio Ray Propagation in the Ionosphere. McGraw-Hill, New York.

Kimura, I. and Kawai, M. (1976). "Ray path in a stratified absorbing medium". IEEE Trans. Antennas & Propag. AP-24, 515-8.

Kolesova, V.I., Kropachev, E.P., Lysenko, L.S., Privalova, L.A. and Anshukova, T.N. (1974). "Global magnetic charts of the 1970 epoch". Geomagn. & Aeron. (USA) 14, 596-602.

Kopka, H. and Möller, H.G. (1968). "MUF calculations including the effect of the earth's magnetic field". Radio Sci. 3, 53-6.

Kuriki, I., Kasuya, I., Hojo, H. and Tanohata, K. (1974). "Analysis of the maximum observed frequencies on oblique ionograms by ray tracing technique". J. Radio Res. Lab. (Japan) 21, 161-90.

Lambert, S. (1974). Ray Tracing in the Ionosphere. Physics Honours Project, Rhodes University.

Lee, M.K. and Nisbet, J.S. (1975). "Propagation predictions and studies using a ray tracing program combined with a theoretical ionospheric model". IEEE Trans. Antennas & Propag. AP-23, 132-6.

Möller, H.G. (1964). Variable-Frequency Pulse Transmission Tests at Oblique Incidence Over Distances between 1000km and 2000km. Stanford Research Institute, Menlo Park, California.

Piggott, W.R. (1976). Private Communication.

Poole, A.W.V. (1974). Private Communication.

Rash, J.P.S. and Poole, A.W.V. (1975). "SANAE-Grahamstown oblique soundings - a preliminary study". Paper presented at S.A. Institute of Physics 20th Annual Conference.

Rash, J.P.S. (1976). "Transmission times of radio waves between SANAE and Grahamstown". Paper presented at S.A. Institute of Physics 21st Annual Conference.

Ratcliffe, J.A. (1959). The Magneto-Ionic Theory and its Applications to the Ionosphere. Cambridge University Press.

Ratcliffe, J.A. (1974). "Experimental methods of ionospheric investigation 1925-1955. J. Atmos. & Terr. Phys. 36, 2095-103.

Rawer, K., Ramakrishnan, S. and Bilitza, D. (1975). Preliminary Reference Profiles for Electron and Ion Densities and Temperatures proposed for the International Reference Ionosphere. IPW - Scientific Report W.B.2., Institute für physikalische Wettraumforschung, Freiburg, F.R.G.

Rush, C.M., Miller, D. and Gibbs,J. (1974). "The relative daily variability of f_oF2 and h_mF2 and their implications for HF radio propagation". Radio Sci. 9, 749-56.

Rush, C.M. and Edwards, W.R. Jr. (1975). "Sensitivity of HF circuit simulations to electron density models". Radio Sci. 10, 867-74.

Smith, M.S. (1970). "The calculation of ionospheric profiles from data given on oblique incidence ionograms". J. Atmos. & Terr. Phys. 32, 1047-56.

Terry, P.D. (1971). Complex Ray Tracing in Ionospheric Radio Propagation. Ph. D. Thesis, Cambridge University.

Terry, P.D. (1974). "Ray tracing in three dimensional geophysical polar co-ordinates". Private Communication.

Titheridge, J.E. (1959). "The use of the extraordinary ray in the analysis of ionospheric records". J. Atmos. & Terr. Phys. 17, 110-25.

Titheridge, J.E. (1975). "The relative accuracy of ionogram analysis techniques". Radio Sci. 10, 589-99.

Wait, J.R. (1962). Electromagnetic Waves in Stratified Media. Pergamon Press, London.

Yabroff, I. (1961). "Computation of whistler ray paths". J. Res. Nat. Bur. Stds. D 65, 485-505.

GLOSSARY OF IMPORTANT SYMBOLS

c	speed of light in vacuo
e	charge on the electron
f	frequency of electromagnetic wave or ray
f_N	plasma frequency
f_H	electron gyrofrequency
h	height above the surface of the earth
h'	virtual height of reflection of a ray
h_i	scale factors for an orthonormal, curvilinear co-ordinate system
k	wave number
m	mass of the electron
n	complex phase refractive index
p	phase
q	refractive index in direction of stratification of plasma
r	radial position co-ordinate
s	integration step size
t	time of travel of wave front along ray
x_i	orthonormal, curvilinear position co-ordinates
x	cartesian position co-ordinates
y	- do -
z	
$\vec{B}_o$	external magnetic field for a plasma
$\vec{B}$	geomagnetic field
B_0	magnitude of dipole geomagnetic field at magnetic equator and surface of the earth
D	distance along the earth's surface between ground-based transmitter and receiver; magnetic declination
F	total magnetic field strength at a point
G	refractive index surface
H	horizontal component of geomagnetic field
I	magnetic dip
J	quantities in Terry (1974) adaptation of Haselgrove
K	and Haselgrove (1960) equations
L	
M	- do -
N	electron density
P'	virtual path of a ray
P	quantities in Terry (1974) adaptation of Haselgrove
Q	and Haselgrove (1960) equations

S_1, S_2	direction cosines of wave normal
U	ionospheric parameter
V	phase velocity
V'	group velocity
V_R	ray velocity
X	ionospheric parameter; east-west component of H
Y	ionospheric parameter; north-south component of H
Z	ionospheric parameter; vertical component of geomagnetic field
α	take-off angle between wave normal of ray and vertical direction
β	take-off angle between wave normal of ray and magnetic meridian
ε_o	permittivity of free space
ζ	angle between wave normal and direction of ray
η	angle between wave normal and vertical direction; quantity in Terry (1974) adaptation of Haselgrove and Haselgrove (1960) equations
θ	latitude (geophysical position co-ordinate)
μ	real part of phase refractive index n
μ'	group refractive index
ν	electron collision angular frequency
ξ	angle between ray direction and vertical direction
ρ_i	components of "refractive index vector"
τ	delay time, or time of travel, of ray
ϕ	longitude (geophysical position co-ordinate)
χ	imaginary part of refractive index n
ψ	angle between wave normal and external magnetic field vector
ω	angular frequency
Θ	latitude of geomagnetic north pole
Φ	longitude of geomagnetic north pole